MONTANUNIVERSITÄT LEOBEN

PETROLEUM ENGINEERING DEPARTMENT

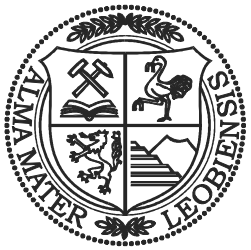

TEXTBOOK SERIES

VOLUME 3

PETROLEUM RECOVERY

by

Zoltán E. HEINEMANN
Professor for Reservoir Engineering

Leoben, January 2003

PREFACE

This volume is the third within the series of textbooks written by Z.E.Heinemann. The previous volumes:

- Flow in Porous Media
- Reservoir Fluids

deal with the properties of porous media, the one and two phase flow in reservoir rocks, phase behavior and thermodynamical properties of oil, gas and brine.

To use this volume it is supposed that the reader has attended the courses mentioned above or possesses profound knowledge of these topics. All methods discussed in this volume have practical importance and are used in today work. However, it is not possible to give a complete overview about the whole range of the classical and modern reservoir engineering tools. The selection was made under the aspect of transmitting basic understandings about the reservoir processes, rather to provide recipes.

This volume is followed by the textbooks

- Well Testing
- Basic Reservoir Simulation
- Enhanced Oil Recovery
- Advanced Reservoir Simulation Management

The seven volumes cover the whole area of reservoir engineering normally offered in graduate university programs worldwide, and is specially used at the MMM University Leoben.

ACKNOWLEDGEMENTS

The author gratefully acknowledges permission to use material from the following sources:

Table 3.1: From “Accurate Formulas for Calculating the Water Influx Superposition Integral” presented at the SPE Eastern Regional Meeting, Pittsburgh, October 1987. ©1987 SPE-AIME. **Figures 2.8, 2.9 and 2.10**: From *Journal of Petroleum Technology,* Vol. 19, Dec ©ember 1967. ©1967 SPE-AIME. **Figure 4.3**: From *Transactions of the SPE of the AIME*, Vol. 165, 1946. ©1946 SPE-AIME. **Figure 4.10**: From *Petroleum Production Handbook, Vol. II: Reservoir Engineering*, 1962. ©1962 SPE-AIME. **Figures 4.12, and 4.13**: From The *Reservoir Engineering Aspects of Waterflooding*, SPE Monograph, 1971. ©1971 SPE-AIME. **Figure 4.14**: From *Transactions of the SPE of the AIME*, Vol. 207, 1956 SPE-AIME. **Figure 5.1**: From *Transactions of the SPE of the AIME*, Vol. 210, 1957. ©1957 SPE-AIME. **Figures 5.15, 5.16, 5.17 and 5.18**: From *Transactions of the SPE of the AIME*, Vol. 207, 1956. ©1956 SPE-AIME. **Figures 5.24 and 5.25:** From “Effect of Flooding Rate and Permeability Ordering on Waterflooding Stratified Reservoirs”, *Paper 7158*, 1978. ©1978 SPE-AIME. **Figures 5.27, 5.28 and 5.29**: From *The Reservoir Engineering Aspects of Waterflooding*, SPE Monograph, 1971. ©1971 SPE-AIME. **Figures 5.30, 5.31 and 5.32**: From *Transactions of the SPE of the AIME*, Vol. 216, 1959. ©1959 SPE-AIME.

Table of Contents

List of Figures

Chapter 1

Introduction

The most important tasks of the reservoir engineer are to estimate the oil and gas reserves and to forecast the production. This volume describes the classic and fundamental methods that are applied for these purposes:

- Volumetric computation of reservoir volume
- Material balance calculations
- Estimation of displacement efficiency
- Estimation of sweep efficiency
- Production decline analysis

This volume is based on the textbooks Heinemann: *"Fluid Flow in Porous Media"* [21.] (1991) and Heinemann and Weinhardt: *"Reservoir Fluids"* [20.].

1.1 General Remarks

First some commonly used notions have to be defined:

- *PETROLEUM* is the common name for all kinds of hydrocarbons existing inside of the earth, independently of its composition and aggregate stage.
- *PETROLEUM IN PLACE* is defined as the total quantity of petroleum estimated in a reservoir:
  O.O.I.P. - Original oil in place m^3 [bbl]. Used symbol: N
  O.G.I.P. - Free gas in a gas cap or in a gas reservoir m^3 [cuft]. Used symbol: G_F.
- *CUMULATIVE PRODUCTION* is the accumulated production at a given date. Used symbols: N_p, G_p.
- *ULTIMATE RECOVERY* is the estimated ultimate production, which is expected

during the life of the property. Used symbols: N_{pmax}, G_{pmax}.

- *RESERVES* are the Ultimate Recovery minus Cumulative Production:

$$N_{pmax} - N_p \quad \text{or} \quad G_{pmax} - G_p \tag{1.1}$$

- *RECOVERY FACTOR*

$$E_R = \frac{Cumulative Production}{O.O.I.P.} = \frac{N_p}{N} \quad \text{or} \quad E_R = \frac{G_p}{G} \tag{1.2}$$

- *ULTIMATE RECOVERY FACTOR*

$$E_{Rmax} = \frac{Ultimate\ Recovery}{O.O.I.P.} = \frac{N_{pmax}}{N} \quad \text{or} \quad E_{Rmax} = \frac{G_{pmax}}{G} \tag{1.3}$$

The amount of reserves determines the whole strategy of future activities concerning

- exploration,
- development and
- production.

Unfortunately, reliable reserve figures are most urgently needed during the early stages of an exploration project, when only a minimum of information is available. During further activities (exploration and production), the knowledge concerning the reservoir contents becomes more and more comprehensive and naturally will reach a maximum at the end of the reservoir's life cycle.

Fig.1.1 shows the life cycle of a reservoir, and the range of recovery estimates.

PERIOD *AB*:

When no well is drilled, any estimate will be supported by the analogous method based on data from similar pools. In this phase probabilities of the

- presence of a trap,
- presence of oil or gas saturation,
- presence of pay and
- amount of recoverable reservoir contents

have to be estimated. No reserves is a real option.

PERIOD *BC*:

The field is being discovered and step by step developed. The production rate increases. The volumetric estimation can be made more and more precise due to the increasing

number of wells available.

PERIOD *CD*:

The field has been developed and the production rate achieved a maximum. The majority of possible informations from

- well logs
- core analysis and
- transient well testing

are available. The volumetric estimation can be made more precise when analysing the reservoir performance. Early simulation studies, called reservoir modeling, make the calculation of the ultimate recovery possible.

PERIOD *DE:*

The recovery mechanisms are well known. Material balance calculations and simulation of the reservoir history provide, in most of the cases, more accurate figures of O.O.I.P. than the volumetric method. These methods are more suited to compute the reserves than the volumetric method.

PERIOD *EF*:

In addition to material balance calculations and simulation studies decline curve analysis becomes more appropriate.

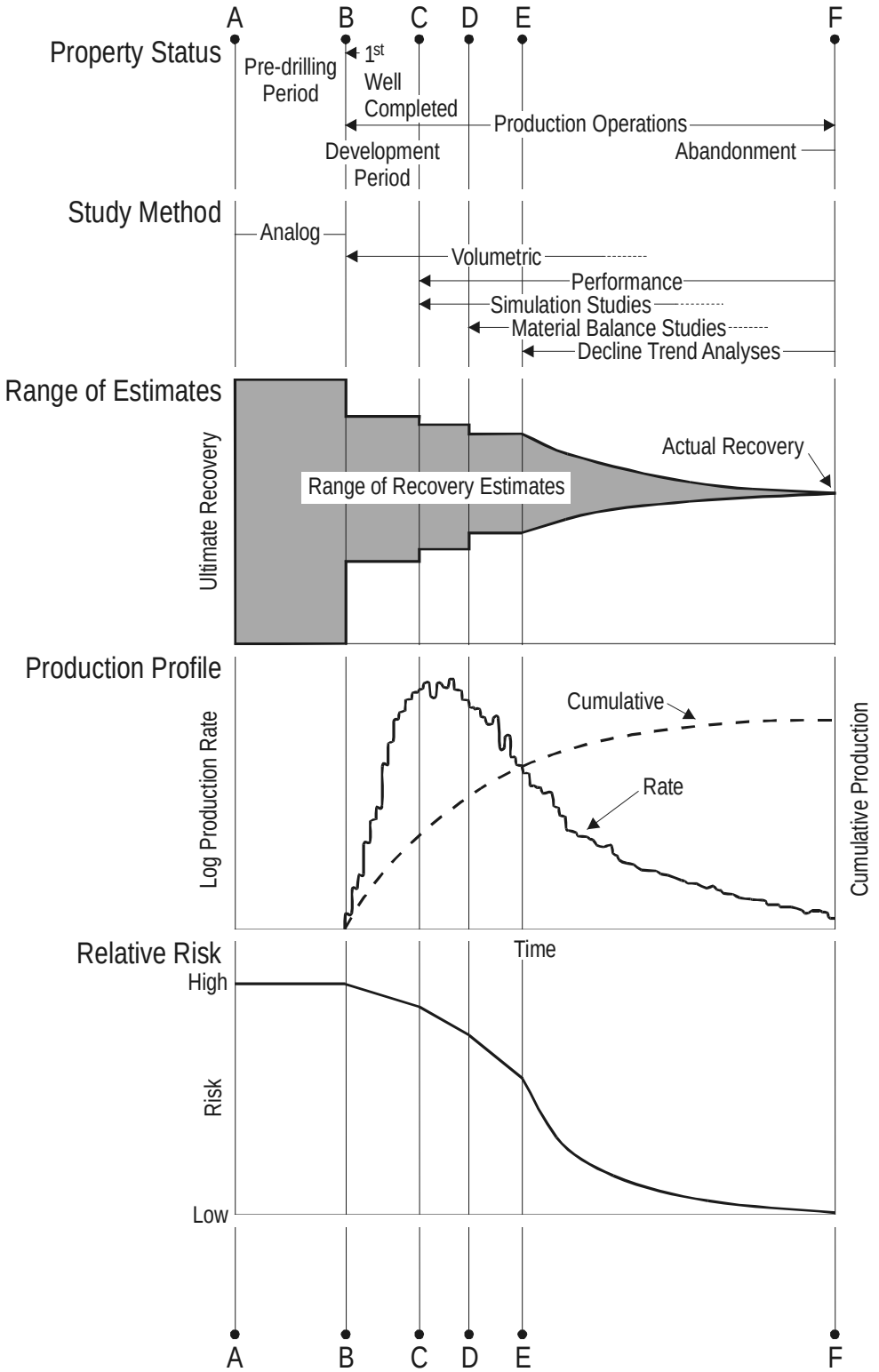

Figure 1.1: Range in estimates of ultimate recovery during the life of a reservoir

1.2 Classification of Reserves

Reserves are divided into classes. The definition of these classes is not common in all countries. Here the recommended nomenclature system of MARTINEZ *et al.*[28.](1983) published at the 11th World Oil Congress, London, is used.

PROVED RESERVES of petroleum are the estimated quantities, as of a specific date, which analysis of geological and engineering data demonstrates, with reasonable certainty, to be recoverable in the future from known reservoirs under the economic and operational conditions at the same date.

PROVED DEVELOPED RESERVES are those proved reserves that can be expected to be recovered through existing wells and facilities and by existing operating methods. Improved recovery reserves can be considered as proved developed reserves only after an improved recovery project has been installed.

PROVED UNDEVELOPED RESERVES are those proved reserves that are expected to be recovered from future wells and facilities, including future improved recovery projects which are anticipated with a high degree of certainty.

UNPROVED RESERVES of petroleum are the estimated quantities, as of a specific date, which analysis of geological and engineering data indicate might be economically recoverable from already discovered deposits, with a sufficient degree of certainty to suggest the likelihood or chance of their existence. Unproved reserves may be further categorized as *PROBABLE RESERVES* where there is a likelihood of their existence, or *POSSIBLE RESERVES* where there is only a chance of their existence. The estimated quantities of unproved reserves should take account of the uncertainties as to whether, and to what extent, such additional reserves may be expected to be recoverable in the future. The estimates, therefore, may be given as a range.

SPECULATIVE RESERVES of petroleum are the estimated quantities, as at a specific date, which have not yet been discovered, but which general geological and engineering judgement suggests may be eventually economically obtainable. Due to the great uncertainties, they should always be given as a range.

Chapter 2

Reserves Calculation by Volumetric Methods

2.1 Computation of Oil and Gas in Place

The following formulas are used:

OOIP - Original oil in place:

$$N = \frac{V\phi(1 - S_{wi})}{B_{oi}}. \tag{2.1}$$

OGIP - Free gas in a gas reservoir or in a gas cap:

$$G_F = \frac{V\phi(1 - S_{wi})}{B_{gi}}. \tag{2.2}$$

Solution gas in an oil reservoir:

$$G_s = \frac{V\phi(1 - S_{wi})R_{si}}{B_{oi}} = NR_{si}, \tag{2.3}$$

where

- V - reservoir volume [m^3]
- ϕ - porosity [-]
- S_{wi} - initial water saturation [-]

B_{oi} - oil formation volume factor (FVF) at initial pressure [m^3/sm^3]

B_{gi} - gas formation volume factor at initial pressure [m^3/sm^3]

R_{si} - initial solution (or dissolved) gas oil ratio [sm^3/sm^3]

The reservoir volume V can be calculated in different ways. Which method is the best depends on the available data, shape of the reservoir, etc..

2.2 Recovery Factor

Ultimate recovery is influenced by a lot of individual physical realities. It depends on the

- drive mechanism of the reservoir,
- mobility of reservoir fluids,
- permeability and variation of permeability, both vertically and in the area,
- inclination and stratification of the layers,
- strategy and methods of field development and exploitation.

In the exploration and early exploitation stage, only analogous or statistical methods can be used to estimate the ultimate recovery factor. It is necessary to examine known reservoirs from the same region.

ARPS *et al.*[2.] examined a large amount of oil fields with depletion drive and with water drive. The results were published by the American Petroleum Institute. The formulas are known as API formulas for estimation of the ultimate recovery factor.

Depletion or gas drive:

$$E_R(\%) = 41.815 \times \left(\frac{\phi(1-S_w)}{B_{ob}}\right)^{0.1611} \left(\frac{k}{\mu_{ob}}\right)^{0.0979} S_w^{0.3722} \left(\frac{p_b}{p_a}\right)^{0.1714} \tag{2.4}$$

Water or gravitation drive:

$$E_R(\%) = 54.898 \left(\frac{\phi(1-Sw)}{B_{oi}}\right)^{0.0422} \left(\frac{k}{\mu_{oi}\mu_{wi}}\right)^{0.077} S_w^{-0.1903} \left(\frac{p_i}{p_a}\right)^{-0.2159} \tag{2.5}$$

where p_i is the initial pressure, p_a the abandonment pressure, and p_b the bubble point pressure. The subscripts *i* and *b* denote that the value is valid at p_i or p_b. The numerical results of the API examination are summarized in Table 2.1.

Table 2.1: API Ultimate Recovery Factor Estimation

	Standard deviation	Sand, Sandstone min.	mean	max.	Carbonates min.	mean	max.
Depletion + Gasdrive	0.229	0.095	0.213	0.460	0.155	0.176	0.207
Water or Gravitationdrive	0.176	0.131	0.284	0.579	0.090	0.218	0.481

2.3 Data Distribution and Probability

The methods for calculation of the reservoir volume, average porosity and permeability are subjects of reservoir geology and log evaluation. These data are more or less uncertain and have to be treated as random variables.

Interpretation of even moderately large amounts of data requires statistical methods. A commonly used method is to gather individual data into groups or classes. This facilitates interpretation as well as numerical computations. Porosity data are used to demonstrate this ascertainment. An example of raw data is given in Table 2.2.

Table 2.2: Porosity Sample Data (n=24 values)

0.165	0.198	0.196	0.185	0.192	0.188
0.187	0.184	0.182	0.205	0.178	0.175
0.192	0.205	0.162	0.162	0.182	0.170
0.184	0.165	0.154	0.179	0.172	0.156
					$\Sigma x = 4.317$

Class boundaries, as given in Table 2.3, coincide in terms of the upper boundary of one class being the same as the lower boundary of the next class. Common convention is to take the values at the boundary into the higher class. The difference between upper and lower boundaries is referred to as the class interval. Normally but not necessarily, the class intervals are equal.

Average porosity can be calculated either from the data in Table 2.2 or in Table 2.3:

$$\bar{\phi} = \frac{\sum_{j=1}^{n} x_j}{n} = \frac{4.317}{24} = 0.1798 \qquad (2.6)$$

$$\overline{\phi}^{*} = \frac{\sum_{i=1}^{n} f_i x_i}{\sum f_i} = \frac{4.33}{24} = 0.1804 \tag{2.7}$$

It is evident that

$$\bar{\phi} = \lim_{n \to \infty} \overline{\phi}^{*} \tag{2.8}$$

Table 2.3: Frequency Distribution

Class Boundaries	Members	Frequency f_i	Class Mark x_i	$f_i.x_i$
0.15-0.16	0.156, 0.157	2	0.155	0.311
0.16-0.17	0.162, 0.162, 0.165, 0.165	4	0.165	0.660
0.17-0.18	0.170, 0.172, 0.175, 0.178, 0.179	5	0.175	0.875
0.18-0.19	0.181, 0.182, 0.182, 0.184, 0.185, 0.187	7	0.185	1.295
0.19-0.20	0.192, 0.192, 0.196, 0.198	4	0.195	0.780
0.20-0.21	0.205, 0.205	2	0.205	0.410
		24		4.330

Histograms and frequency polygons are used to show the probability density. Fig. 2.1 shows both of them for the porosity data included in the foregoing tables. The frequency polygon is drawn through the midpoints of the classes. The areas below the histogram and the frequency polygon are equal.

The cumulative frequency polygons are shown in Fig. 2.2. Based on this diagram, one can conclude that 60% of the samples have a porosity less than about 18.5%. Two important statistical properties of the data group are

the *variance*

$$\sigma^2 = \frac{\sum_{j=1}^{n} (x_j - \bar{x})^2}{n} \tag{2.9}$$

and the *standard deviation*

$$\sigma = \sqrt{\frac{\sum_{j=1}^{n} (x_j - \bar{x})^2}{n}} \tag{2.10}$$

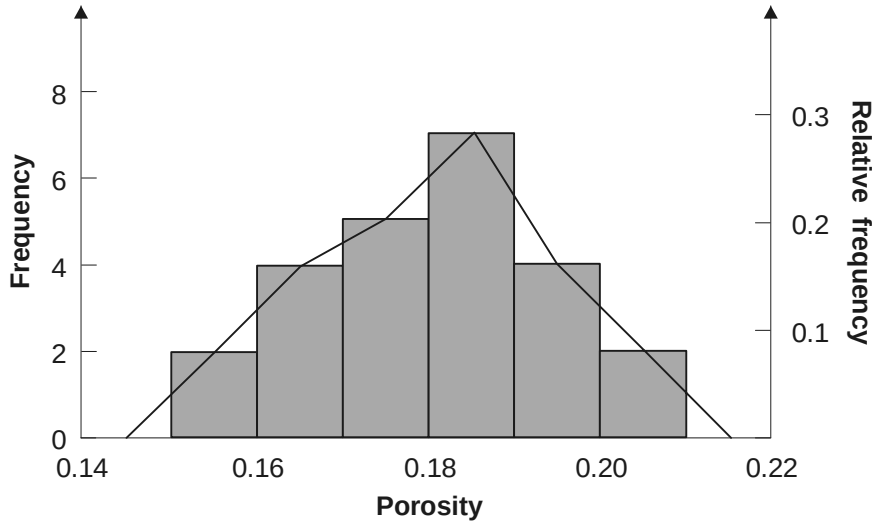

Figure 2.1: Histogram for porosity data (Table 2.3)

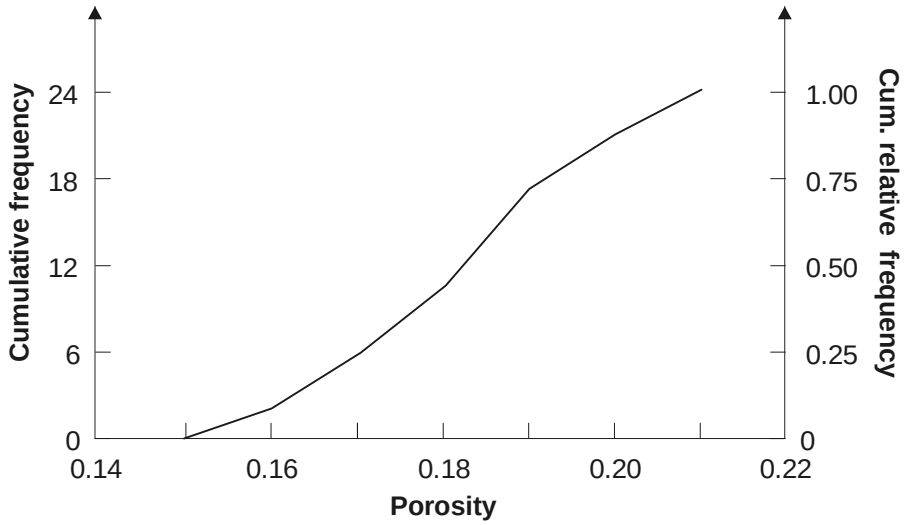

Figure 2.2: Cumulative frequency of porosity data (Table 2.3)

For the foregoing example, these are

$$\sigma^2 = \frac{\sum_{j=1}^{n} (\phi_j - \bar{\phi})^2}{n} = 0.0002; \quad \sigma = 0.014. \tag{2.11}$$

The local maximum of the probability density is called *the modus.* If the distribution is symmetrical, the modus is equal to the mean value.

2.3.1 Triangular Distribution

In the majority of practical cases, it is not possible to get a reliable histogram or frequency polygon. One has to be content with estimating the **upper**, the **lower** and the **modus**.

For the data given in Table 2.2 the following estimation would be possible:

$$\phi_{min} = 0.150,\ \phi_{max} = 0.210,\ \phi_{mod} = 0.185,\ \bar{\phi} = 0.180. \tag{2.12}$$

Fig. 2.3 illustrates the triangular distribution of this data. The height of the triangle is selected in a way so that the surface value becomes 1. The probability that the value (ϕ) will be less than the modes (ϕ_{mod}) is

$$p = \frac{\phi_{mod} - \phi_{min}}{\phi_{max} - \phi_{min}} \tag{2.13}$$

and 1 - p that it will be higher. The cumulative probability can be calculated as follows:

$$F = p\left(\frac{\phi - \phi_{min}}{\phi_{max} - \phi_{min}}\right)^2, \quad \phi_{min} \le \phi \le \phi_{mod}, \tag{2.14}$$

$$F = 1 - (1-p)\left(\frac{\phi_{max} - \phi}{\phi_{max} - \phi_{min}}\right)^2, \quad \phi_{mod} \le \phi \le \phi_{max}. \tag{2.15}$$

The variance is

$$\sigma = \frac{(\phi_{max} - \phi_{min})^2}{18}[1 - p(1-p)]. \tag{2.16}$$

Fig. 2.4 shows the F-function for the triangular probability distribution in Fig. 2.3. It is very similar to the diagram in Fig. 2.2. In fact, cumulative relative frequency and cumulative probability have the same meaning.

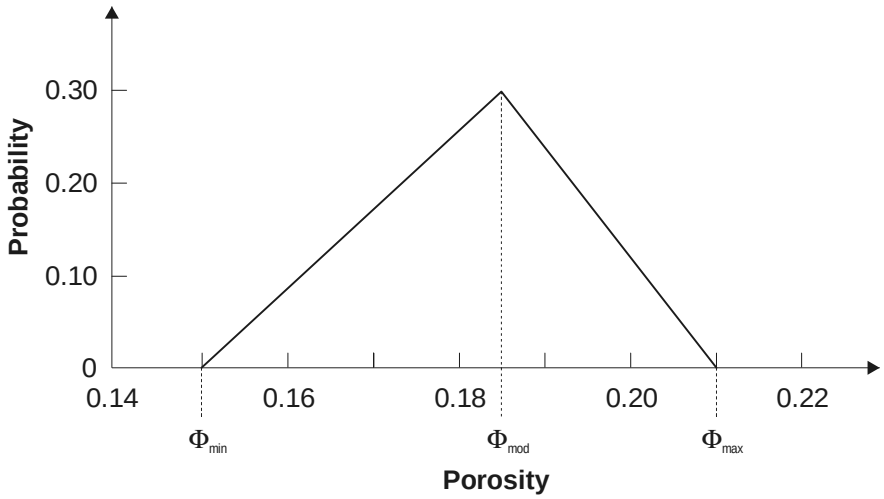

Figure 2.3: Triangular probability distribution

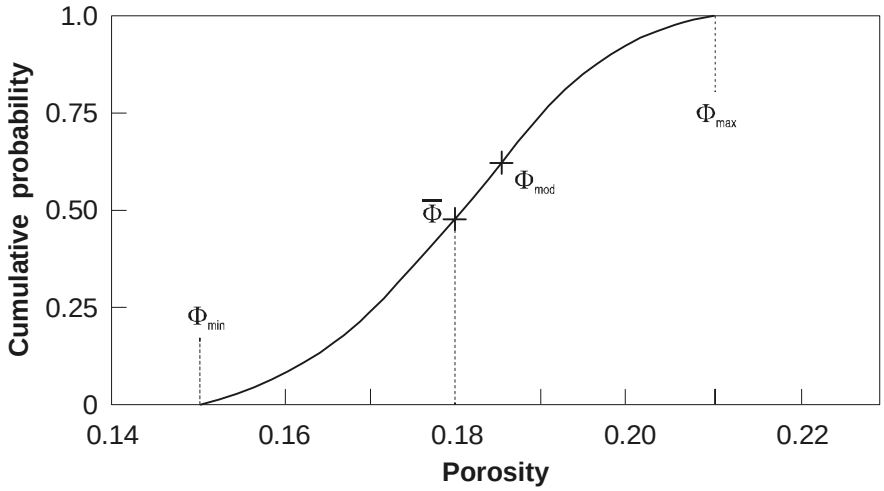

Figure 2.4: Cumulative probability calculated from Fig. 2.3

2.3.2 Uniform Distribution

An uniform distribution is illustrated in Fig. 2.5. The randomly occurring values are evenly distributed in the range from minimum to maximum values. The cumulative probability is defined by:

$$F = \int_{\phi_{min}}^{\phi_{max}} p(\phi)d\phi = \frac{\phi - \phi_{min}}{\phi_{max} - \phi_{min}}, \ \phi_{min} \le \phi \le \phi_{max}. \tag{2.17}$$

For $\phi = \phi_{min}$, F = 0 and for $\phi = \phi_{max,}$ F = 1.

The variance is

$$\sigma^2 = \frac{(\phi_{max} - \phi_{min})^2}{12}. \tag{2.18}$$

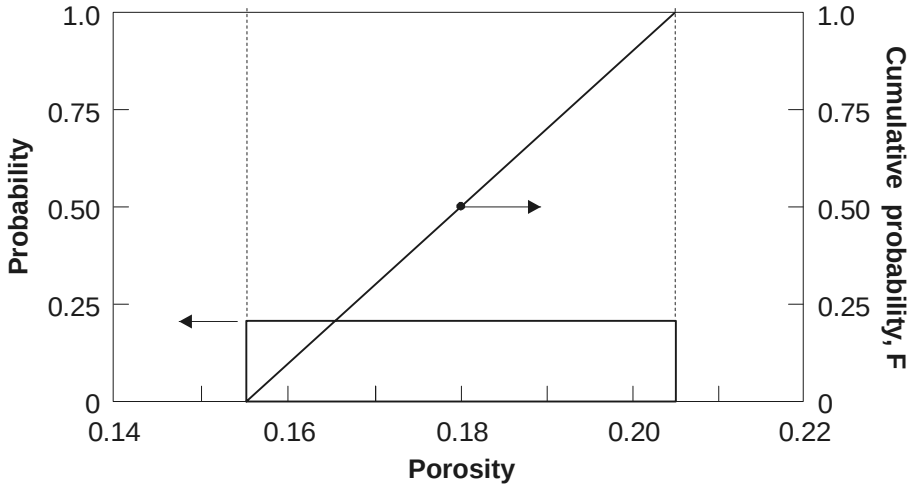

Figure 2.5: Uniform probability distribution

2.3.3 Dependent Distribution

Reservoir data applied for computation purposes of the reservoir are not independent. For example, the water saturation may be calculated from the ARCHIE[1.] formulas:

$$F = a\phi^{-m} \tag{2.19}$$

$$R_t = FR_w S_w^{-n} \tag{2.20}$$

thus

$$S_w = \left(\frac{aR_w}{R_t}\right)^{\frac{1}{n}} \phi^{-\frac{m}{n}} \tag{2.21}$$

where

R_w - the connate water resistivity Ωm [Ωft],
R_t - the formation resistivity Ωm [Ωft],
F - the formation factor,
a, m, n - positive constants.

It is evident, that S_w increases if ϕ decreases. Fig. 2.6 shows such a dependence for a triangular distribution of the connate water saturation.

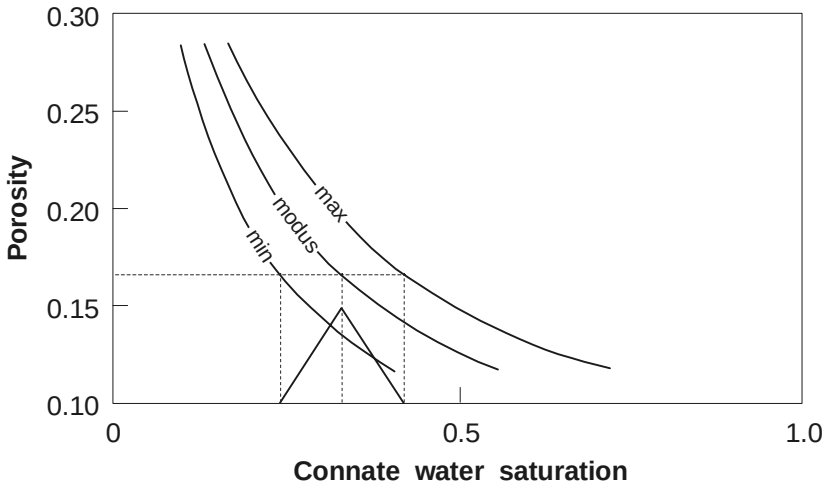

Figure 2.6: Use of dependent distribution

2.4 Monte Carlo Simulation Method

Calculate the following formula:

$$z = xy. \tag{2.22}$$

x and y are stochastic variables. Their cumulative probabilities between their minimum and maximum values are known. The task is to determine the probability distribution and the expected value of z.

The computation is simple, but less suitable for hand calculations than for the computer. For calculations it is necessary to use a random number generator.

Values entering into Eq. 2.22 are repeatedly selected by random numbers taken from an appropriate range of values, as it is shown in Fig. 2.7. Within several hundred to several thousand trials, the number of z values for prefixed classes are counted. The result is a histogram and the cumulative relative frequency for the z variable.

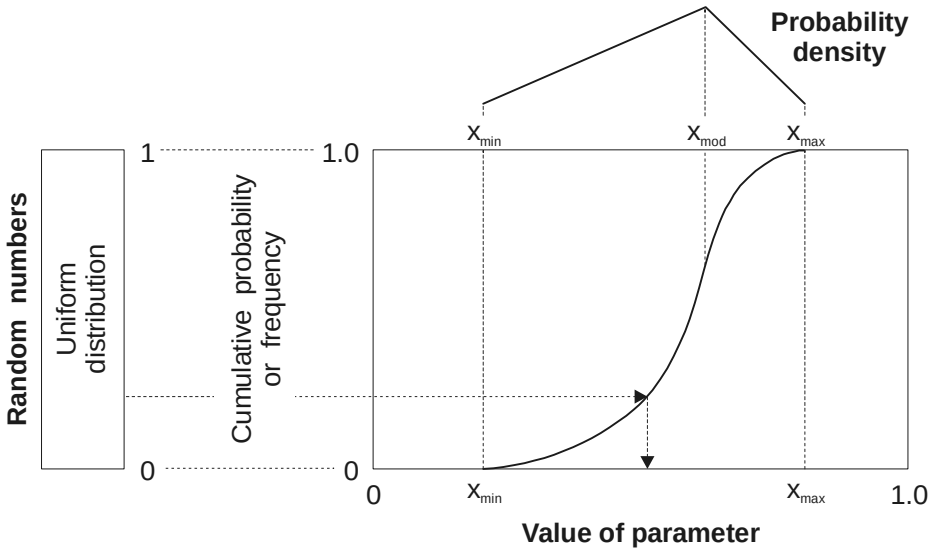

Figure 2.7: Selecting random values from a triangular distribution (after McCray, 1975)

Example 2.1

Calculating the porosity (ϕ) and water saturation (S_w) from well logs (after Walstrom *et al.*[39.](1967).

The calculation steps are as follows:

1. Determine ϕ from the relation:

   $$\rho_B = \rho_F\phi + \rho_{Ma}(1-\phi).$$

2. Use the value of ϕ to determine formation factor F from the Archie formula:

   $$F = a\phi^{-m}.$$

3. Use the value of F and randomly chosen values of other quantities to determine S_w from the relation

   $$R_t = FR_wS_w^{-n},$$

where

ρ_B - the bulk density kg m^{-3}[1b/cuft],
ρ_F - the fluid density kg m^{-3}[1b/cuft],
ρ_{Ma} - the rock matrix density kg m^{-3}[1b/cuft],
R_w - the connate water resistivity Ωm [Ωft],
R_t - the formation resistivity Ωm [Ωft],
F - the formation factor,
a, m, n - positive constants.

The range of parameter used in this example is given in Table 2.4. Uniform distribution was assumed for all quantities, except parameters a and ρ_F, which where assumed to be constants. The results of the simulation are shown in Fig. 2.8, Fig. 2.9 and Fig. 2.10, these reflect the results of several hundred cases, wherein each case was processed through steps 1, 2 and 3. Here it may be noted that although uniform distribution was assumed for quantities entering the calculations, the resulting probability densities are not symmetrical. The functional relationship of the quantities may skew the results.

Table 2.4: Ranges of Parameters Used in a Log-Interpretation Example (metric units)

	Parameter	Lower Limit	Upper Limit
R_t	True resistivity Ωm	19.000	21.000
R_w	Connate water resistivity Ωm	0.055	0.075
n	Exponent in the ARCHIE equation	1.800	2.200
a	Coefficient in the ARCHIE equation	0.620	0.620
m	Exponent in the ARCHIE equation	2.000	2.300
ρB	Bulk density kg/m^3	2.360	2.380
ρ_{MA}	Rock mineral density kg/m^3	2.580	2.630
ρ_F	Reservoir fluid density kg/m^3	0.900	0.900

Table 2.5: Ranges of Parameters Used in a Log-Interpretation Example (field units)

	Parameter	Lower Limit	Upper Limit
R_t	True resistivity Ωft	62.300	68.900
R_w	Connate water resistivity Ωft	0.180	0.246
n	Exponent in the ARCHIE equation	1.800	2.200
a	Coefficient in the ARCHIE equation	0.620	0.620
m	Exponent in the ARCHIE equation	2.000	2.300
ρB	Bulk density *lb/cu ft*	147.300	148.600
ρ_{MA}	Rock mineral density *lb/cu ft*	161.000	164.200
ρ_F	Reservoir fluid density *lb/cu ft*	56.200	56.200

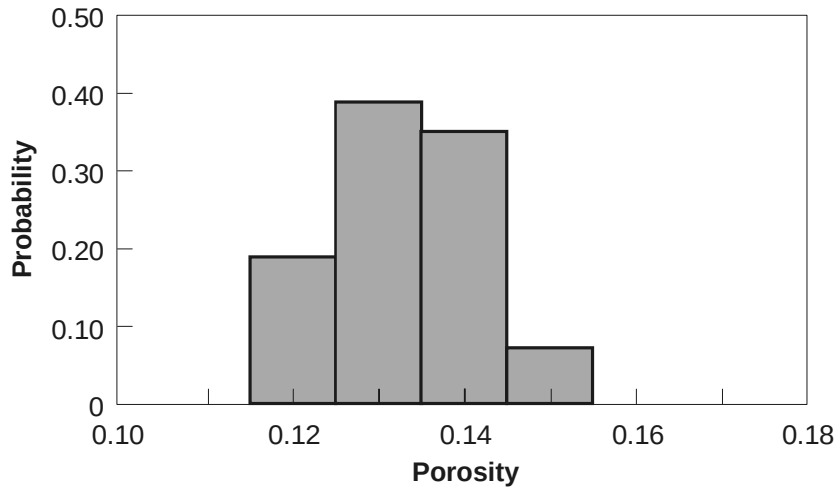

Figure 2.8: Calculated porosity (after Walstrom *et al*. 1967)

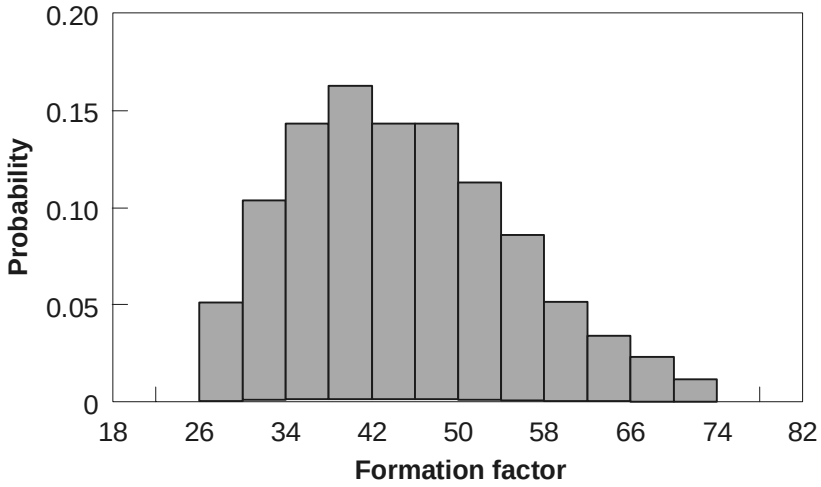

Figure 2.9: Formation factor (after Walstrom *et al*. 1967)

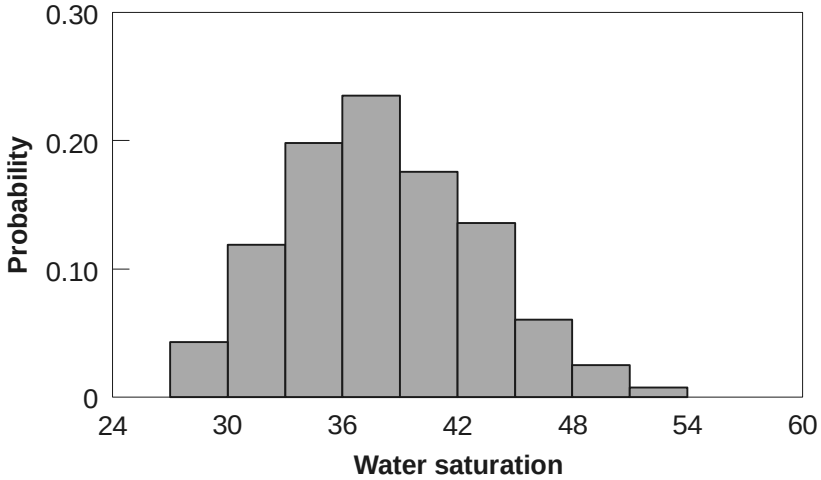

Figure 2.10: Calculated water saturation (after Walstrom *et al*. 1967)

Example 2.2

Calculation of oil recovery

The ultimate recovery was estimated by combination of the Eq. 2.1 and Eq. 2.5:

$$N_{pmax} = NE_R = 0.54898V\left(\frac{\phi(1-S_w)}{B_{oi}}\right)^{1.04222}\left(\frac{k\mu_{wi}}{\mu_{oi}}\right)^{0.077} S_w^{-0.1903}\left(\frac{p_i}{p_a}\right)^{-0.2159} \quad (2.23)$$

Symmetric triangular distribution was assumed for all the quantities in Eq. 2.23, except the parameter μ_{wi} which is constant 0.7 cP. The limits are shown in Table 2.6 and Table 2.7.

The ultimate recovery from this reservoir can be characterized with the following figures

of a Monte Carlo simulation with 5000 trials.

Expected ultimate recovery:	16,540,000 m^3	or	104.03 *MMbbl*
with standard deviation of:	1,100,000 m^3	or	6.91 *MMbbl*

Probability distribution:

with	more than	but	less than
99%	13.82	-	$19.24.10^3 m^3$ [86.9 - 121.0 MMbbl]
90%	14.70	-	$18.38.10^6 m^3$ [92.4 - 115.6 MMbbl]
80%	15.08	-	$18.00.10^6 m^3$ [94.8 - 113.2 MMbbl]

Taking for all parameters the most unfavorably and the most favorably the following realistically figures can be calculated:

Worst case:	Best case:
$12.227x10^6$ m^3	$21.726x10^6$ m^3
(76.9x106 bbl)	(136.6x106bbl)

Table 2.6: Range of Parameters Used in the Ultimate Recovery Calculation Example (metric units)

	Parameter	Unit	Lower Limit	Upper Limit
V	Reservoir volume	$10^6 m^3$	285.000	370.00
ϕ	Porosity		0.165	0.19
S_w	Initial water saturation		0.220	0.28
B_{oi}	Formations volume factor		1.480	1.50
μ_{oi}	Reservoir oil viscosity	cP	2.850	2.95
k	Reservoir permeability	darcy	0.800	1.50
p_i	Initial pressure ($p_i = p_b$)	MPa	22.000	22.50
p_a	Abandonment pressure	MPa	18.000	20.00

Table 2.7: Range of Parameters Used in the Ultimate Recovery Calculation Example (field units)

	Parameter	Unit	Lower Limit	Upper Limit
V	Reservoir volume	$10^5 ac\ ft$	2.310	3.000
ϕ	Porosity		0.165	0.190
S_w	Initial water saturation		0.220	0.280
B_{oi}	Formations volume factor		1.480	1.500
μ_{oi}	Reservoir oil viscosity	cP	2.850	2.950
k	Reservoir permeability	mD	800.000	1.500
p_i	Initial pressure ($p_i = p_b$)	psi	3.190	3.262
p_a	Abandonment pressure	psi	2.610	2.900

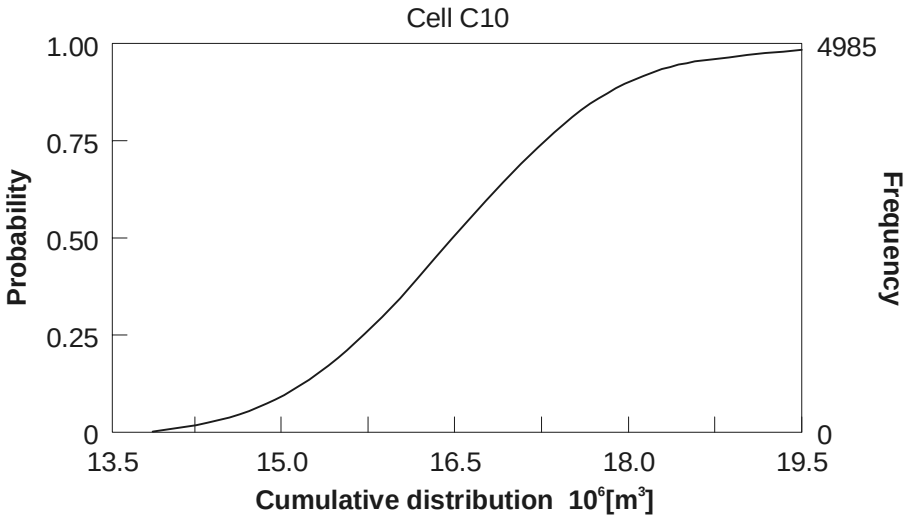

Figure 2.11: Ultimate recovery calculation with Monte Carlo simulation

Chapter 3

Material Balance

3.1 Tarner's Formulation

Fig. 3.1 shows a schematic illustration of an oil reservoir. The rock volume is V and the porosity ϕ. Apart from a certain saturation of connate water S_{wi}, the rock is saturated with hydrocarbons. Thus, the effective reservoir volume is

$$V\phi(1 - S_{wi}) = V_P(1 - S_{wi}) . \tag{3.1}$$

The reservoir temperature is defined as T, the initial pressure as p_i. The virgin reservoir is in a state of hydrostatic and thermodynamic equilibrium.

The original oil in place is defined as N in sm^3 or stb (stock tank barrels). At reservoir conditions gas is dissolved in the oil. The amount is expessed by the initial solution GOR (gas-oil ratio) R_{si} sm^3/sm^3 or scft/stb.

The formation volume of the oil is NB_{oi}. If the reservoir contains the same or a greater amount of gas than soluble at reservoir conditions (pressure and temperature), the reservoir is saturated and the surplus gas forms a gas cap. Otherwise, the reservoir is undersaturated.

Should the gas cap contain an amount of G sm^3 or scft gas, then its formation volume will be GB_{gi}. Usually the volume of the gas cap is expressed in relation to the oil volume:

$$GB_{gi} = mNB_{oi} . \tag{3.2}$$

When regarding surface and formation volumes the following relations can be set up:

Fluid	Surface	Formation
Oil	N sm^3[stb]	NB_{oi} m^3[bbl]
Dissolved Gas	NR_{si} sm^3[scft]	--
Free Gas	G_F sm^3[scft]	$G_F B_{gi} = mN\ B_{oi}$ m^3[cuft]

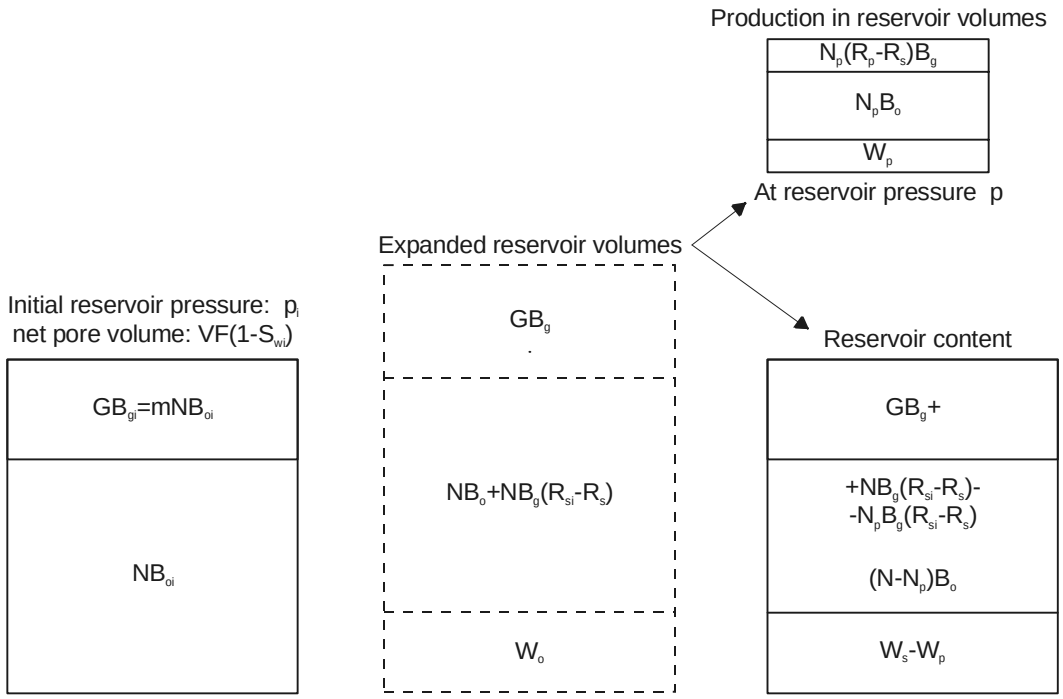

Figure 3.1: The scheme of the material balance of an oil reservoir

The effective pore volume, expressed by the amounts of oil and gas, is:

$$NB_{oi} + GB_{gi} = V_P(1 - S_{wi})\,. \tag{3.3}$$

After a certain time period, an amount of

Oil	N_p	sm^3 [stb],
Gas	$G_p=N_pR_p$	sm^3 [scft],
Water	W_p	sm^3 [bbl]

will have been produced. R_p is the cumulative production GOR. As a consequence of production, the reservoir pressure decreases from p_i to p.

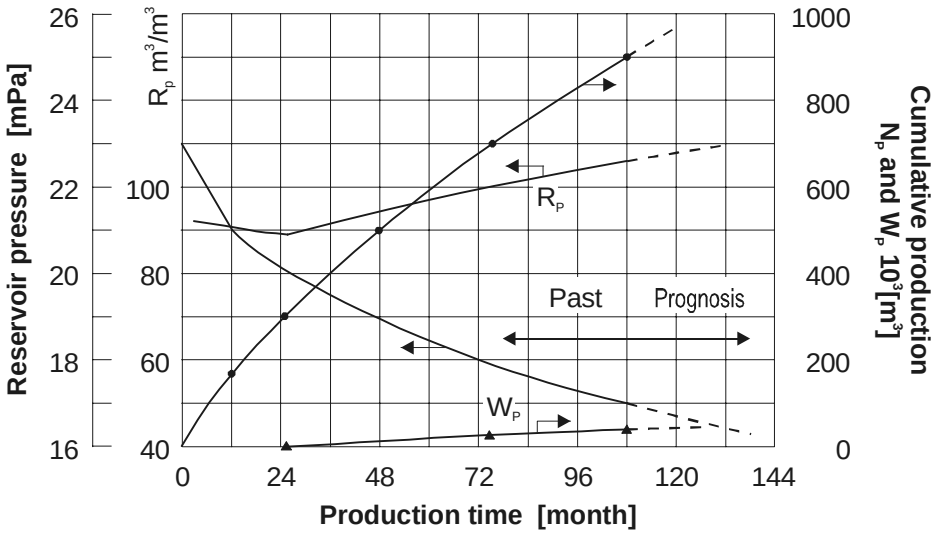

Figure 3.2: Pressure drop and production of a reservoir

Let us now consider the reverse situation. At first pressure drops to p. Thus, the gas cap expands and gas evolves from the oil. From the aquifer an amount of W_e water will flow into the reservoir. The expanded system would have a reservoir volume at pressure p of

$$NB_o + mNB_{oi}\frac{B_g}{B_{gi}} + NB_g(R_{si} - R_s) + W_e\,. \tag{3.4}$$

At the same pressure the produced fluids would have a total reservoir volume of

$$N_pB_o + N_pB_g(R_p - R_s) + W_p \;=\; N_p[B_o + B_g(R_p - R_s)] + W_p\,. \tag{3.5}$$

The effective pore volume corresponding to Eq. 3.1 remains unchanged which consequently makes the following assertion valid:

[expanded volume] - [initial volume] = [produced volume]

or

Eq. 3.4 - Eq. 3.3 = Eq. 3.5

After substituting:

$$N(B_o - B_{oi}) + N\left[mB_{oi}\left(\frac{B_g}{B_{gi}} - 1\right) + B_g(R_{si} - R_s)\right] + W_e \tag{3.6}$$

$$= N_p[B_o + B_g(R_p - R_s)] + W_p$$

From this

$$N = \frac{N_p[B_o + B_g(R_p - R_s)] - (W_e - W_p)}{mB_{oi}\left(\frac{B_g}{B_{gi}} - 1\right) + B_g(R_{si} - R_s) - (B_{oi} - B_o)}. \tag{3.7}$$

This is the formula of **TARNER's**[37.] material balance. If in addition to production, water is injected at the cumulative amount of W_I and/or gas at the cumulative amount of G_pI, then the term ($W_I + G_pIB_g$) has to be added to the numerator. I indicates how much of the produced gas was reinjected into the reservoir.

Every specific term in Eq. 3.7 has a certain meaning:

$$N = \frac{\overbrace{N_p\left[B_o + B_g(R_p - R_s)\right]}^{\text{produced hydrocarbons}} - \overbrace{(W_e + W_I - W_p)}^{\text{net water influx}} - \overbrace{G_I B_g}^{\text{injected gas}}}{\underbrace{mB_{oi}\left(\frac{B_g}{B_{gi}}\right)}_{\text{gas cap expansion}} + \underbrace{B_g(R_{si} - R_s)}_{\text{desoluted gas expansion}} - \underbrace{(B_{oi} - B_o)}_{\text{reservoir oil shrinkage}}} \tag{3.8}$$

Reservoir volume of

Eq. 3.6 is then divided by B_g

(3.9)

Eq. 3.9 is divided by its right hand side:

$$\frac{N\left[\left(\frac{B_o}{B_g}-R_s\right)-\left(\frac{B_{oi}}{B_g}-R_{si}\right)\right]+mNB_{oi}\left(\frac{1}{B_{gi}}-\frac{1}{B_g}\right)+\frac{1}{B_g}(W_e-W_p)}{N_p\left(\frac{B_o}{B_g}-R_s\right)+N_pR_p}=1 \qquad (3.10)$$

3.2 Drive Indices

Splitting up the left side of Eq. 3.10 leaves three fractions which describe the shares of the specific drive mechanisms in reference to the whole cumulative production effected by

- the solution gas drive,
- the gas drive and
- the water drive.

These are considered the drive indices. The *solution gas drive index* (a two phase expansion of the oil) is defined as

$$I_s=\frac{N\left[\left(\frac{B_o}{B_g}-R_s\right)-\left(\frac{B_{oi}}{B_g}-R_{si}\right)\right]}{N_p\left(\frac{B_o}{B_g}-R_s\right)+N_pR_p}. \qquad (3.11)$$

The *gas drive index* (expansion of the gas cap) is defined as

$$I_g=\frac{mNB_{oi}\left(\frac{1}{B_{gi}}-\frac{1}{B_g}\right)}{N_p\left(\frac{B_o}{B_g}-R_s\right)+N_pR_p}. \qquad (3.12)$$

The *water drive index* (expansion of the aquifer) is defined as

$$I_w=\frac{\frac{1}{B_g}(W_e-W_p)}{N_p\left(\frac{B_o}{B_g}-R_s\right)+N_pR_p}. \qquad (3.13)$$

The relation between the indices is given by

$$I_s + I_g + I_w = 1 . \tag{3.14}$$

Cumulative oil-, gas- and water production (N_p, R_p, W_p) are given by production statistics. The PVT-properties (B_o,B_g,R_s) are determined by laboratory measurement or by correlations. The volumetric reserve calculation covers the petroleum in place (N, G). The average reservoir pressure is recorded by regular measurements of static well bottom-hole pressures. The application of these data enables a sufficient description of the water influx as a function of time.

3.3 Water Influx

Operating a reservoir over years, the cumulative oil, gas and water production $N_p(t)$, $G_p(t)$, and $W_p(t)$ are naturally known. The reservoir pressure declines and the actual values $p(t)$ will be determined by regulare pressure surveys. The fluid properties, as $B_o(p)$, $B_g(p)$ and $R_s(p)$, are messured in PVT Labs or determined from different types of charts, e.g.: from Standing correlation. Also the OOIP (N) and the gas cap factor m can be estimated by volumetric calculation (see Chapter 3.).

The only quantity in Eq. 3.6, which is entierly unknown, is the water influx $W_e(t)$. The Material Balance calculation is the only method which enables to determine it as function of time. From Eq. 3.6:

$$W_e(t) = N_p[B_o + B_g(R_p - R_s)] \tag{3.15}$$

$$-N\left[B_o - B_{oi} + mB_{oi}\left(\frac{B_g}{B_{gi}} - 1\right) + B_g(R_{si} - R_s)\right] + W_p$$

The aquifer is a water bearing formation, hydrodynamically connected to the hydrocarbon reservoir. Its form, size and permeability can vary greatly. Hydrological reflection could help to set up hypotheses. However, these can never be verified in detail since no wells will be drilled to explore an aquifer.

One of the boundaries of the aquifer is the water-oil-contact (WOC). This interior boundary is usually well known, whereas the exterior boundary is an object of speculation.

The exterior boundary can be considered closed if the whole amount of water flowing into the reservoir is due to the expansion of the aquifer. In this case, the aquifer is finite closed. Faults and layer pinch outs form such boundaries.

The aquifer can be considered a finite open one, if the pressure at the exterior boundary is constant. A connection to the atmosphere through outcropping or hydrodynamic contact to a karstic formation are the possibilities to form such boundaries. Fig. 3.4 shows a schematic illustration of an aquifer.

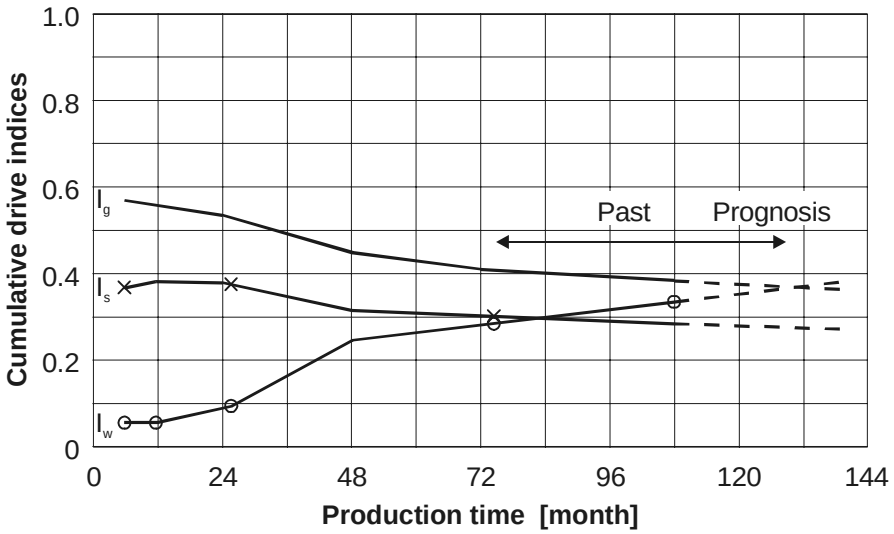

Figure 3.3: Cumulative drive indices

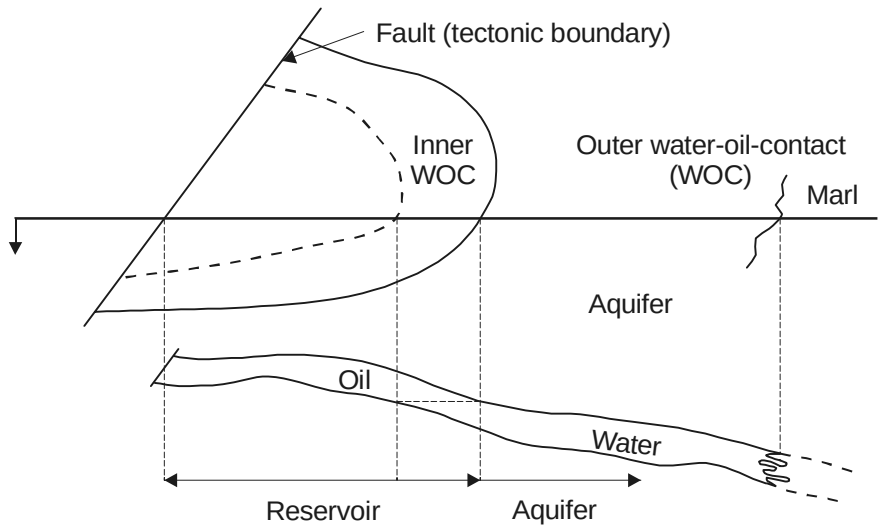

Figure 3.4: Oil reservoir with an aquifer

The cumulative water influx is calculated from the rate:

$$W_e(t) = \int_o^t q(t)dt. \tag{3.16}$$

Production induces pressure decline at the interior boundary of the aquifer. Let us make a theoretical consideration. We assume a unique and sudden pressure drop $\Delta p = p_i - p$ at this

boundary, where p_i is the initial reservoir pressure. The pressure drop will cause water intrusion into the reservoir. Initially, this is a consequence of the expansion of water and rock and it is independent of the distance to the exterior boundary and regardless of whether the boundary is closed or not. The depression zone stretches with time - either fast or slowly, dependent on permeability - whereby the water influx rate permanently decreases. This situation is given until the depression radius reaches the exterior boundary. We call this time interval as transient period.

In case of a closed exterior boundary, water influx decreases rapidly and tends to zero, if the pressure in the whole aquifer has dropped by Δp. In this case, the function of the cumulative water influx $W_e(t)$ has an asymptotic value (see Fig. 3.5).

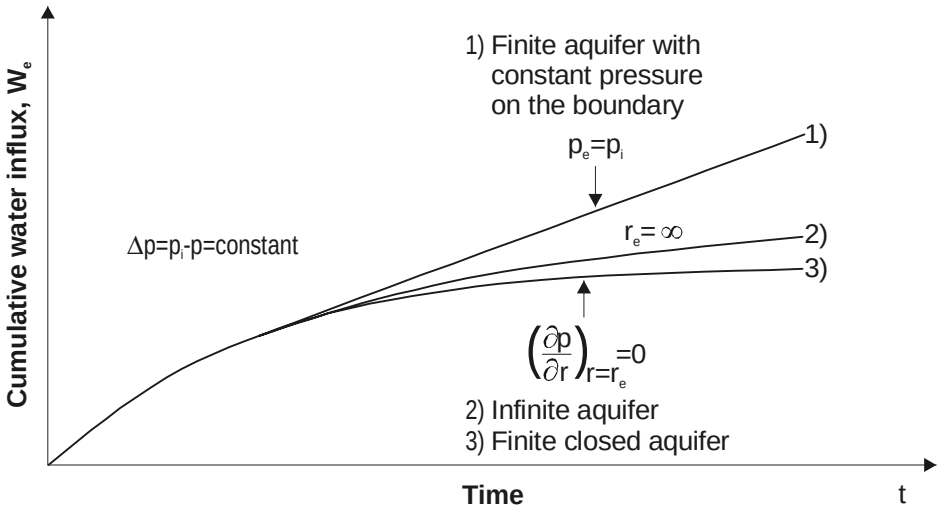

Figure 3.5: Cumulative water influx at a constant reservoir pressure

If there is an aquifer with constant pressure at the exterior boundary, a stabilization of the influx rate takes place and therefore the function $W_e(t)$ becomes linear with increasing time.

If the aquifer is small or the permeability high, the transient period becomes short and can be neglected. Under this consideration we distinguish between three types of aquifer models or water influxes:

1. Semi-steady-state,
2. Steady-state,
3. Non-steady-state:
    3.1. Transient
    3.2. Pseudo-steady-state.

3.3.1 Semi-Steady-State Water Influx

Sometimes the cumulative water influx can be considered solely as a function of the

pressure drop. That means, the time in which the pressure change took place has no influence on the intruded water amount, consequently Eq. 3.16 becomes:

$$W_e = C_1[p_i - p(t)]\,. \tag{3.17}$$

In such a case the aquifer has always a limited size and a closed external boundary. The coefficient C_1 can be expressed by the parameters of the aquifer:

$$C_1 = Ah\phi c_e \tag{3.18}$$

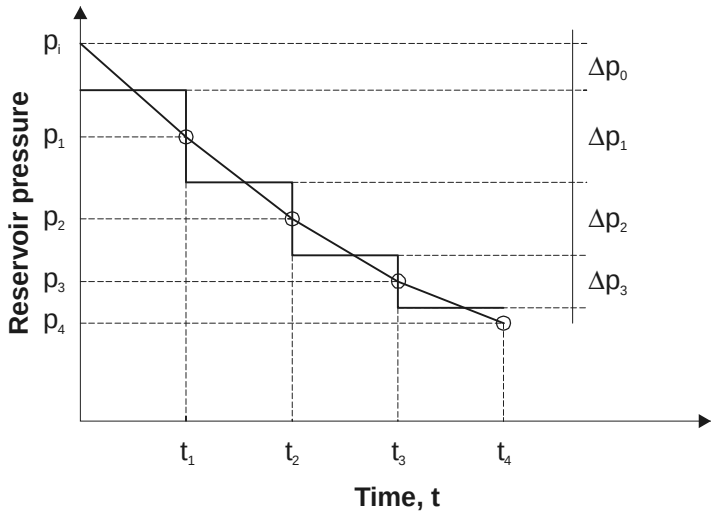

Figure 3.6: Change in reservoir pressure

3.3.2 Steady-State Water Influx

In case of a constant pressure at the exterior boundary and high aquifer permeability the transient period can be neglected. This is equivalent to the assumption of incompressible water inside the aquifer. Thus the water influx rate is proportional to the pressure difference between the two boundaries:

$$q(t) = C_2[p_i - p(t)] \tag{3.19}$$

The cumulative water influx is calculated by integration:

$$W_e(t) = C_2\int_o^t [p_i - p(t)]\,dt \tag{3.20}$$

This is the **SCHILTHUIS**[35.]-formula (1936). The coefficient C_2 is calculated by **DARCY'**s law with the help of the specific aquifer parameters. In the case of linear

aquifers (Fig. 3.7)

$$C_{2L} = \frac{bhk}{\mu L}, \tag{3.21}$$

where

- b - width of the aquifer,
- h - thickness of the aquifer,
- L - length of the aquifer,
- k - permeability of the aquifer,
- μ - viscosity of the water.

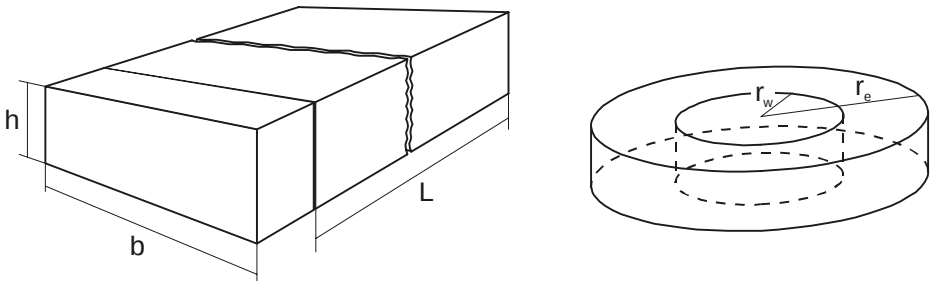

Figure 3.7: Idealized aquifers

In the case of radialsymmetric aquifers (Fig. 3.7 B), the coefficient is:

$$C_{2r} = \frac{2\pi hk}{\mu \ln \frac{r_e}{r_w}}, \tag{3.22}$$

where replace 2π by 7.08×10^{-3} for field units to get [bbl/psi d]. There are

- r_w - inner radius,
- r_e - outer radius of the aquifer.

The pressure $p(t)$ in Eq. 3.20 is the pressure at the inner boundary. In most of the practical cases it will be replaced by the average reservoir pressure, given for discrete time points: $t_0 = 0, t_1, t_2, ..., t_n$. Although this pressure can be plotted with a smooth continuous line, it is more practical to approximate it with a step function or with linear functions as shown in Fig. 3.6. For Eq. 3.20 both approximations give the same results.

$$W_e(t) = C_2 \sum_{j=1}^{n} \int_{t_{j-1}}^{t_j} [p_i - p(t)]dt \qquad (3.23)$$

$$= C_2 \sum_{j=1}^{n} \left[p_i - \frac{p_j + p_{j-1}}{2} \right] (t_j - t_{j-1})$$

$$= C_2 \sum_{j=1} (p_i - \bar{p}_j)(t_j - t_{j-1})$$

3.3.3 Non-Steady-State Water Influx

Usually the water influx has non-steady-state character. We distinquish between transient and pseudo-steady state flow regime. Note that both are non-steady state flow.

The theoretical funded and general applicable method, covering transient, pseudo-steady-state and steady-state flow as well, was published by van Everdingen and Hurst[16.](1949). The method was slighly modified by Vogt and Wang[41.](1988), making it more convenient for computer programming. The derivation was discussed in the Volume 1 of this Textbook series (Heinemann, Z.E.: "Fluid Flow in Porous Media", Chapter 3). We use the Vogt-Wang formulation as our standard method.

Under pseudo steady state conditions the water influx results from the uniform expansion of the aquifer, which means that the rate of pressure change is equal in the whole aquifer domain.

3.3.3.1 Vogt-Wang Aquifer Model

It was assumed that the reservoir area can be approximated by a segment of a circle. The radius is

$$r_w = \left(\frac{2A}{\omega} \right)^{1/2}, \qquad (3.24)$$

where ω is the arc in radian (= 2π for complete circle) and r_e is the outer radius of the aquifer.

The dimensionless outer radius is

$$r_{eD} = \frac{r_e}{r_w}. \qquad (3.25)$$

The dimensionless time is

$$t_D = \frac{k}{\phi\mu_w c_e r_w^2} t = \alpha t \qquad \text{(x 0.00634 for field units, } t \text{ in days).} \tag{3.26}$$

The cumulative water influx at the time t_{Dj} is

$$W_{ej} = C_3 \left\{ \frac{p_o - p_1}{t_{D1}} \tilde{Q}(t_{Dj}) + \left(\frac{p_1 - p_2}{t_{D2} - t_{D1}} - \frac{p_o - p_1}{t_{D1}} \right) \tilde{Q}(t_{Dj} - t_{D1}) \ldots \right. \tag{3.27}$$
$$\left. + \left(\frac{p_{j-1} - p_j}{t_{Dj} - t_{Dj-1}} - \frac{p_{j-2} - p_{j-1}}{t_{Dj-1} - t_{Dj-2}} \right) \tilde{Q}(t_{Dj} - t_{Dj-1}) \right\}$$

The $\tilde{Q}(t_D)$ functions are given in Table 3.1 only for an infinite acting radial aquifer. In case of finite aquifers we refer to the paper of VOGT and WANG[41.](1988).

In radial symmetrical homogeneous case the coefficient C_3 can be calculated as

$$C_3^{id} = \omega\phi h c_e r_w^2 \qquad \text{(x 0.1781 for } bbl/psi\text{).} \tag{3.28}$$

Example 3.2 - Example 3.4 demonstrate how the coefficients C_1-C_3 and the function $W_e(t)$ are calculated.

Usually the aquifer parameters are unknown. It is possible however (as shown in Example 3.1) to determine the water influx of the past with help of the material balance equation. First it is essential to ascertain the semi-steady-state, steady state or non-steady-state character of the water influx.

Example 3.1 is continued by Example 3.5. If either C_1 nor C_2 is a constant but the coefficient C_1 calculated at various times increase steadily whereas C_2 continuously decreases, coefficient C_3 can be determined with sufficient accuracy. The dispersion of the C_3-values indicates how appropriate r_{eD} and α were chosen. If α is too small, the function

$$W_e = f\left[\sum \Delta \left(\frac{\Delta p}{\Delta t_D} \right) \tilde{Q} \right] \tag{3.29}$$

is not linear, but has an upward curvature. If α is too big, the curvature is directed downwards. Only numerous repetitions of the calculation using various values of r_{eD} provide a favorable solution.

Table 3.1: Dimensionless Functions for an Infinite Radial Aquifer
($Q(t_D)$ after van EVERDINGEN and HURST, 1949)
($\tilde{Q}(t_D)$ after VOGT and WANG, 1988

t_D	$Q(t_D)$	t_D	$\tilde{Q}(t_D)$
0.1000E-01	0.1120000E+00	0.1000E-01	0.75225280E-03
0.2500E-01	0.1742500E+00	0.1780E-01	0.18364557E-02
0.5000E-01	0.2780000E+00	0.3160E-01	0.44321290E-02
0.7500E-01	0.3410000E+00	0.5620E-01	0.10722197E-01
0.1000E+00	0.4040000E+00	0.1000E+00	0.26043625E-01
0.2500E+00	0.6890000E+00	0.1780E+00	0.63654354E-01
0.5000E+00	0.1020000E+01	0.3160E+00	0.15612493E+00
0.7500E+00	0.2610000E+01	0.5620E+00	0.38757698E+00
0.1000E+01	0.1569000E+01	0.1000E+01	0.97310597E+00
0.2500E+01	0.5649000E+01	0.1780E+01	0.24730688E+01
0.5000E+01	0.4539000E+01	0.3160E+01	0.63361924E+01
0.7500E+01	0.6028500E+01	0.5620E+01	0.16497206E+02
0.1000E+02	0.7411000E+01	0.1000E+02	0.43576673E+02
0.2500E+02	0.1457300E+02	0.1780E+02	0.11676082E+03
0.5000E+02	0.2485500E+02	0.3160E+02	0.31559709E+03
0.7500E+02	0.3424700E+02	0.5620E+02	0.86662947E+03
0.1000E+03	0.4312900E+02	0.1000E+03	0.24102943E+04
0.2500E+03	0.9108400E+02	0.1780E+03	0.67814908E+04
0.5000E+03	0.1626980E+03	0.3160E+03	0.19176731E+05
0.7500E+03	0.2295150E+03	0.5620E+03	0.54886840E+05
0.1000E+04	0.2935140E+03	0.1000E+04	0.15847778E+06
0.2500E+04	0.6487810E+03	0.1780E+04	0.46108726E+06
0.5000E+04	0.1192198E+04	0.3160E+04	0.13431358E+07
0.7500E+04	0.1706688E+04	0.5620E+04	0.39470205E+07
0.1000E+05	0.2203861E+04	0.1000E+05	0.11665744E+08
0.2500E+05	0.5005726E+04	0.1780E+05	0.34650488E+08
0.5000E+05	0.9363099E+04	0.3160E+05	0.10279585E+09
0.7500E+05	0.1353145E+05	0.5620E+05	0.30704301E+09
0.1000E+06	0.1758628E+05	0.1000E+06	0.92078873E+09
0.2500E+06	0.4066000E+05	0.1780E+06	0.27708710E+10
0.5000E+06	0.7699000E+05	0.3160E+06	0.83166975E+10
0.7500E+06	0.1120000E+06	0.5620E+06	0.25105398E+11
0.1000E+07	0.1462000E+06	0.1000E+07	0.76014114E+11
0.2500E+07	0.3427000E+06	0.1780E+07	0.23075497E+12
0.5000E+07	0.6544000E+06	0.3160E+07	0.69814848E+12
0.7500E+07	0.9562500E+06	0.5620E+07	0.21230343E+13
0.1000E+08	0.1252000E+07	0.1000E+08	0.64719162E+13
0.2500E+08	0.2961000E+07	0.1780E+08	0.19772497E+14
0.5000E+08	0.5689000E+07	0.3160E+08	0.60187517E+14
0.7500E+08	0.8341000E+07	0.5620E+08	0.18414932E+15
0.1000E+09	0.1095000E+08	0.1000E+09	0.56428423E+15

The VAN EVERDINGEN-HURST solution requires the calculation of the sum at every time t_D for every j. This is for limited aquifers not necessary if the early transient period is over.

3.3.3.2 Fetkovich Aquifer Model

Fetkovich[17.] presented a simplified approach for such cases that utilizes the pseudo-steady-state aquifer productivity index and an aquifer material balance to represent a finite compressibility system.

Assuming that the flow obeys DARCY's law and is at pseudo-steady-state or steady-state, the generalized rate equation for an aquifer without regarding the geometry can be written:

$$q_w = J_w(\bar{p} - p_{wf}). \tag{3.30}$$

J_w is defined as the productivity index of the aquifer. p_{wf} is the pressure at the inner radius and $\bar{p}$ is the average aquifer pressure. The later value can be calculated from a material balance for a constant compressibility:

$$\bar{p} = -\frac{W_e}{c_e W} + p_i, \tag{3.31}$$

where W is the water content and $c_e = c_w + c_\phi$ the total compressibility of the aquifer. The maximum encroachable water at $\bar{p} = 0$ is:

$$W_{ei} = c_e W p_i \tag{3.32}$$

After substituting Eq. 3.32 into Eq. 3.31:

$$\bar{p} = -\frac{p_i}{W_{ei}} W_e + p_i \tag{3.33}$$

The calculation is reduced to the following steps:

- For a time interval $\Delta_{j+1}t = t_{j+1} - t_j$ the constant influx rate would be:

$$q_w = J_w(\bar{p}_j - \bar{p}_{wfj+1}), \tag{3.34}$$

where $\bar{p}_j$ is the average aquifer pressure for the time t_j and $\bar{p}_{wfj+1}$ is the average inner boundary pressure during the period $\Delta_{j+1}t$.

- The total efflux during the timer interval $\Delta_{j+1}t$ would be

$$\Delta W_{ej+1} = W_{ej+1} - W_{ej} = q_w \Delta_{j+1} t \tag{3.35}$$

- The cumulative efflux to the time $\Delta_{j+1}t$ would be:

$$W_{ej+1} = W_{ej} + \Delta W_{ej+1} = \sum_{n+1}^{j+1} \Delta W_{en} \tag{3.36}$$

- The aquifer average pressure for the next time interval:

$$\bar{p}_{j+1} = -\frac{p_i}{W_{ei}} W_{ej+1} + p_i \tag{3.37}$$

The efflux of the aquifer is naturally the water influx for the reservoir.

The VAN EVERDINGEN-HURST[16.] method in the original form and in the modified form by VOGT and WANG[41.] as well uses three parameters: C_3, α and r_{eD}. The first two are numerical constants, the third relates to the mathematical assumption of a radial symmetrical aquifer.

The Fetkovich[17.] method uses only two parameters (J_w and W_{ei}) and no relation was made to any geometrical form. In spite of that J_w and W_{ei} can be calculated for the radial symmetric case easily as described in the volume "*Fluid Flow in Porous Media*":

$$J_w = \frac{2\pi hkf}{\mu\left(\ln\frac{r_e}{r_w} - \frac{3}{4}\right)} \tag{3.38}$$

$$W_{ei} = f\pi(r_e^{\,2} - r^2{}_w)hc_e p_i \tag{3.39}$$

where f=1 if the circle is in full size. For field units replace 2π by 7.08×10^{-3} in Eq. 3.38 to get [bbl/psi d]. There Eq. 3.34 - Eq. 3.37 give the exact solution of the time step go to zero. For practical cases a time step of some months gives results accurate enough.

Example 3.1

An oil reservoir contains $N = 3.6 \times 10^6 m^3$[$2.264 \times 10^7 bbl$] oil. The ratio of the gas-/oil-pore volume is m = 0.3. The change of the reservoir pressure and the cumulative productions are given in columns (1)-(5) in Table 3.4 and Table 3.5. Columns (6)-(8) tabulate the values for B_g, B_o and R_s at the corresponding reservoir pressure. The task is to calculate water influx.

Solution

From Eq. 3.6:

$$W_e = N_p[B_o + B_g(R_p - R_s)]$$

$$-N\left[B_o - B_{oi} + mB_{oi}\left(\frac{B_g}{B_{gi}} - 1\right) + B_g(R_{si} - R_s)\right] + W_p$$

The routine of the calculation procedure can be set up as follows (the numbers indicate the column numbers):

$$(9) = (3) \times [(6) + (7) \times ((4) - (8))] - N$$
$$\times [(6) - B_{oi} + mB_{oi}((7)/B_{gi} - 1) + 7 \times (R_{si} - (8))] + (5)$$

The results are written in Column (9)

Example 3.2

Figure 3.4 shows an oil reservoir with a semicircular aquifer. The parameters of the aquifer are

r_w	-	1000 m [3280 ft]
r_e	-	5000 m [16400 ft]
h	-	7.2 m [23.6 ft]
ϕ	-	0.23
k	-	0.0225×10^{-12} m^2 [~ 22.2 mD]
μ_w	-	0.00025 Pas [0.25 cp]

At the time *t = 0* reservoir pressure is reduced by *1 MPa [145 psi]* and is then kept constant. The water influx can be considered steady-state. The cumulative water influx after 3 years is to be calculated.

Solution

From Eq. 3.22 for the semicircular aquifer:

$$C_{2r} = \frac{1}{2}\frac{2\pi hk}{\mu \ln \frac{r_e}{r_w}} = \frac{\pi 7.2 \times 0.0225 \times 10^{-12}}{0.25x10^{-3} \ln 5} = 1.265 \times 10^{-90} \quad m^3 Pa^{-1} s^{-1}$$

$$= 109.3 \quad m^3 MPa^{-1} d^{-1}$$

In field units:

$$C_{2r} = \frac{1}{2}\frac{7.08 \times 10^{-3} \times 23.6 \times 22.2}{0.25 \times \ln 5} = 4.6095 \quad bbl/psi\ d$$

The cumulative water influx after 1000 days totals

$$W_e = C_{2r} \Delta p t = 109.3 \times 1 \times 1000 = 109 \times 10^3 \quad m^3$$

In field units:

$$W_e = 4.6095 \times 145 \times 1000 = 677410 \quad bbl$$

Example 3.3

The task is to determine cumulative water influx after a production time of *t = 1000 days* at non-steady-state conditions (Fig. 3.4). During this time the reservoir pressure is reduced linear by 1 MPa [145 psi]. The aquifer acting infinite.

The parameters of the aquifer are:

A	=	14x10^6	m^2	[3459 *ac*]
h	=	7.2	*m*	[23.6 *ft*]
ϕ	=	0.23		
k	=	0.225x10^{-12}	m^2	[~ 222 *mD*]
c_ϕ	=	6x10^{-10}	Pa^{-1}	[4.13685x10^{-6} 1/*psi*]
c_w	=	5x10^{-10}	Pa^{-1}	[3.4473x10^{-6} 1/*psi*]
μ_w	=	0.25x10^{-3}	*Pas*	[0.25 *cP*]

A is the area of the aquifer.

Solution

The radii of the reservoir are

$$r_w = \left(\frac{2A}{\pi}\right)^{\frac{1}{2}} = \left(\frac{28 \times 10^6}{\pi}\right) = 2985 \ \ m$$

In field units:

$$r_w = \left(\frac{2 \times 3459 \times 43560}{\pi}\right)^{\frac{1}{2}} = 9794 \ \ ft$$

The effective compressibility of the aquifer is

$$c_e = c_w + c_\phi = (6 + 5) \times 10^{-10} = 1.1 \times 10^{-9} \ \ Pa^{-1}$$

In field units:

$$c_e = 3.448 \times 10^{-6} + 4.137 \times 10^{-6} = 7.585 \times 10^{-6} \ \ 1/psi$$

According to Eq. 3.26:

$$\alpha = \frac{k}{\mu \phi c_e r_w^2} = \frac{0.225 \times 10^{-12}}{0.25 \times 10^{-3} \times 0.23 \times 1.1 \times 10^{-9} \times 2985^2}$$

$$= 0.39924 \times 10^{-6} \ s^{-1} = 0.0345 \ d^{-1}$$

In field units:

$$\alpha = 6.34 \times 10^{-3} \frac{222}{0.25 \times 10^{-3} \times 0.23 \times 7.585 \times 10^{-6} \times 9794^2} = 0.0345 \ d^{-1}$$

From Table 3.1, at $t_D = \alpha t = 34.5$ we get:

$$\tilde{Q}(t_D) = 380.5562$$

Eq. 3.28, since the reservoir is semicircular

$$C_3^{id} = \pi\phi h c_e r_w^2 = \pi 0.23 \times 7.2 \times 1.1 \times 10^{-9} \times 2985^2$$
$$= 0.051 \ m^3 Pa^{-1} = 51000 \ m^3 MPa^{-1}$$

In field units:

$$C_3^{id} = 0.17801\pi \times 0.23 \times 23.6 \times 7.585 \times 10^{-6} \times 9794^2 = 2208 \ bbl/psi$$

From Eq. 3.26:

$$W_e = C_3^{id} \frac{\Delta p}{t_D} \tilde{Q}(t_D) = 51000 \times 1 \times 380.5562/34.5 = 568000 \ m^3$$

In field units:

$$W_e = 2208 \times 145 \times 380.5562/34.5 = 3.53246 \times 10^6 \ bbl$$

Example 3.4

A reservoir produces three years. Reservoir pressure has decreased from 30 MPa [4350 psi] to 27 MPa [3915 psi]. The data known are tabulated in columns (1)-(3) in Table 3.4 and Table 3.5. The cumulative water influx after 3 years is to be calculated. The parameters of the aquifer are the same as in Example 3.3.

Solution

Constants $\alpha = 0.0345 \ d^{-1}$ and $C_3 = 51\ 000 \ m^3 \ MPa^{-1}$ [2233 *bbl/psi*] were already calculated in Example 3.3.

The water influx results in

$$W_e = C_3 \sum_{j=0}^{n-1} \Delta_{j+1} \left(\frac{\Delta p}{\Delta t_D} \right) \tilde{Q}(t_{Dn} - t_{Dj}) = 51000 \times 26.189 = 1.3356 \times 10^6 \ m^3$$

In field units:

$$W_e = 2208 \times 379.74 = 8.38465 \times 10^6 \ bbl$$

Example 3.5

A water influx equation for the reservoir in Example 3.1 has to be determined. The radius of the reservoir is ~ 1000 m [3280 ft], the data of the aquifer are:

ϕ	=	0.23		
k	=	$8\text{x}10^{-15}$	m^2	[8 *mD*]
c_e	=	$1.1\text{x}10^{-9}$	Pa^{-1}	[$7.585\text{x}10^{-6}$ 1/*psi*]
μ_w	=	$0.25\text{x}10^{-3}$	*Pas*	[0.25 *cP*]

Solution

First, it is essential to determine whether the water influx is steady-state or non-steady-state. The procedure is comprised in Table 3.6 and Table 3.7. The coefficients C_1 and C_2 are calculated for all t_j by using Eq. 3.17 and Eq. 3.23.

Due to the fact that C_1 increases and C_2 decreases, the water influx can be considered non-steady-state.

The aquifer is assumed infinite and α is calculated as follows:

$$\alpha = \frac{k}{\mu\phi c_e r_w^2} = \frac{8\times10^{-15}}{0.25\times10^{-3}\times0.23\times1.1\times10^{-9}\times10^{6}} =$$

$$= 1.2648\times10^{-7}s^{-1} = 0.0109\,d^{-1} \approx 1/3 month^{-1}$$

In field units:

$$\alpha = \frac{6.34\times10^{-3}\times8}{0.23\times0.25\times7.585\times10^{-6}\times3280^2} = 0.0190 d^{-1} \approx (1/3) month^{-1}$$

In Table 3.8 and Table 3.9, the terms

$$\sum_{j=0}^{n-1} \Delta_{j+1}\left(\frac{\Delta p}{\Delta t_D}\right)\tilde{Q}(t_{Dn} - t_{Dj}),\ n = 1, \ldots 6$$

are calculated for the last three time points. The coefficients C_3 are calculated in Table 3.6 and Table 3.7 using Eq. 3.26. The values C_3 can be regarded with fair accuracy as constants during the last 60 months. The value C_3 = 5300 m^3 MPa^{-1}[230 *bbl/psi*] can be accepted for prediction purposes.

Table 3.2: Calculation of Water Influx into an Oil-Reservoir - Example 3.1 (metric units)

t *month*	p *MPa*	N_p 10^3m^3	R_p	W_p 10^3m^3	B_o	B_g	R_s	W_e 10^3m^3
(1)	(2)	(3)	(4)	(5)	(6)	(7)	(8)	(9)
0	23				1.3032*	0.00480*	97.8*	0.0
6	22	87.8	94.0	0.0	1.2957	0.00502	93.9	5.8
12	21	183.7	92.0	0.1	1.2879	0.00526	90.0	11.1
27	20	308.9	89.0	1.1	1.2800	0.00552	86.0	39.5
48	19	502.8	95.0	3.3	1.2719	0.00581	82.0	166.8
75	18	693.20	99.0	13.2	1.2636	0.00613	77.9	292.2
108	17	905.0	105.0	21.8	1.2550	0.00649	73.8	468.5

Table 3.3: Calculation of Water Influx into an Oil-Reservoir - Example 3.1 (field units)

t *month*	p *psi*	N_p 10^3bbl	R_p *scf/bbl*	W_p $10^3/bbl$	B_o	B_g	R_s *scf/bbl*	W_e $10^3/bbl$
(1)	(2)	(3)	(4)	(5)	(6)	(7)	(8)	(9)
0	3335				1.3032*	0.00480*	549.2	0
6	3190	552	527	0.0	1.2957	0.00502	527.0	36
12	3045	1155	516	0.6	1.2879	0.00526	505.0	70
27	2900	1943	499	6.9	1.2800	0.00552	483.0	248
48	2755	3162	532	20.7	1.2719	0.00581	460.0	1049
75	2610	4359	555	82.9	1.2636	0.00613	437.0	1837
108	2465	5691	589	136.9	1.2550	0.00649	414.0	2946

Table 3.4: Calculation of Water Influx into an Oil-Reservoir - Example 3.1 (metric units

Date	*Reservoir pressure MPa*	Δ_p *MPa*	*t days*	$t_{Dj}=$ αt	t_D-$t_{Dj}=$ *37.8-*t_{Dj}	$\frac{\Delta p}{\Delta t_D}$	$\Delta_{j+1}\left(\frac{\Delta p}{\Delta t_D}\right)$	$\tilde{Q}(t_{Dn}-t_{Dj})$	(8)x(9)
(1)	(2)	(3)	(4)	(5)	(6)	(7)	(8)	(9)	(10)
76.7.1	30.0	0.10			37.8	0.0158	0.0158	454.475	7.181
77.1.1	29.8	0.25	183	6.3	31.5	0.0397	0.0239	314.080	7.506
77.7.1	29.5	0.40	365	12.6	25.2	0.0635	0.0238	223.422	5.317
78.1.1	29.0	0.70	548	18.9	18.9	0.1111	0.0476	132.683	6.316
78.7.1	28.1	0.75	730	25.2	12.6	0.1190	0.0079	67.573	0.538
79.1.1	27.5	0.55	913	31.5	6.3	0.0873	-0.0323	20.704	-0.669
79.9.1	27.0		1095	37.8					Σ 26.189

$\alpha = 0.0345$
Δt_D = const. = 6.3

Table 3.5: Calculation of Water Influx into an Oil-Reservoir - Example 3.1 (field units)

Date	*Reservoir pressure psi*	Δ_p *psi*	*t days*	$t_{Dj}=$ αt	t_D-$t_{Dj}=$ *37.8-*t_{Dj}	$\frac{\Delta p}{\Delta t_D}$	$\Delta_{j+1}\left(\frac{\Delta p}{\Delta t_D}\right)$	$\tilde{Q}(t_{Dn}-t_{Dj})$	(8)x(9)
(1)	(2)	(3)	(4)	(5)	(6)	(7)	(8)	(9)	(10)
76.7.1	4350.0	14.5			37.8	0.229	0.229	454.475	104.12
77.1.1	4321.0	36.3	183	6.3	31.5	0.576	0.347	314.080	108.84
77.7.1	4277.5	58.0	365	12.6	25.2	0.921	0.345	223.422	77.09
78.1.1	4205.0	101.5	548	18.9	18.9	1.611	0.690	132.683	91.58
78.7.1	4074.0	108.8	730	25.2	12.6	1.725	0.114	67.573	7.8
79.1.1	3987.5	79.8	913	31.5	6.3	1.266	-0.459	20.704	-9.70
79.9.1	3915.0		1095	37.8					Σ 379.74

$\alpha = 0.0345$
Δt_D = const. = 6.3

Table 3.6: Determination of the Aquifer Type (metric units)

No	*t*	*p*	W_e	p_i-p	C_1	Δp_j	$\Sigma\Delta p$	C_2	$\Sigma\Delta_{j+1}$	C_3
							$(t\text{-}t_j)$		$\left(\frac{\Delta p}{\Delta t_D}\right)\tilde{Q}$	
	month (1)	*MPa* (2)	$10^3 m^3$ (3)	*MPa* (4)	(3)/(4) (5)	*MPa* (6)	(7)	(3)/(7) (8)	(9)	(3)/(9)
0	0	23.0								
1	6	22.0	5.8	1.0	5.8	0.5	3.0	1.93		
2	12	21.0	11.1	2.0	5.6	1.0	12.0	0.93		
3	27	20.0	39.5	3.0	13.2	1.0	49.5	0.80		
4	48	19.0	166.8	4.0	41.7	1.0	123.0	1.36	30.444	5480
5	75	18.0	292.2	5.0	58.5	1.0	244.5	1.19	54.460	5360
6	108	17.0	468.5	6.0	78.1	1.0	426.0	1.10	88.209	5310

$N = 3600000\ m^3$

Table 3.7: Determination of the Aquifer Type (field units)

No	*t*	*p*	W_e	p_i-p	C_1	Δp_j	$\Sigma\Delta p$	C_2	$\Sigma\Delta_{j+1}$	C_3
							$(t\text{-}t_j)$		$\left(\frac{\Delta p}{\Delta t_D}\right)\tilde{Q}$	
	month (1)	*psi* (2)	$10^3 bbl$ (3)	*psi* (4)	(3)/(4) (5)	*psi* (6)	(7)	(3)/(7) (8)	(9)	(3)/(9)
0		3335								
1	6	3190	36.5	145	2.52	72.5	435	83.90		
2	12	3045	69.8	290	2.42	145.0	1740	40.01		
3	27	2900	248.4	435	5.72	145.0	7177	34.60		
4	48	2755	1049.0	580	18.09	145.0	17835	58.80	4413	237.6
5	75	2610	1838.0	725	25.38	145.0	35452	51.80	7897	232.6
6	108	2465	2946.0	870	33.88	145.0	61770	47.70	12790	230.5

$N = 2.26 \text{x} 10^7\ bbl$

Table 3.8: Calculation of the $\sum \Delta_{j+1}\left(\frac{\Delta_p}{\Delta t_D}\right)\tilde{Q}(t_D - t_{Dj})$ Function for Example 3.5 (field units)

No	t_D	Δp_j *psi*	$\frac{\Delta p}{\Delta t_D}$	$\Delta_{j+1}\left(\frac{\Delta p}{\Delta t_D}\right)$
0	0	145	72.5000	72.5000
1	2	145	72.5000	0.0000
2	4	145	29.0000	-43.5000
3	9	145	20.7060	-8.2940
4	16	145	16.1095	-4.5965
5	25	145	13.1805	-2.9290

For 6th time point: t_{Dn} = 36

No	t_{Dn}-t_{Dj}	$\tilde{Q}(t_D - t_{Dj})$	$\Delta_{j+1}\left(\frac{\Delta p}{\Delta t_D}\right)\tilde{Q}$
0	36	414.157	30 026.310
1	34	378.317	0.000
2	32	326.557	-14 205.215
3	27	249.154	-2 066.540
4	21	148.294	-681.645
5	11	96.536	-282.750
			Σ 12 790.160

For 5th time point: t_{Dn} = 25

No	t_{Dn}-t_{Dj}	$\tilde{Q}(t_D - t_{Dj})$	$\Delta_{j+1}\left(\frac{\Delta p}{\Delta t_D}\right)\tilde{Q}$
0	25	220.337	15 974.505
1	23	191.521	0.000
2	21	162.704	-7.077.595
3	16	99.872	-828.385
4	9	37.394	-171.825
			Σ 7 896.700

For 4th time point: t_{Dn} = 16

No	t_{Dn}-t_{Dj}	$\tilde{Q}(t_D - t_{Dj})$	$\Delta_{j+1}\left(\frac{\Delta p}{\Delta t_D}\right)\tilde{Q}$
0	25	220.337	15 974.505
1	23	191.521	0.000
2	21	162.704	-7.077.595
3	16	99.872	-828.385
4	9	37.394	-171.825
			Σ 7 896.700

Table 3.9: Calculation of $\sum \Delta_{j+1}\left(\frac{\Delta_p}{\Delta t_D}\right)\tilde{Q}(t_D - t_{Dj})$ Function for Example 3.5 (metric units)

No	t_D	Δp_j *MPa*	$\frac{\Delta p}{\Delta t_D}$	$\Delta_{j+1}\left(\frac{\Delta p}{\Delta t_D}\right)$
0	0	1	0.5000	0.5000
1	2	1	0.5000	0.0000
2	4	1	0.2000	-3.0000
3	9	1	0.1428	-0.0572
4	16	1	0.1111	-0.0317
5	25	1	0.0909	-0.0202

For 6th time point: t_{Dn} = 36

No	t_{Dn}-t_{Dj}	$\tilde{Q}(t_D - t_{Dj})$	$\Delta_{j+1}\left(\frac{\Delta p}{\Delta t_D}\right)\tilde{Q}$
0	36	414.157	207.078
1	34	378.317	0.000
2	32	326.557	-97.967
3	27	249.154	-14.252
4	21	148.294	-4.701
5	11	96.536	-1.950
			Σ 88.208

For 5th time point: t_{Dn} = 25

No	t_{Dn}-t_{Dj}	$\tilde{Q}(t_D - t_{Dj})$	$\Delta_{j+1}\left(\frac{\Delta p}{\Delta t_D}\right)\tilde{Q}$
0	25	220.337	110.169
1	23	191.521	0.000
2	21	162.704	-48.811
3	16	99.872	-5.713
4	9	37.394	-1.185
			Σ 54.460

For 4th time point: t_{Dn} = 16

No	t_{Dn}-t_{Dj}	$\tilde{Q}(t_D - t_{Dj})$	$\Delta_{j+1}\left(\frac{\Delta p}{\Delta t_D}\right)\tilde{Q}$
0	16	99.872	49.936
1	14	81.107	0.000
2	12	62.342	-18.703
3	7	25.029	-0.793
			Σ 30.440

3.4 Finite Difference Material Balance Equation

The time is divided into a finite number of optional intervals. At time j, Eq. 3.9 becomes

$$N\left[\left(\frac{B_o}{B_g}-R_s\right)_j-\left(\frac{B_{oi}}{B_{gj}}-R_{si}\right)\right]+mNB_{oi}\left(\frac{1}{B_{gi}}-\frac{1}{B_{gj}}\right)+\frac{1}{B_{gj}}(W_{ej}-W_{pj}) \tag{3.40}$$
$$=N_p\left[\left(\frac{B_o}{B_g}-R_s\right)_j\right]+G_{pj}$$

For time $j+1$

$$N_{pj+1} = N_{pj}+\Delta_{j+1}N_p = N_{pj}+q_o\Delta_{j+1}t$$
$$G_{pj+1} = G_{pj}+\bar{R}\Delta_{j+1}N_p = G_{pj}+q_o\bar{R}\Delta_{j+1}t \quad , \tag{3.41}$$
$$W_{pj+1} = W_{pj}+\Delta_{j+1}W_p = W_{pj}+q_w\Delta_{j+1}t$$

where

q_o	-	oil production rate	m^3/d [bbl/d],
q_w	-	water production rate	m^3/d [bbl/d],
$\bar{R}$	-	the average production GOR.	

In order to simplify calculations, the water influx is assumed steady-state.
(Calculations are similar, but more complicated for non-steady-state water influx).

According to Fetkovich[17.] equation Eq. 3.35,

$$W_{ej+1} = W_{ej}+J_w(p_{aj}-\bar{p})\Delta_{j+1}t, \tag{3.42}$$

where p_{aj} is the avarage aquifer pressure at time j and

$$\bar{p} = \frac{p_{j+1}+p_j}{2} \tag{3.43}$$

is the average reservoir pressure in a time period (t_j, t_{j+1}). Thus, Eq. 3.40 at time $j+1$ leads to

$$N\left[\left(\frac{B_o}{B_g}-R_s\right)_{j+1}-\left(\frac{B_{oi}}{B_{gj}}-R_{si}\right)\right]+mNB_{oi}\left(\frac{1}{B_{gi}}-\frac{1}{B_{gj+1}}\right)+\frac{1}{B_{gj+1}}(W_{ej}-W_{pj}) \quad (3.44)$$

$$+\frac{1}{B_{gj+1}}[J_w(p_{aj}-\bar{p})-q_w]\Delta_{j+1}t$$

$$= N_{pj}\left(\frac{B_o}{B_g}-R_s\right)_{j+1}+G_{pj}+\Delta_{j+1}N_p\left[\left(\frac{B_o}{B_g}-R_s\right)_{j+1}+\bar{R}\right]$$

From Eq. 3.44 either the production for the time intervall *j,j+1*

$$\Delta_{j+1}N_p = \frac{mNB_{oi}\left(\frac{1}{B_{gj}}-\frac{1}{B_{gj+1}}\right)+N\left[\left(\frac{B_o}{B_g}-R_s\right)_{j+1}-\left(\frac{B_{oi}}{B_{gj+1}}-R_{si}\right)\right]}{\left(\frac{B_o}{B_g}-R_s\right)_{j+1}+\bar{R}} \quad (3.45)$$

$$+\frac{-N_{pj}\left(\frac{B_o}{B_g}-R_s\right)_{j+1}-G_{pj}+\frac{(W_e-W_p)}{B_{gj+1}}+\frac{J_w(p_{aj}-\bar{p})-q_w}{B_{gj+1}}\Delta_{j+1}t}{\left(\frac{B_o}{B_g}-R_s\right)_{j+1}+\bar{R}}$$

or the duration

$$\Delta_{j+1}t = \frac{mNB_{oi}\left(\frac{1}{B_{gj}}-\frac{1}{B_{gj+1}}\right)+N\left[\left(\frac{B_o}{B_g}-R_s\right)_{j+1}-\left(\frac{B_{oi}}{B_{gj+1}}-R_{si}\right)\right]}{q_o\left[\left(\frac{B_o}{B_g}-R_s\right)_{j+1}+\bar{R}\right]-\frac{J_w(p_{aj}-\bar{p})-q_w}{B_{gj+1}}} \quad (3.46)$$

$$+\frac{-N_{pj}\left(\frac{B_o}{B_g}-R_s\right)_{j+1}-G_{pj}+\frac{W_e-W_{pj}}{B_{gj+1}}}{q_o\left(\frac{B_o}{B_g}-R_s\right)_{j+1}+\bar{R}-\frac{J_w p_{aj}-\bar{p}-q_w}{B_{gj+1}}}$$

can be expressed.

Application of the differential form of **MB** equation:

1. Eq. 3.44 is applied for the production forecast $\Delta_{j+1}\ N_p$, if the reservoir pressure drops from p_j to p_{j+1} in a time period $\Delta_{j+1}\ t$.
2. Eq. 3.46 enables the calculation of the time period $\Delta_{j+1}\ t$ corresponding to a given pressure change $\Delta_{j+1}p$ and production $\Delta_{j+1}\ N_p$.
3. For the third case, where the pressure change in a certain time interval $\Delta_{j+1}\ t$ at a given production rate has to determined, a NEWTON- RAPHSON iteration must be applied to calculate $\Delta_{j+1}\ N_\mathrm{p}$ and $\Delta_{j+1}\ t$ according to $\Delta_{j+1}p$.

Subtraction of Eq. 3.40 from Eq. 3.44 leads to

$$N\Delta_{j+1}\left(\frac{B_o}{B_g}-R_s\right)-NB_{oi}\Delta_{j+1}\left(\frac{1}{B_g}\right)-mNB_{oi}\Delta_{j+1}\left(\frac{1}{B_g}\right)+(W_e-W_p)_j\Delta_{j+1}\left(\frac{1}{B_g}\right)$$
$$+\frac{1}{B_{gj+1}}[J_w(p_{aj}-\bar{p})-q_w]\Delta_{j+1}t= \tag{3.47}$$
$$=N_{pj}\Delta_{j+1}\left(\frac{B_o}{B_g}-R_s\right)+\Delta_{j+1}N_p\left[\left(\frac{B_o}{B_g}-R_s\right)_{j+1}+\bar{R}\right]$$

where

$$\Delta_{j+1}\left(\frac{1}{B_g}\right)=\frac{1}{B_{gj+1}}-\frac{1}{B_{gj}}, \tag{3.48}$$
$$\Delta_{j+1}\left(\frac{B_o}{B_g}-R_s\right)=\left(\frac{B_o}{B_g}-R_s\right)_{j+1}-\left(\frac{B_o}{B_g}-R_s\right)_j.$$

After reordering:

$$\frac{(N-N_p)\Delta_{j+1}\left(\frac{B_o}{B_g}-R_s\right)-(1+m)NB_{oi}\Delta_{j+1}\left(\frac{1}{B_g}\right)}{\Delta_{j+1}N_p\left[\left(\frac{B_o}{B_g}-R_s\right)_{j+1}+\bar{R}\right]} \tag{3.49}$$
$$+\frac{(W_e-W_p)\Delta_{j+1}\left(\frac{1}{B_g}\right)+\frac{1}{B_{gj+1}}[J_w(p_{aj}-\bar{p})-q_w]\Delta_{j+1}t}{\Delta_{j+1}N_p\left[\left(\frac{B_o}{B_g}-R_s\right)_{j+1}+\bar{R}\right]}=1$$

Again, it is possible to split this term into three fractions, each representing one specific drive index at a production of $\Delta_{j+1}\ N_p$:

The **solution gas drive index**:

$$i_s = \frac{(N - N_p)\Delta_{j+1}\left(\frac{B_o}{B_g} - R_s\right) - NB_{oi}\Delta_{j+1}\left(\frac{1}{B_g}\right)}{\left[\left(\frac{B_o}{B_g} - R_s\right)_{j+1} + \bar{R}\right]\Delta_{j+1}N_p} \tag{3.50}$$

The gas **drive index**:

$$i_g = \frac{mNB_{oi}\Delta_{j+1}\left(\frac{1}{B_g}\right)}{\left[\left(\frac{B_o}{B_g} - R_s\right)_{j+1} + \bar{R}\right]\Delta_{j+1}N_p}, \tag{3.51}$$

The **water drive index**:

$$i_w = \frac{(W_e - W_p)\Delta_{j+1}\left(\frac{1}{B_g}\right) + \frac{1}{B_{gj+1}}[J_w(p_{aj} - \bar{p}) - q_w]\Delta_{j+1}t}{\left[\left(\frac{B_o}{B_g} - R_s\right)_{j+1} + \bar{R}\right]\Delta_{j+1}N_p} \tag{3.52}$$

Again

$$i_s + i_g + i_w = 1 \tag{3.53}$$

is valid.

In contrast to the indices applied in Eq. 3.11 - Eq. 3.13, which refer to the total cumulative production, these are only valid for the production in the time interval $\Delta_{j+1}\, t$.

3.5 Undersaturated Oil Reservoirs

Up to this point, the compressibility of both the connate water and the reservoir rock has been neglected due to the compressibility of gas and the two phase compressibility of oil.

In case of an unsaturated reservoir, oil is in single phase state if pressure ranges from initial pressure p_i to bubble point pressure p_b. Since the compressibility of water is in its order of magnitude comparable to that of oil, it has to be taken into consideration also.

A simplification can be achieved by introducing an apparent oil compressibility c_{oe} representing all three phases:

$$S_o c_{oe} = c_o S_o + c_w S_w + c_\phi . \tag{3.54}$$

Since $S_o = 1 - S_w$, then

$$c_{oe} = c_o + c_w \frac{S_w}{1 - S_w} + c_\phi \frac{1}{1 - S_w} . \tag{3.55}$$

The volume of the reservoir oil at initial pressure p_i is

$$V_p(1 - S_{wi}) = NB_{oi} . \tag{3.56}$$

If the reservoir pressure drops to p as a consequence of the production N_p, the volume of the total reservoir contents taking the water influx into account would be

$$NB_{oi}[1 + c_{oe}(p_i - p)] + W_e . \tag{3.57}$$

Due to the fact that the compressibility of the pore volume is conveyed to the oil, the pore volume is considered constant as in Chapter 3.1. The difference between the volumes according Eq. 3.57 and Eq. 3.56 lies in the volume of cumulative production at pressure p:

$$N_p B_o + W_p . \tag{3.58}$$

Thus,

$$NB_{oi} c_{oe}(p_i - p) + W_e = N_p B_o + W_p \tag{3.59}$$

Substitution of Eq. 3.55 leads to

$$N\left[B_{oi} c_o (p_i - p) + \frac{B_{oi}(c_\phi + S_{wi} c_w)(p_i - p)}{1 - S_{wi}}\right] + W_e = N_p B_o + W_p . \tag{3.60}$$

Since

$$B_o = B_{oi}[1 + c_o(p_i - p)] , \tag{3.61}$$

Eq. 3.60 can be written as follows:

$$N\left[B_o - B_{oi} + \frac{B_{oi}(c_\phi + S_{wi} c_w)(p_i - p)}{1 - S_{wi}}\right] + W_e = N_p B_o + W_p . \tag{3.62}$$

Analogous forms can be set up for Eq. 3.45, Eq. 3.46 and Eq. .

The equations of material balance for unsaturated reservoirs can be applied solely between initial and bubble point pressure. In case of pressure being below bubble point pressure, the equations for saturated reservoirs must be applied.

3.6 Gas Reservoirs

The compressibility of rock and connate water are again neglected. The formation volume at initial presure p_i is defined as

$$V_p(1 - S_{wi}) = GB_{gi} \tag{3.63}$$

The production G_p effects a drop of the reservoir pressure. The total reservoir content including the water influx then adds up to

$$GB_g + W_e . \tag{3.64}$$

The difference between Eq. 3.63 and Eq. 3.64 is conditioned by the volume of cumulative production at pressure p_j:

$$GB_g + W_e - GB_{gi} = G_pB_g + W_p \tag{3.65}$$

and thus

$$G = \frac{G_pB_g}{B_g - B_{gi}} - \frac{W_e - W_p}{B_g - B_{gi}} . \tag{3.66}$$

The formation volume factor can be calculated from the real gas equation.

$$B_g = C \cdot \frac{ZT}{p} \qquad C = \frac{p_o}{Z_oT_o} \tag{3.67}$$

Since C and T (reservoir temperature) are constant, Eq. 3.66 can be written as follows:

$$G = G_p \frac{\left(\frac{Z}{p}\right)}{\left(\frac{Z}{p}\right) - \left(\frac{Z}{p}\right)_i} - \frac{W_e - W_p}{B_g - B_{gi}} \tag{3.68}$$

If no water influx is present, a gas reservoir is called *volumetric.* Thus, the second term on the right side of the equatin vanishes and Eq. 3.68 can be transformed to

$$\left(\frac{p}{Z}\right) = \left(\frac{p}{Z}\right)_i \left(1 - \frac{G_p}{G}\right). \tag{3.69}$$

A specific property of a volumetric reservoir is that the fraction *p/Z* is a linear function of the cumulative production. Therefore, the presence of a water influx is easily observed by this function not being linear (see Fig. 3.8).

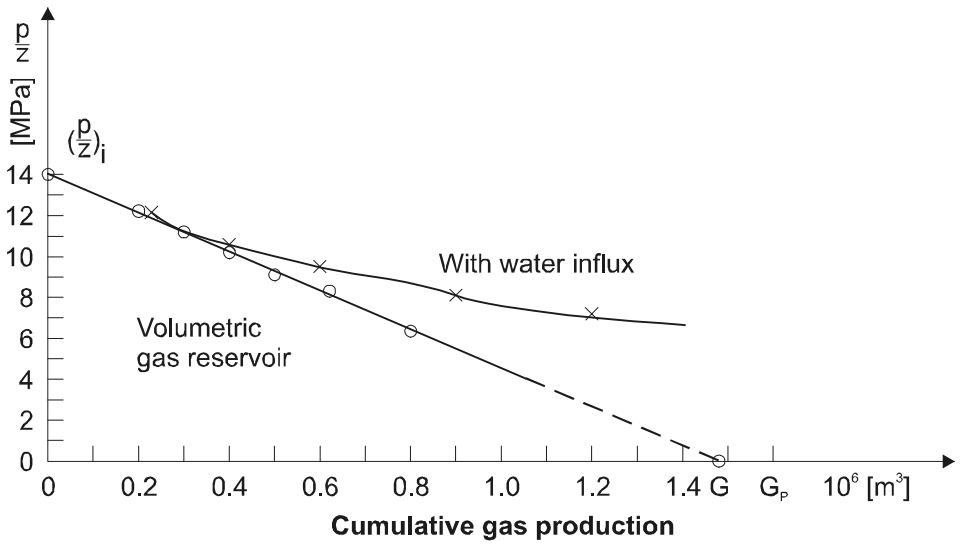

Figure 3.8: Pressure-drop in a gas reservoir

3.7 Calculation of Original Fluid in Place

The material balance formulas as used in Chapters 3.1, 3.4, 3.5 can be regarded as specific cases. The general form of the material balance equation is

$$N\left[B_o - B_{oi} + B_g(R_{si} - R_s) + \frac{B_{oi}(c_\phi + S_{wi}c_w)(p_i - p)}{1 - S_{wi}}\right] + GB_{gi}\left(\frac{B_g}{B_{gi}} - 1\right) + W_e$$
$$= N_p[B_o + B_g(R_p - R_s)] + W_p - (W_I + G_I B_g) \qquad (3.70)$$

where W_I is the cumulative injected water and G_I the cumulative injected gas. Eq. 3.70 includes the material balance equations derivated earlier:

- The compressibility of the pore volume and the connate water can be neglected if the reservoir contains free gas. Then $R_{si} > R_s$ and/or $GB_{gi} = mNB_{oi} \neq 0$. Disregarding gas and water injection means that Eq. 3.70 is identical with Eq. 3.6.
- If the reservoir pressure is above bubble point pressure $R_s = R_{si}$, $R_p = R_{si}$, and $GB_{gi} = 0$. Therefore, Eq. 3.70 becomes identical with Eq. 3.62.

- In a gas reservoir, $N = 0$, $N_p = 0$. Thus Eq. 3.70 is identical with Eq. 3.65.

The water influx can be calculated by the modified VAN EVERDINGEN-HURST method (see Eq. 3.26):

$$W_e = C\sum_{j=0}^{n-1}\Delta_{j+1}\left(\frac{\Delta p}{\Delta t_D}\right)\tilde{Q}(t_{Dn}-t_{Dj}) = C\eta_w, \tag{3.71}$$

where

$$\eta_w = \sum_{j=0}^{n-1}\Delta_{j+1}\left(\frac{\Delta p}{\Delta t_D}\right)\tilde{Q}(t_{Dn}-t_{Dj}) \tag{3.72}$$

Further, the following notions are defined:

$$\varepsilon_o = B_o - B_{oi} + B_g(R_{si}-R_s), \tag{3.73}$$

$$\varepsilon_w = \frac{B_{oi}(c_\phi + S_w c_w)(p_i - p)}{1-S_{wi}}, \tag{3.74}$$

$$\varepsilon_{ow} = \varepsilon_o + \varepsilon_w, \tag{3.75}$$

$$\varepsilon_g = B_g - B_{gi}, \tag{3.76}$$

$$Q_F = N_p[B_o + B_g(R_p - R_s)] + W_p - (W_I + G_I B_g). \tag{3.77}$$

Substituting Eq. 3.71 - Eq. 3.77 into Eq. 3.70 the following simple form is obtained:

$$N\varepsilon_{ow} + G\varepsilon_g + C\eta_w = Q_F. \tag{3.78}$$

In order to determine the functions ε, η and Q_F, it is necessary to have knowledge of both the average reservoir pressure as a function of time and cumulative production. If the corresponding values are known at *n* dates, it is possible to set up a system of *n* linear equations:

$$\begin{aligned} &N\varepsilon_{ow1} + G\varepsilon_{g1} + C\eta_{w1} = Q_{F1} \\ &N\varepsilon_{ow2} + G\varepsilon_{g2} + C\eta_{w2} = Q_{F2} \\ &\text{.....} \\ &N\varepsilon_{own} + G\varepsilon_{gn} + C\eta_{wn} = Q_{Fn} \end{aligned} \tag{3.79}$$

Solutions for *N*, *G* and *C* could be obtained by the method of the GAUSS's normal equations, whereby Eq. 3.79 is gradually multiplied with the coefficients of the first,

second and third unknown and than summed up:

$$N\sum\varepsilon^2_{owj} + G\sum\varepsilon_{gj}\varepsilon_{owj} + C\sum\eta_{wj}\varepsilon_{owj} = \sum Q_{Fj}\varepsilon_{owj} \tag{3.80}$$
$$N\sum\varepsilon_{owj}\varepsilon_{gj} + G\sum\varepsilon^2_{gj} + C\sum\eta_{wj}\varepsilon_{gj} = \sum Q_{Fj}\varepsilon_{gj}$$
$$N\sum\varepsilon_{owj}\eta_{wj} + G\sum\varepsilon_{gj}\eta_{wj} + C\sum\eta^2_{wj} = \sum Q_{Fj}\eta_{wj}$$

where

$$\sum = \sum_{j=1}^{n} \quad . \tag{3.81}$$

3.8 Graphical Evaluation of Material Balance

Let us consider Eq. 3.78:

$$N\varepsilon_{ow} + G\varepsilon_g + C\eta_w = Q_F \tag{3.82}$$

or with

$$G = \frac{mNB_{oi}}{B_{gi}} \tag{3.83}$$

in the form:

$$N\left[\varepsilon_{ow} + \frac{mNB_{oi}}{B_{gi}}\varepsilon_g\right] + C\eta_w = Q_F \tag{3.84}$$

HAVLENA and ODEH[19.] used this equation for graphical evaluation of reservoir performances.

We investigate several special cases illustrated in Fig. 3.9 and Fig. 3.10.

3.8.1 Reservoirs Without Water Influx: $W_e = 0$

a) For an oil reservoirs without a gas cap $m = 0$ and Eq. 3.84 becomes:

$$Q_F = N\varepsilon_{ow}. \tag{3.85}$$

Illustrated in the coordinate system ε_{ow} vs Q_F, Eq. 3.85 results in a straight line through the origin of the coordinate system with a slope *N*.

b) For an oil reservoir with a gas cap and supposing that m is known and Eq. 3.84 becomes:

$$Q_F = N\left[\varepsilon_{ow} + m\left(\frac{B_o}{B_g}\right)_i \varepsilon_g\right]. \tag{3.86}$$

Illustrated in the coordinate system $\varepsilon_{ow} + m(B_o/B_g)_i \varepsilon_g$ vs. Q_F , Eq. 3.86 appears as a straight line through the origin of the coordinate system with a slope *N*.

c) For an oil reservoir with a gas cap of unknown size must one select a value for m. A diagram is drawn according to the case b). If m is too large, the series of points will bend downwards and upwards if *m* is too small. After several attempts, the correct *m* will result in a straight line.

d) For a gas reservoir Eq. 3.82 becomes:

$$G_p B_g = G\varepsilon_g . \tag{3.87}$$

Illustrated in the coordinate system ε_g vs G_pB_g, Eq. 3.87 is straight line through the origin of the coordinate system with a slope *N*.

3.8.2 Reservoirs With Water Influx

a) For an oil reservoir without a gas cap: *m = 0*. Eq. 3.84 can then be written as

$$\frac{Q_F}{\varepsilon_{ow}} = N + C\frac{\eta_w}{\varepsilon_{ow}} . \tag{3.88}$$

Illustrated in the coordinate system Q_F/ε_{ow} vs. $\eta_m/\varepsilon_{ow,}$ Eq. 3.88 is a straight line with a slope *C*. The intersection of the straight line with the axis of coordinates gives *N*.

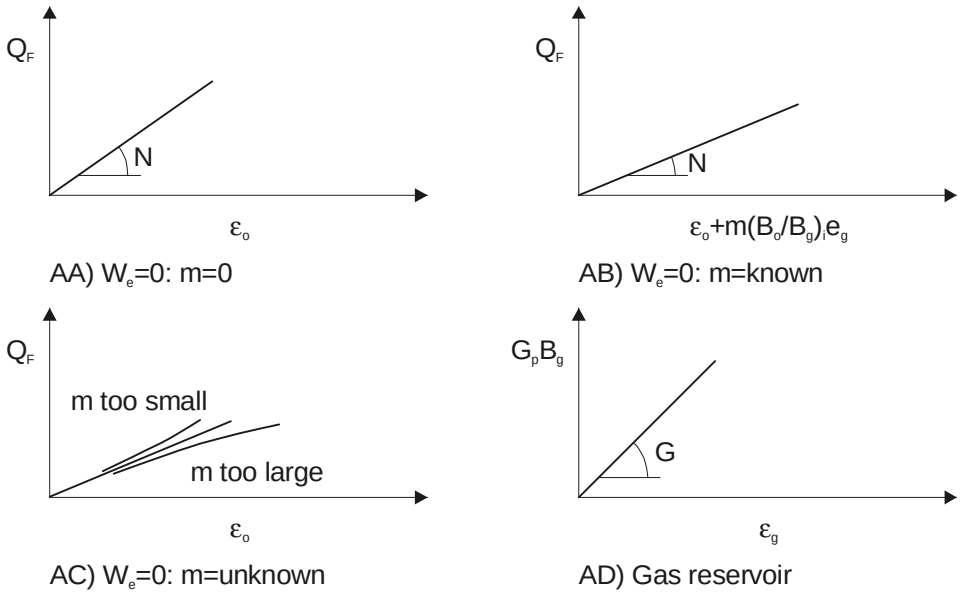

Figure 3.9: Graphical illustration of material balance without water influx ($W_e = 0$)

b) For an oil reservoir with a gas cap of known size Eq. 3.84 can be written as

$$\frac{Q_F}{\varepsilon_o + m\left(\frac{B_o}{B_g}\right)_i \varepsilon_g} = N + C\frac{\eta_w}{\varepsilon_o + m\left(\frac{B_o}{B_g}\right)_i \varepsilon_g} \tag{3.89}$$

The analogy to case a) is obvious.

c) Gas reservoir Eq. 3.82 can be written in the following form:

$$\frac{G_p B_g + W_p}{\varepsilon_g} = G + C\frac{\eta_w}{\varepsilon_g}. \tag{3.90}$$

Evaluation is made as in case a).

In order to calculate

$$\eta_w = \sum_{j=0}^{n-1} \Delta_{j+1}\left(\frac{\Delta p}{\Delta t_D}\right)\tilde{Q}(t_{Dn} - t_{Dj}) \tag{3.91}$$

one must estimate the parameters

$$r_{eD} = \frac{r_e}{r_w} \quad \text{and} \quad \alpha = \frac{k}{\mu c_e \phi r_w^2} \tag{3.92}$$

correctly. If η_w has a large value, Eq. 3.88 will be a rather flat curve.

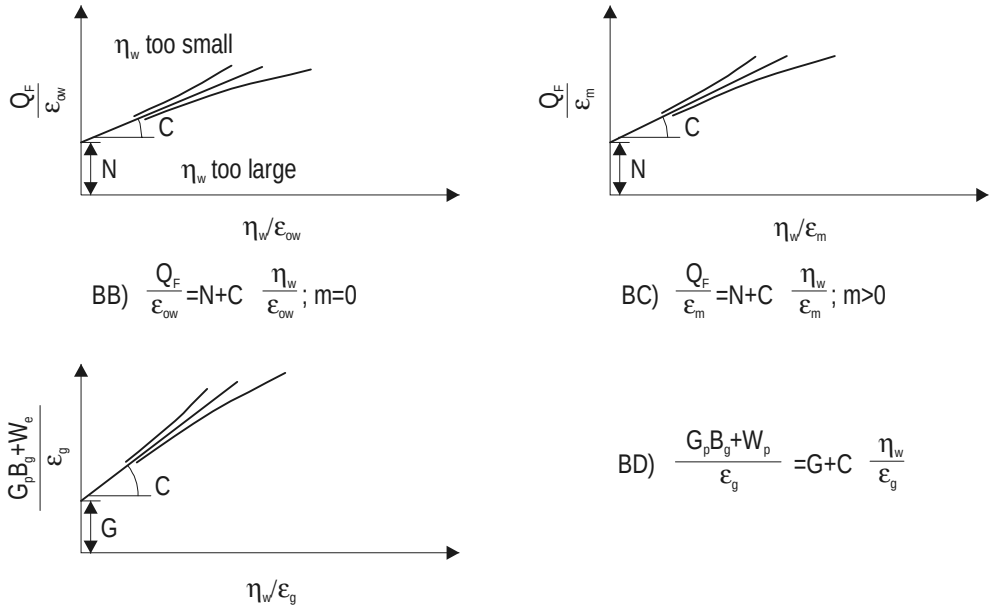

Figure 3.10: Graphical illustration of material balance with balance with water influx (W_e>0)

3.9 Recovery Factor

The ultimate recovery factor is defined as the relation between the ultimate recovery and the original oil in place, short OOIP:

$$E_R = \frac{N_{pmax}}{N}. \tag{3.93}$$

The recovery factor can be applied either for the whole or selected parts of the reservoir. The recovery factor at a specific point is considered equal to that of the displacement efficiency inferred by the existing oil recovery mechanisms at just this point. If several oil recovery mechanisms exist in a reservoir, they will result in an overall oil recovery (various possible combinations of elementary mechanisms are considered extra):

$$E_R = \sum_{j=1}^{n} E_{vj}E_{Dj}, \tag{3.94}$$

where E_{vj} is the volumetric efficiency of recovery mechanism j.

Of course,

$$\sum_{j=1}^{n} E_{vj} = 1 . \tag{3.95}$$

It is customary to split E_v into two factors:

E_A - areal sweep efficiency

E_I - vertical sweep efficiency.

The contribution of recovery mechanism j to the recovery factor is defined by the multiplication of the following three factors:

$$\Delta_j E_R = E_{Dj} E_{Aj} E_{Ij} . \tag{3.96}$$

Chapter 4

Displacement Efficiency

4.1 Solution Gas Drive

Imagine a part of the reservoir with 1 m^3[bbl] pore volume, an immobile water saturation S_{wi} and oil saturation $S_{oi} = 1 - S_{wi}$. The oil is saturated with gas at initial reservoir pressure.

In case of a pressure drop, the fluids will expand and gas will liberate from the oil. The total fluid volume will increase. Since the pore volume remains constant, surplus fluid must be displaced. An essential precondition for displacement is the mobility of the phase. In this case, the immobility of the water is inferred from the constant value of water saturation (expansion of the water was neglected). The involved gas develops a disperse, free gas phase consisting of small immobile gas bubbles. The oil is the only phase capable of flowing out of the regarded volume. A further pressure drop enlarges the number and size of the gas bubbles. The bubbles start to connect themselves and consequently develop continuous channels. The gas begins to move, more and more gas rather than oil will flow out. Pressure drops rapidly and as a result only oil with lost interior energy will remain.

4.1.1 MUSKAT's (1945) Equation of Solution Gas Drive

A pressure below the bubble point p_b is assumed. Water, oil and gas saturations represent the reservoir fluid volumes:

$$S_o + S_g + S_w = 1 \tag{4.1}$$

An unit pore volume at this pressure contains S_o / B_o sm^3[stb] stock tank oil and

$$_s\frac{S_o}{B_o} + (1 - S_o - S_w)\frac{1}{B_g} \ldots sm^3[scf] \tag{4.2}$$

gas. The first term in this formula is the amount of dissolved, the second term the amount of free gas. As pressure drops from p_i to p, Q_o $sm^3[stb]$ oil and Q_g $sm^3[scf]$ gas are produced from this volume unit. Further pressure drops of a differently small dp cause an increase of production by dQ_o and dQ_g. Naturally these terms must coincide with the changes of the oil and gas contents:

$$\frac{dQ_o}{dp} = -\frac{d}{dp}\left(\frac{S_o}{B_o}\right) = -\frac{1}{B_o}\frac{dS_o}{dp} + \frac{S_o}{B_o^2}\frac{dB_o}{dp} \tag{4.3}$$

and

$$\begin{aligned}\frac{dQ_o}{dp} &= -\frac{d}{dp}\left[R_s\frac{S_o}{B_o} + (1 - S_w - S_o)\frac{1}{B_g}\right] \\ &= -\frac{R_s}{B_o}\frac{dS_o}{dp} + \frac{R_s S_o}{B_o^2}\frac{dB_o}{dp} - \frac{S_o}{B_o}\frac{dR_s}{dp} - (1 - S_w - S_o)\frac{d}{dp}\left(\frac{1}{B_g}\right) + \frac{1}{B_g}\frac{dS_o}{dp}\end{aligned} \tag{4.4}$$

The momentary GOR results in:

$$R = \frac{dQ_g}{dQ_o} = R_s + \frac{B_o}{B_g}\frac{k_g}{k_o}\frac{\mu_o}{\mu_g}. \tag{4.5}$$

Eq. 4.5 demands a reduction of saturation both of oil and gas in such a way that the equation for the GOR is fulfilled when regarding the present saturations.

A combination of Eq. 4.3, Eq. 4.4 and Eq. 4.5 thus leads to

$$\begin{aligned}R_s + \frac{B_o}{B_g}\frac{k_g}{k_o}\frac{\mu_o}{\mu_g} = &\frac{\frac{R_s}{B_o}\frac{dS_o}{dp} - \frac{R_s S_o}{B_o^2}\frac{dB_o}{dp} + \frac{S_o}{B_o}\frac{dR_s}{dp}}{\frac{1}{B_o}\frac{dS_o}{dp} - \frac{S_o}{B_o^2}\frac{dB_o}{dp}} \\ &+ \frac{(1 - S_w - S_o)\frac{d}{dp}\left(\frac{1}{B_g}\right) - \frac{1}{B_g}\frac{dS_o}{dp}}{\frac{1}{B_o}\frac{dS_o}{dp} - \frac{S_o}{B_o^2}\frac{B_o}{dp}}\end{aligned} \tag{4.6}$$

Thus $\frac{dS_o}{dp}$ can be defined as

$$\frac{dS_o}{dp} = \frac{S_o \frac{B_g}{B_o} \frac{dR_s}{dp} + S_o \frac{k_g}{k_o} \frac{\mu_o}{B_o \mu_g} \frac{dB_o}{dp} + (1 - S_w - S_o) B_g \frac{d}{dp}\left(\frac{1}{B_g}\right)}{1 + \frac{k_g}{k_o} \frac{\mu_o}{\mu_g}} \tag{4.7}$$

This is a nonlinear first order differential equation. The oil saturation at pressure p is calculated by integration from p_i to p.

The following functions are introduced:

$$\lambda(p) = \frac{B_g}{B_o} \frac{dR_s}{dp} ,$$

$$\varepsilon(p) = B_g \frac{d}{dp}\left(\frac{1}{B_g}\right) \tag{4.8}$$

$$\eta(p) = \frac{1}{B_o} \frac{\mu_o}{\mu_g} \frac{dB_o}{dp},$$

$$\omega(p, S_o) = 1 + \frac{k_g}{k_o} \frac{\mu_o}{\mu_g} .$$

These are the MUSKAT functions and are given either graphically (Fig. 4.1) or in tables, but never analytically. Therefore integration can only be carried out numerically. The finite difference form of Eq. 4.7 is defined as

$$\Delta S_o = \Delta p \left[\frac{S_o \lambda(p) + S_o \frac{k_g}{k_o} \eta(p) + (1 - S_w - S_o)\varepsilon(p)}{\omega(p, S_o)} \right] \tag{4.9}$$

and the cumulative amount of produced oil as

$$N_p = V_p \sum_{pi}^{p} \Delta\left(\frac{S_o}{B_o}\right) = V_p \left[\left(\frac{S_o}{B_o}\right)_i - \left(\frac{S_o}{B_o}\right) \right]. \tag{4.10}$$

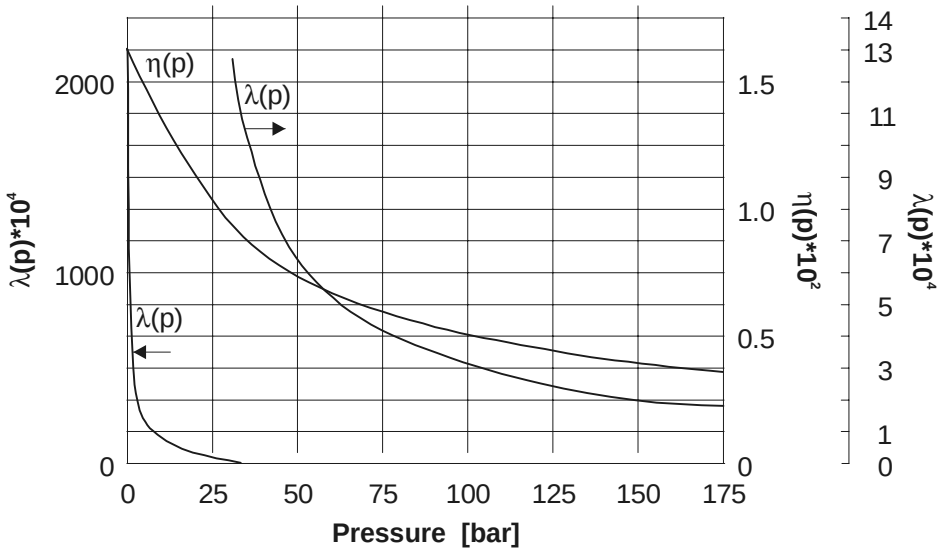

Figure 4.1: MUSKAT's function: λ and η

The method of MUSKAT is advantageous if a greater number of calculations are to be executed, whereby the effects of various factors on the solution gas drive are to be analysed. The fluid and rock characteristics remain unchanged. The functions $\lambda(p)$, $\eta(p)$, $\varepsilon(p)$, $\omega(p, S_o)$ are calculated only once. The corresponding values are obtained from the given curves.

Nevertheless there are various methods to solve Eq. 4.7 or Eq. 4.9. Several authors have analysed the effects of various factors influencing the progress of expansion and recovery.

MUSKAT and TAYLOR[32.](1946) using Eq. 4.7, analysed the influence of

μ_o	-	viscosity
p_i	-	initial pressure
R_{si}	-	solution gas-oil ratio
k_{rg}/k_{ro}	-	relative permeability ratio, see Fig. 4.2
S_{wi}	-	connate water saturation

Recovery as a function of the oil viscosity μ_o in case of solution gas drive is illustrated in Fig. 4.3. Essential for production planning of a volumetric reservoir is the calculation of the pressure decrease $p(N_p)$, the gas -oil ratio $R(N_p)$ and the production index $J(N_p)$, each as a function of the cumulative oil production N_p. In case the initial production rates of each well are known, N_p may be calculated with the help of the productivity index as a function of time.

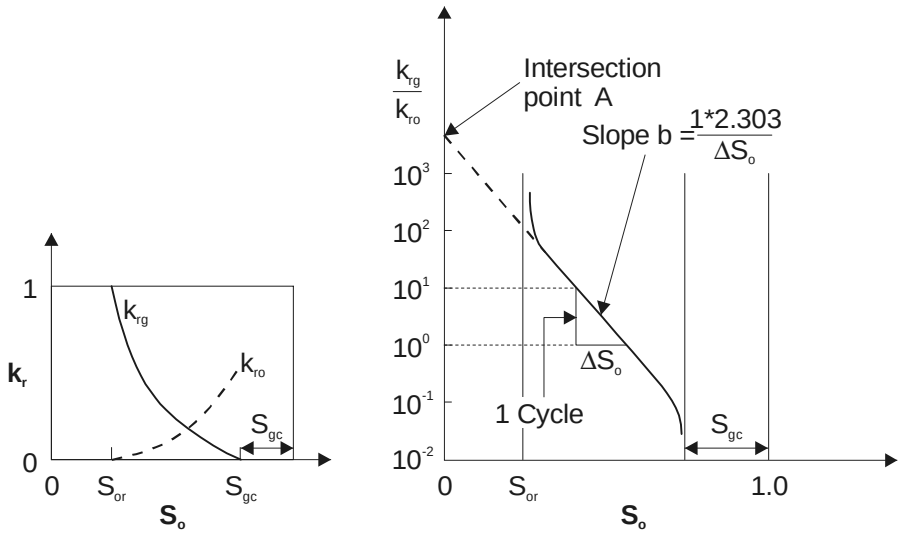

Figure 4.2: The relative gas and oil permeabilities and their relation as a function of the oil saturation

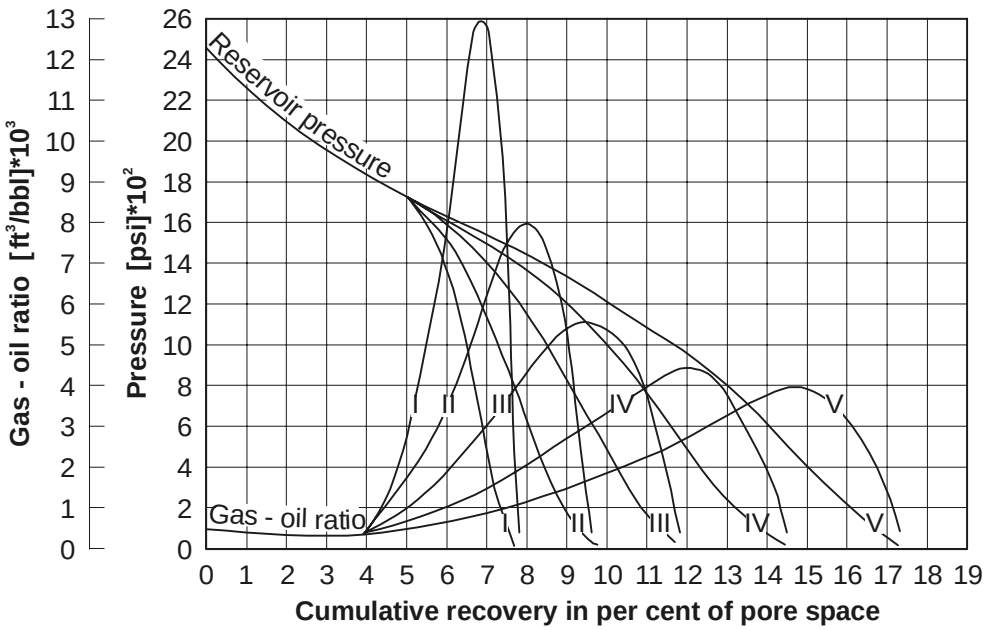

Curve I: atmospheric-pressure viscosity = 11.04 cp.
Curve II: atmos. pres. viscosity = 5.52 cp.
Curve III: atmos. pres. viscosity = 2.76 cp.
Curve IV: atmos. pres. viscosity = 1.38 cp.
Curve V: atmos. pres. viscosity = 0.69 cp.
Gas solubility at 2500 lb. per sq. in. = 534 cu. ft. per bbl. in all cases

Figure 4.3: Pressure and gas oil ratio histories of solution gas-drive reservoirs producing oil of different viscosities (after MUSKAT and TAYLOR, 1946)

4.1.2 Calculation of the Solution Gas Drive According to PIRSON

The task is again the calculation of the pressure drop and GOR as a function of the cumulative produced oil. The equations will be written for N m^3 O.O.I.P..

Fluid saturation equation:

$$S_L = S_w + \frac{(N - N_p)B_o}{NB_{oi}} (1 - S_w) \quad . \tag{4.11}$$

GOR equation:

$$R = R_s + \frac{B_o}{B_g} \frac{k_{rg}}{k_{ro}} \frac{\mu_o}{\mu_g}. \tag{4.12}$$

PIRSON[33.](1958) applied the material balance form in its difference form which is advantageous because it converges and the number of numerical operations is minimal.

Since only the solution gas drive is acting the drive index i_s = 1 can be set in Eq. 3.53 and the production increase can be calculated as follows:

$$\Delta_{j+1}N_p = \frac{(N - N_{pj}) \ \Delta_{j+1}\left(\frac{B_o}{B_g} - R_s\right) - NB_{oi} \ \Delta_{j+1}\frac{1}{B_g}}{\left(\frac{B_o}{B_g} - R_s\right)_{j+1} + \bar{R}} \tag{4.13}$$

where

$$\bar{R} = \frac{R_j + R_{j+1}}{2}.$$

j or $j + 1$ refer to two subsequent dates.

Further, the production capacity is defined by the productivity index:

$$J = \lim_{p_{wf} \to p} [q_o / (p - p_{wf})] \tag{4.14}$$

where

p - the reservoir pressure

p_{wf} - the bottom hole flowing pressure

q_o - the oil production rate

$J_i = J(p_i)$ is the productivity index at initial reservoir pressure. The change of the productivity index during recovery may be calculated with the help of the two phase DARCY-equation:

$$J = J_i k_{ro} \frac{(B_o \mu_o)_i}{B_o \mu_o} \quad . \tag{4.15}$$

In order to avoid cumulative errors, it is advisable to check this method using the finite form of the material balance equation. For this, the following formula is applied:

$$\frac{N_{pj+1}\left(\frac{B_o}{B_g} - R_s\right)_{j+1} + \sum_{j=1}^{j+1} \Delta N_p \bar{R}}{N\left[\left(\frac{B_o}{B_g} - R_s\right)_{j+1} - \left(\frac{B_{oi}}{B_{gj+1}} - R_{si}\right)\right]} = 1 \tag{4.16}$$

Fig. 4.4 shows the characteristic functions $p(N_p)$, $R(N_p)$ and $J(N_p)$ of a solution gas drive reservoir with initial pressure $p_i = p_b$.

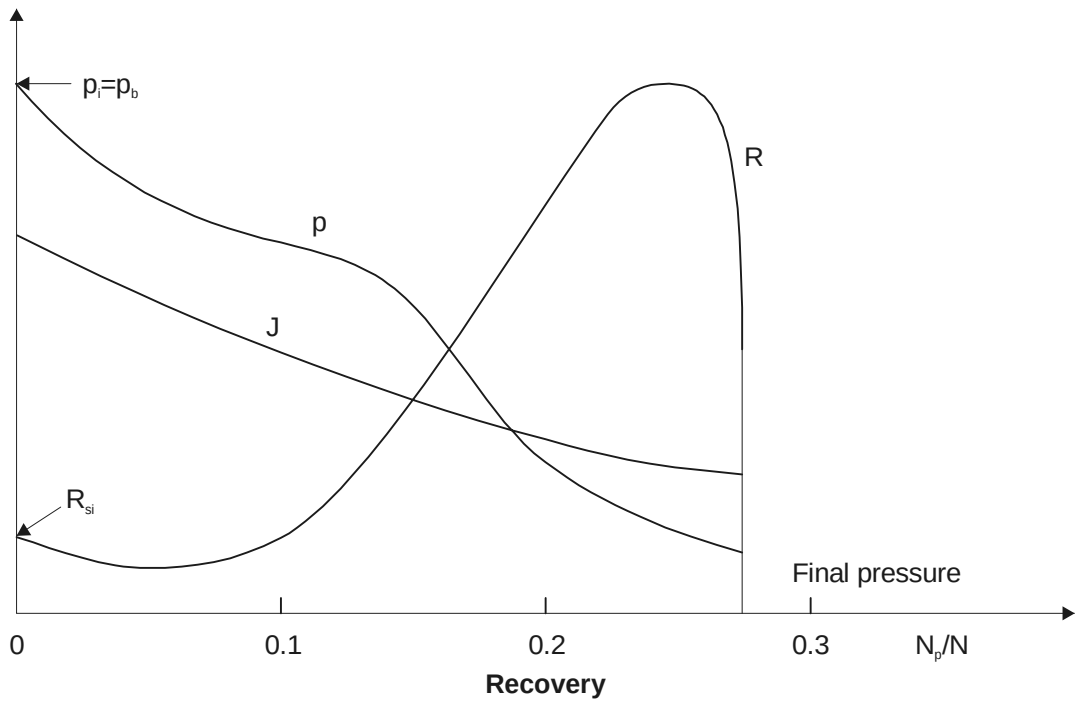

Figure 4.4: Pressure, production index and GOR as a function of the production N_p/N

4.2 Frontal Displacement

Due to pressure drop in the oil zone of the reservoir, the aquifer and gas cap expand, whereby the oil is displaced front-like by gas and water. This front is considered solely a transition zone between the displaced and displacing phase. Its size is very small in relation to the reservoir.

Not only natural depletion, but also artificial methods such as gas and water injection perform frontal displacement. Gas injection wells are situated inside the gas cap, water injection wells at the exterior boundary of the reservoir. If reservoirs have a minor thickness and inclination, the displacing phase can also be injected inside the oil zone. However, direction of flow and distribution of saturation are in this case much more complicated.

In modern reservoir engineering, these processes are calculated with numerical solutions of very complicated systems of differential equations. But this does not imply that analytical solutions of more simple and idealized models are superfluous. An essential aspect of these models is the possibility to make universal assertions and to have a quick overall picture of the considered case.

This chapter analyses several idealized models in order to describe frontal displacement.

4.2.1 BUCKLEY-LEVERETT Theory

This theory proves that displacement can proceed as a front and provides a clear description of how phase mobility and gravity influence this procedure. The calculation of front saturation and average saturation behind the front are additional aspects underlining the importance of this theory.

The BUCKLEY-LEVERETT[4.](1942) theory has proven successful for solutions of more complicated problems such as condensation gas drive, CO_2 gas drive or polymer flooding.

Explanations considering this theory were already given in the volume "*Fluid Flow in Porous Media"* (HEINEMANN[21.](1995)). Therefore it is only necessary to recall the most important aspects.

BUCKLEY and LEVERETT[4.](1942) assumed that:

1. the two fluids are non-compressible and immiscible,
2. the porous medium is homogeneous,
3. the displacement is one dimensional and stable,

4. the filtration can be described by the multiphase DARCY-law,
5. the capillary force is neglectable.

The equations for a one dimensional two phase filtration are

$$u_1 = -\frac{kk_{r1}}{\mu_1}\left(\frac{\partial p_1}{\partial x} + \rho_1 g \sin\alpha\right), \tag{4.17}$$

$$u_2 = -\frac{kk_{r2}}{\mu_2}\left(\frac{\partial p_2}{\partial x} + \rho_2 g \sin\alpha\right), \tag{4.18}$$

where α is the inclination of the direction of displacement. Phase 1 is the displacing phase, and can either be water or gas. Phase 2 is the displaced phase: oil or gas.

The difference between the two phase pressures p_1 and p_2 is regarded as the capillary pressure:

$$p_2 - p_1 = P_c(S_1). \tag{4.19}$$

This is neglected according to condition (5). Therefore,

$$p_2 = p_1 = p \ . \tag{4.20}$$

Let

$$u = u_1 + u_2 \tag{4.21}$$

be the overall filtration velocity, which is according to condition (1) independent of x.

The portion of the displacing phase f_1 referring to the overall flow is calculated with the help of Eq. 4.17 and Eq. 4.18.

Therefore

$$f_1(S_1) = \frac{u_1}{u} = \frac{\dfrac{\mu_2}{k_{r2}} - \dfrac{k(\rho_1 - \rho_2)g\sin\alpha}{u}}{\dfrac{\mu_1}{k_{r1}} + \dfrac{\mu_2}{k_{r2}}} \tag{4.22}$$

or

$$f_1(S_1) = \frac{1}{1 + \dfrac{k_{r2}}{k_{r1}}\dfrac{\mu_1}{\mu_2}}\left[1 - \frac{kk_{r2}(\rho_1 - \rho_2)g\sin\alpha}{\mu_2 u}\right]. \tag{4.23}$$

The function f_1 depends - due to the relative permeabilities - on the saturation S_1. Fig. 4.6 shows this function at a constant displacement velocity.

In the volume "*Fluid Flow in porous Media*" (HEINEMANN[21.](1995)) it was shown that every saturation value moves with the constant velocity:

$$w = \frac{u}{\phi} \frac{df_1}{dS_1} \quad . \tag{4.24}$$

This term is only a function of u and S_i. Thus, it is only necessary to know the initial saturation distribution and the displacement velocity in order to calculate the saturation distribution during the whole displacing process. This discontinuity is regarded as the front of displacement.

Fig. 4.5 illustrates the displacement process. The initial saturation can be zero (for example in case of a gas displacement) or it can be so small that *fluid* 1 becomes immobile ($S_{1i} < S1_c$, $S1_c$ is defined as the critical saturation). Otherwise it is large enough to be mobile.

Two periods are to be distinguished. The first period lasts until the front has reached L. This is regarded as the breakthrough. The front saturation S_{1F} can be determined graphically with the f_i-curve as shown in Fig. 4.7 The procedure is as follows:

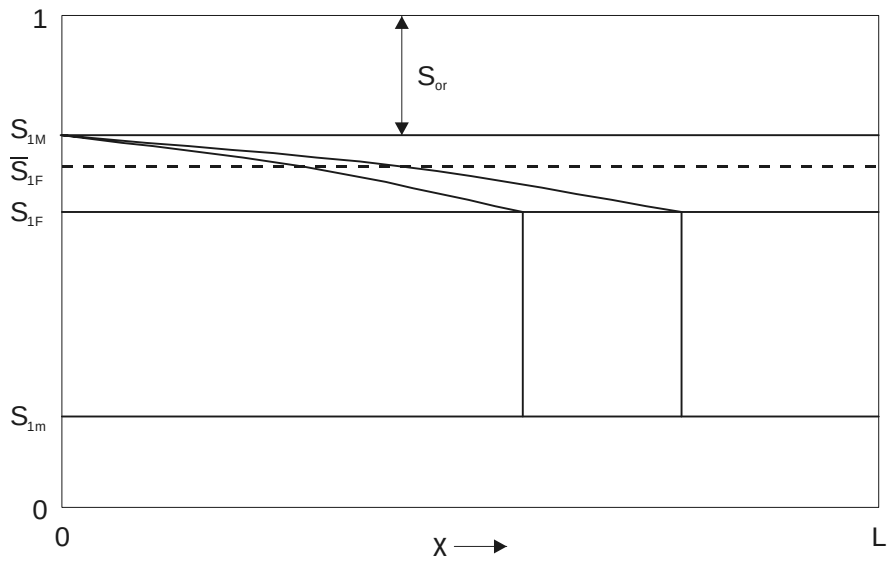

Figure 4.5: Illustration of the displacing process according to Buckley and Leverett

First a tangent is drawn from point S_{1i} to the curve. The tangential point indicates directly the front saturation and the fraction value of the front. In case the initial saturation (S_{1i}) is higher than the critical saturation (S_{1c}), the tangent is drawn from this initial value situated on the fractional flow curve to the curve itself.

Evidently the front saturation (S'_{1F}) will be smaller than before. The same is valid for the average saturation behind the front ($S'_{1F} < \bar{S}_{1F}$). Thus, the efficiency of the frontal displacement is smaller for $S_{1i} > S1_c$ than for $S_{1i} < S_{1c}$.

The average values of saturation behind the front ($\bar{S}_{1F} < \bar{S}_{1F}$) remain constant during the progression of the front until breakthrough is achieved.

On the right hand side of Fig. 4.7 a part of the fractional flow curve is drawn in magnification. The part of the curve between f_{1F} and $f_1 = 1$ describes the displacement conditions after breakthrough.

The proportion of the displacing phase f_{1L} increases continuously at the exit of the medium. Saturation at $x = L$ is S_{1L} and average saturation is $\bar{S}_{1L}$. The last value is the intersection on the $f = 1$ lines with the tangent drawn from the point $f_{1L}(S_{1L})$.

Eq. 4.24 enables the calculation of the date of breakthrough:

$$t_d = \frac{L}{w_f} = \frac{\phi L(\bar{S}_{1F} - S_{1i})}{u}. \tag{4.25}$$

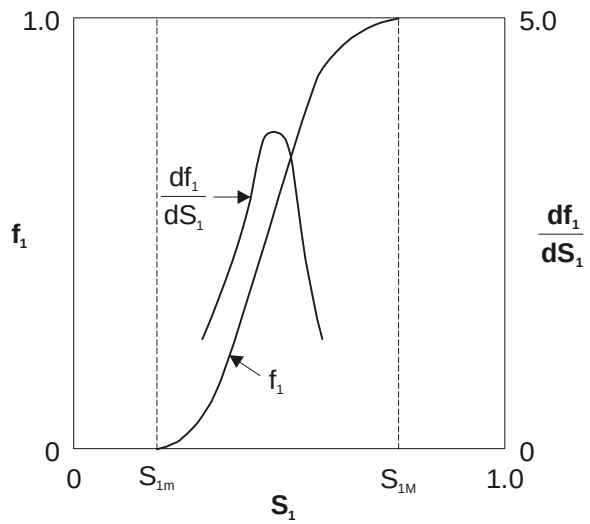

Figure 4.6: The fractional flow curve and its derivative

The displacing efficiency at and after breakthrough is defined as

$$E_D = \frac{\bar{S}_1 - S_{1i}}{1 - S_{1i}}. \tag{4.26}$$

4.2.2 Oil Displacement by Water

Fig. 4.8 left shows the relative permeability curves of a highly water wet and highly oil wet sandstone. Corresponding to this diagram is Fig. 4.9 right, which displays the fractional flow curves at the same viscosity ratio and horizontal displacement.

In case of a given relative permeability function, the viscosity ratio has a deciding influence on the fractional flow curve and therefore on displacement efficiency. Fig. 4.9 was calculated on the basis of Fig. 4.8. The influence of gravity is considered as an advantage if the displacing phase is the heavier one and displacement progresses from bottom to top, or if it is the lighter phase and displacement progresses from top to bottom.

The value f_w describes the fraction of water in the overall flow at reservoir conditions. The notion q_o and q_w are defined as the oil and water production in reference to the volume at surface conditions, therefore:

$$\frac{B_w q_w}{B_w q_w + B_o q_o} = f_w . \tag{4.27}$$

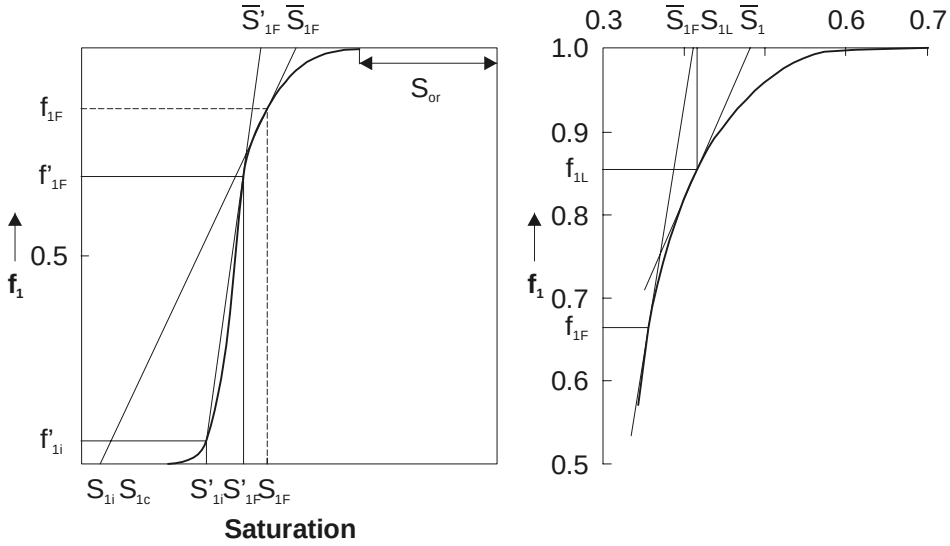

Figure 4.7: The fractional flow curve and graphical method of determining the front saturation and the average saturation behind the front.

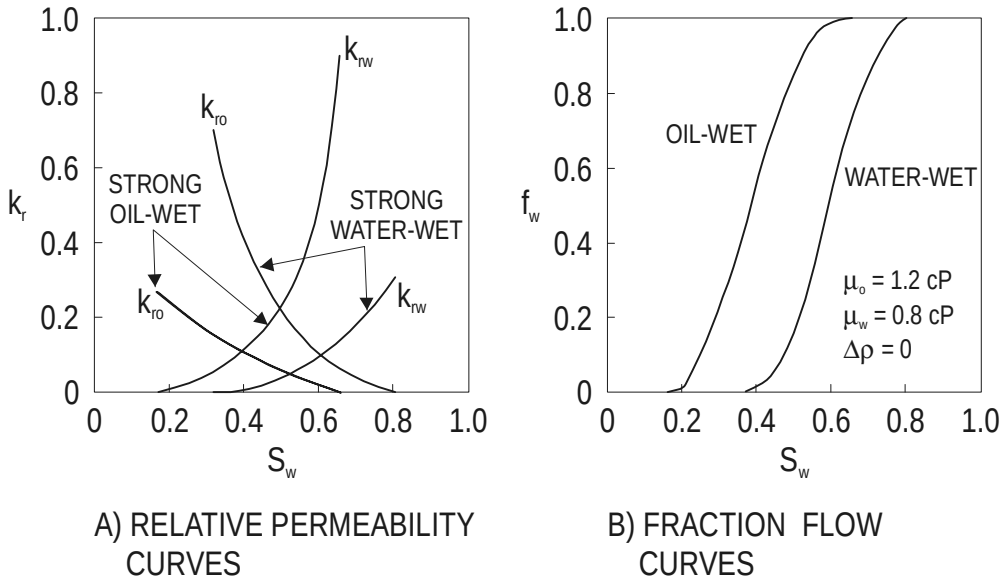

Figure 4.8: Influence of the wettability on relative permeability and fractional curves

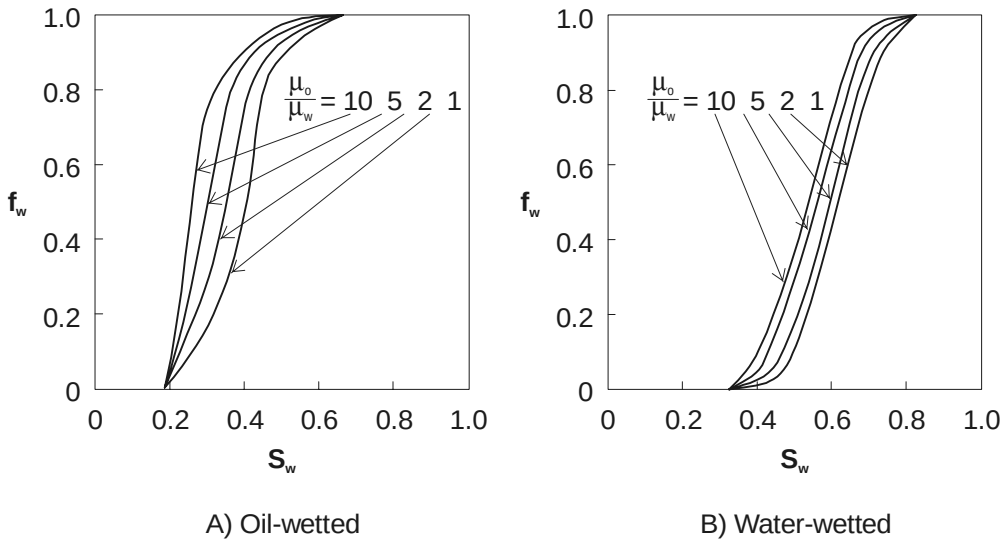

Figure 4.9: The influence of the viscosity on the fractional flow curve

In production statistics, the notions *water cut* (WC) or *water oil ratio* (WOR) are applied to describe water production

$$WC = \frac{q_w}{q_w + q_o}, \tag{4.28}$$

$$WOR = \frac{q_w}{q_o}. \tag{4.29}$$

From Eq. 4.27 and Eq. 4.29:

$$WOR = \frac{B_o}{B_w}\frac{f_w}{1-f_w} \tag{4.30}$$

4.2.3 Influence of Free Gas Saturation on Water Displacement

Often water displacement takes place when a gas saturation has developed as a consequence of solution gas drive or gas displacement. Gas is mobile if $S_g > S_{gc}$. Now the relative permeabilities are a function of two variables:

$$k_{rw} = k_{rw}(S_w, S_o), \qquad k_{ro} = k_{ro}(S_w, S_o), \qquad k_{rg} = k_{rg}(S_w, S_o). \tag{4.31}$$

These are illustrated by a triangular diagram (Fig. 4.10). Fig. 4.11 shows a schematic illustration of the displacing process. The first section shows the existence of two mobile phases: oil and gas. The connate water is immobile and the free gas is displaced by the accumulating oil. Due to the fact that gas has a greater mobility than oil, the remaining gas saturation behind the front will be practically immobile. The gas saturation is also diminished by pressure increase effecting compression and solution in the oil.

A three phase displacement can only be calculated numerically. An approximation is possible by applying the two phase flow equations because there are only two mobile phases present at a specific section. The BUCKLEY-LEVERETT[4.](1942) solution is satisfactory for the calculation of the oil-gas and water-oil front saturations and material balance can be used to calculate the extension of the oil bank.

According to laboratory experiments, the gas saturation in an oil bank (S_{gt}) depends on the initial gas saturation (S_{gi}). Fig. 4.12 shows a summary of several results achieved by CRAIG[8.](1971).

4.2.3.1 The Residual Oil Saturation

The residual oil saturation is defined by the relative permeability function. This is the non-reducible oil saturation achieved during a steady-state-measurement of relative permeability at an increasing water saturation (imbibition).

Therefore, this saturation does not coincide with the oil saturation after displacement by water since it depends on several other parameters such as velocity of displacement, oil viscosity, capillary pressure function, injected pore volume.

Fig. 4.13 demonstrates the effects of gas saturation on oil saturation after a complete water

flooding in the case of water wet reservoir rock. This free gas saturation can have a beneficial effect on the displacing efficiency (assuming that no other factors oppose).

In case of an oil wet reservoir, no specific associations between initial gas saturation and oil saturation after a water flooding are detectable. The influence depends on pore structure, viscosity ratio, injected amount of water and displacing velocity.

The presence of gas diminishes the mobility of water and thereby can be considered beneficial for displacement. This facts results, as shown in Fig. 4.14, in a smaller amount of water needed.

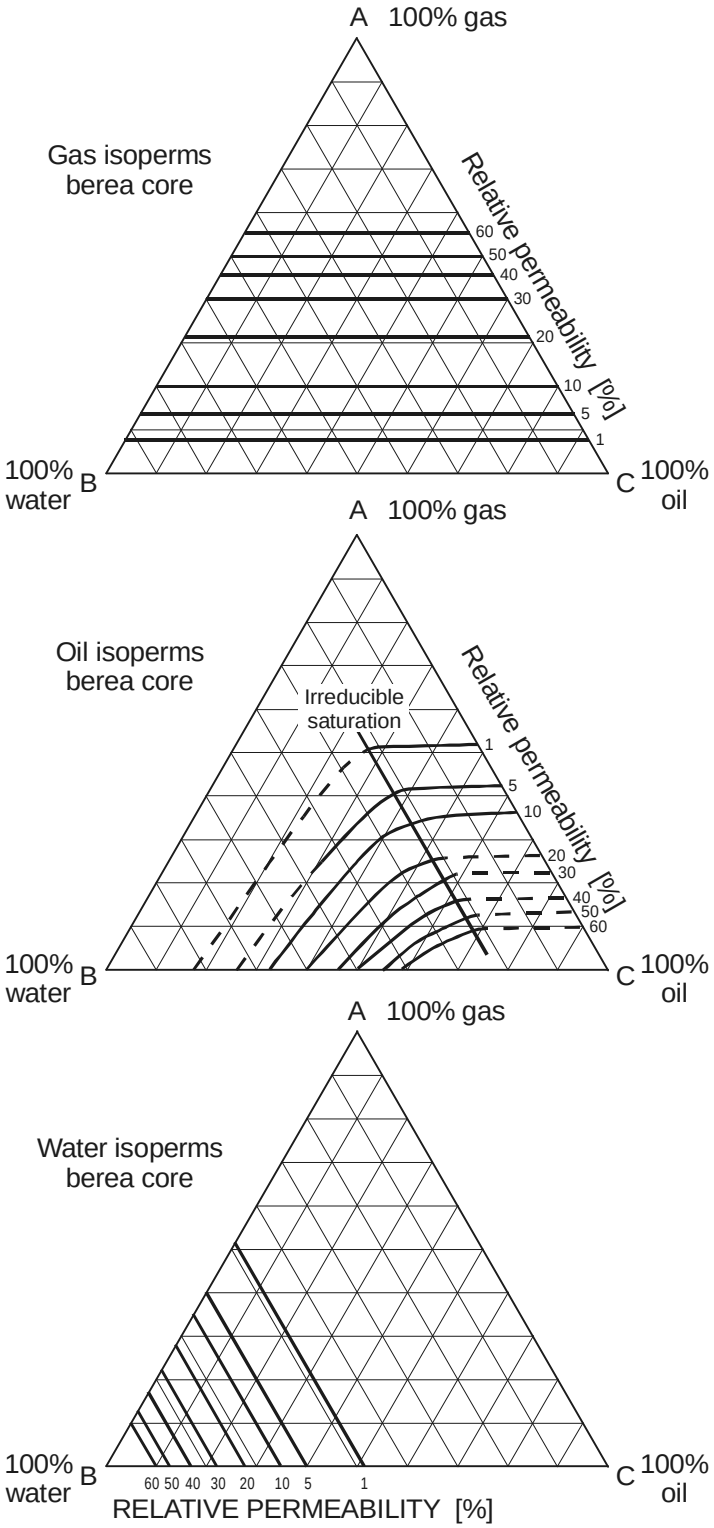

Figure 4.10: Three-phase relative permeability functions (from Petroleum Production Handbook, Vol. 11, 1962)

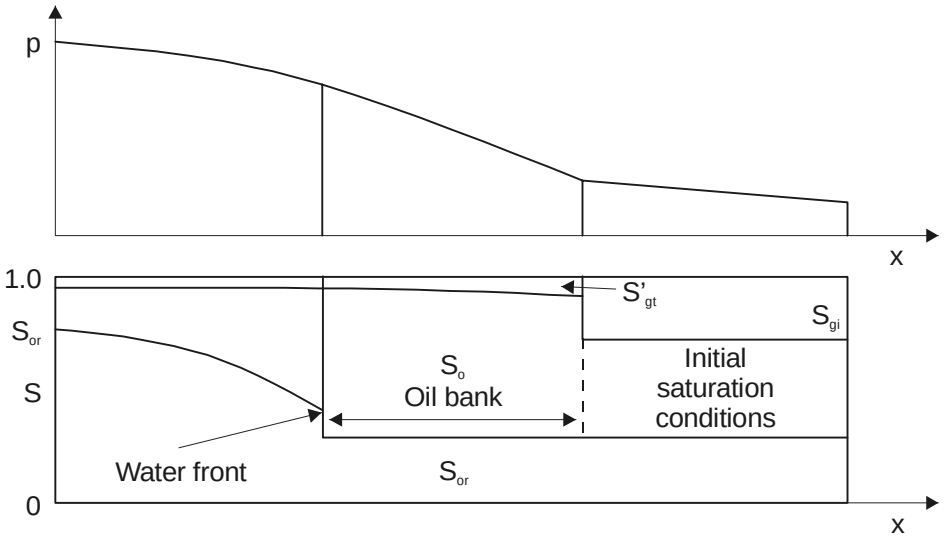

Figure 4.11: Water displacement at free gas saturation

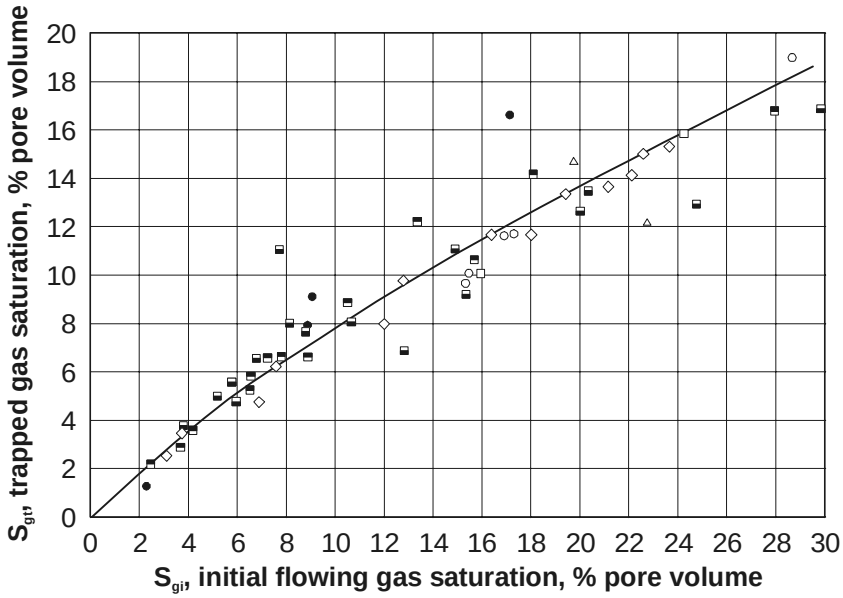

Figure 4.12: Correlation between initial gas saturation and residual gas saturation (after CRAIG, 1971)

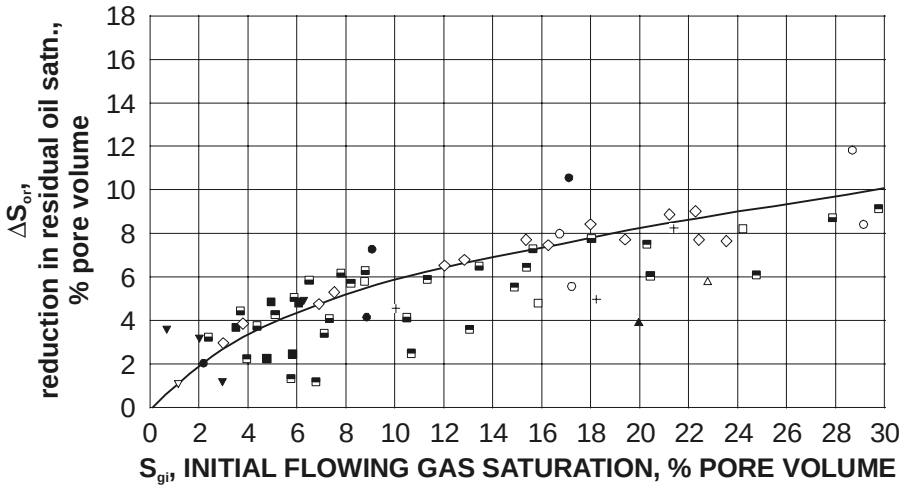

Figure 4.13: Influence of initial gas saturation on the efficiency of water displacement (after CRAIG, 1971)

4.2.4 Displacement by Gas

By assuming that the phases are incompressible and the gas will not dissolve in oil, the BUCKLEY-LEVERETT[4.](1942) theory can be applied for frontal gas displacement. This is the case when displacement occurs at constant pressure with very small depression.

The critical gas saturation at which the gas becomes immobile lies between 0 and 0.12. Fig. 4.15 shows for the same relative permeability functions for different *fractional flow curves.* μ_g is assumed 2 x 10-5 *Pas* [0.02 *cP*] and $\rho_o - \rho_g = 700$ *kg/m*^{3} [43.71 *lbm/cuft*].

Diagram b) displays the influence of the oil viscosity in case of horizontal displacement and diagram c) the influence of gravity. At low velocities, gas displacement in a vertical direction can also achieve favorable results also with viscous oils.

The influence of the displacement velocity is illustrated in diagram d).

The BUCKLEY-LEVERETT[4.](1942) theory may be applied for calculation of the displacement caused by the expanding gas cap or better by a gas injection into the gas cap. In these cases, one can assume that the gas does not condensate in the oil (i.e. it does not dissolve). Gas injection into the oil zone is sometimes associated (i.e. it does not dissolve). Gas injection into the oil zone is sometimes associated with a pressure higher than a reservoir pressure, which means that gas dissolved in the oil enlarges the volume and diminishes the viscosity of the oil. This process is called condensation gas drive. Fig. 4.16 shows a linear gas displacement at constant connate water saturation S_{wi}. At the front, the gas saturation is S_{gf} which increases at $x = 0$ to the value $S_{gmax} = 1 - S_{wi} - S_{or}$.

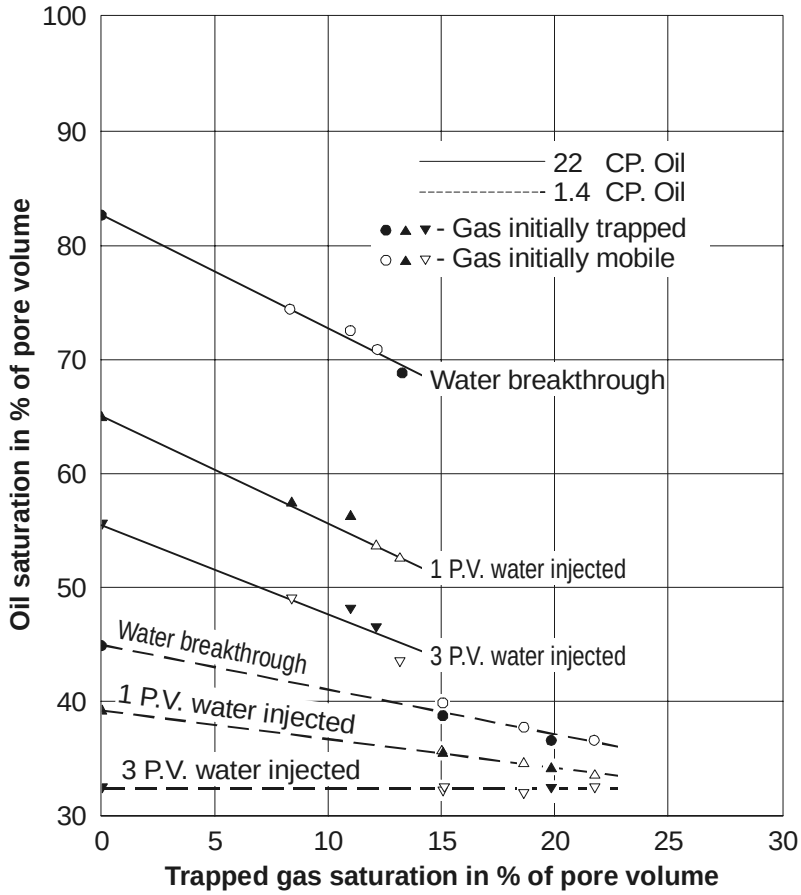

Figure 4.14: Relation between residual gas saturation and oil saturation in case of water flooding (after KYTE et al, 1956)

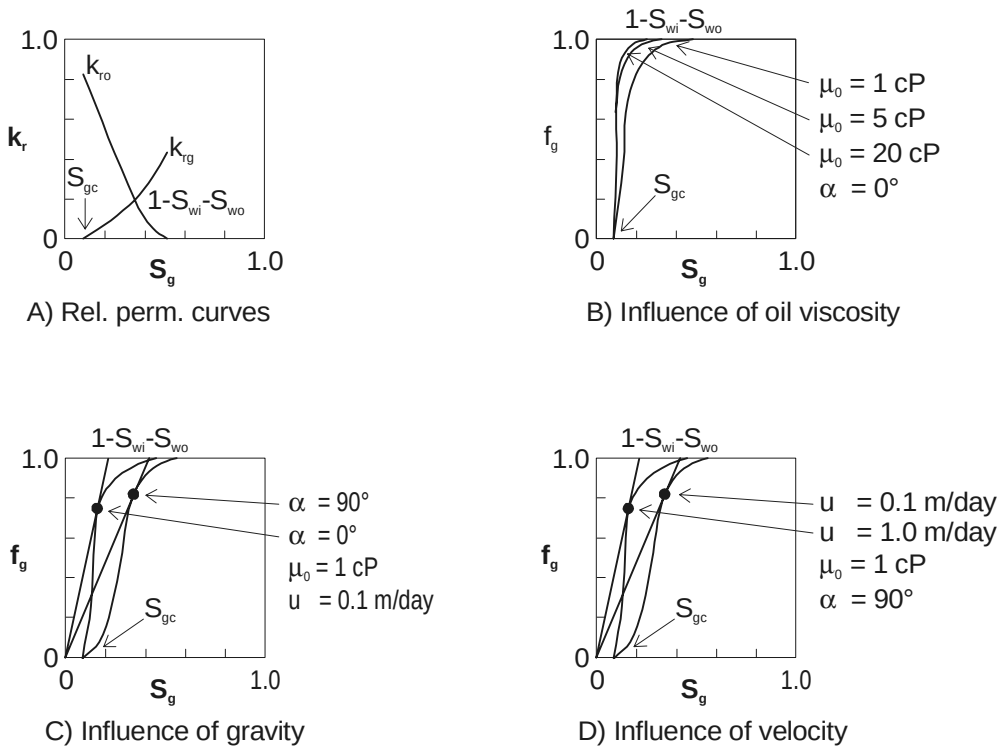

Figure 4.15: Illustration of gas displacement when using the BUCKLEY-LEVERETT theory

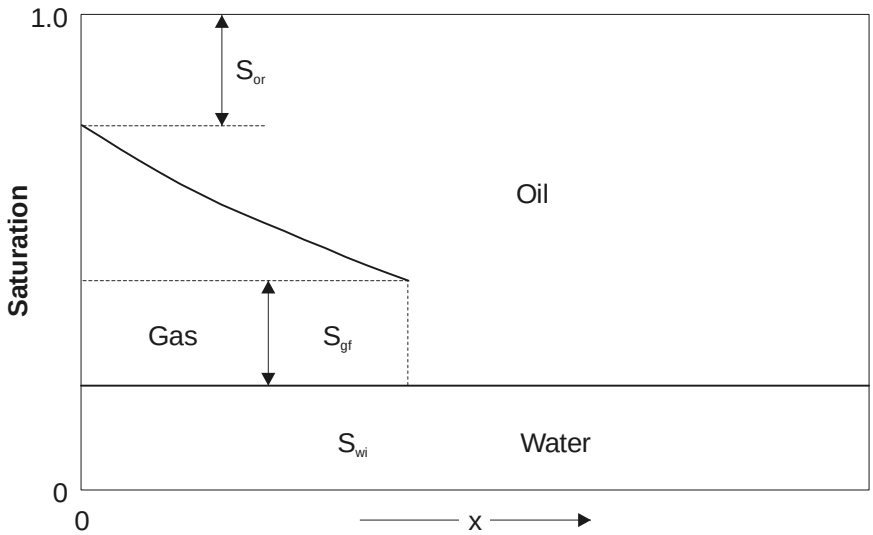

Figure 4.16: Distribution of saturation in case of condensation gas drive

For a specific date *t*, gas balance can be defined as follows:

Injected gas = free gas + additional dissolved gas.

$$q_g t = \frac{A\phi}{B_g}\left[S_{gf}\, x_f + \int_{S_{gf}}^{1-S_{wi}-S_{or}} x(S_g)\, dS_g \right. \\ \left. + A\phi \frac{(R_s - R_{si})}{B_o}\left[(1 - S_{wi} - S_{gf}) x_f - \int_{S_{gf}}^{1-S_{wi}-S_{or}} x(S_g)\, dS_g \right] \right] \tag{4.32}$$

q_g is the gas injection rate, A the surface and R_s - R_{si} the increase of dissolved gas. The distance x_f or $x(S_g)$ are calculated according to the BUCKLEY-LEVERETT[4.](1942) theory from Eq. 4.25:

$$x_f = w_f\, t = \frac{ut}{\phi}\, f'_{gf} = \frac{B_g q_g t}{A\phi}\, f'_{gf} \tag{4.33}$$

and

$$x(S_g) = \frac{B_g q_g t}{A} f'_{gf} \tag{4.34}$$

x_f and $x(S_g)$ are inserted into Eq. 4.32:

$$q_g t = \frac{A\phi}{B_g}\frac{B_g q_g t}{A\phi}\left\{ S_{gf}\, f'_{gf} + 1 - f_{gf} \right. \\ \left. + \frac{B_g (R_s - R_{si})}{B_o}\left[(1 - S_{wi} - S_{gf}) f'_{gf} - 1 + f_{gf} \right] \right\} \tag{4.35}$$

or

$$f_{gf} + a = f'_{gf}\,(S_{gf} + b)\,, \tag{4.36}$$

where

$$a = \frac{B_g (R_s - R_{si})}{B_o - B_g (R_s - R_{si})}, \tag{4.37}$$

$$b = (1 - S_w)\frac{B_g (R_s - R_{si})}{B_o - B_g (R_s - R_{si})}. \tag{4.38}$$

Comparison of Eq. 4.35 with the common BUCKLEY-LEVERETT[4.](1942) equation for $S_{gi} = 0$ leads to

$$f_{gf} = f'_{gf}\, S_{gf}. \tag{4.39}$$

This proves that the condensation gas drive can be designed graphically by coordinate transformation (see Fig. 4.17). The tangent to the f_g curve is drawn from the point (-b,a), left from the origin.

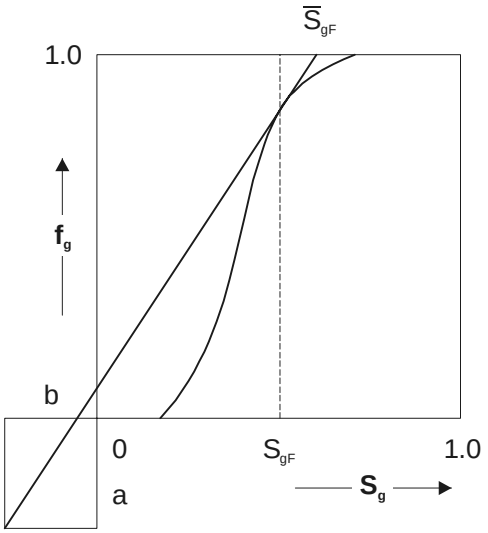

Figure 4.17: Graphical determination of the front saturation by condensation gas drive

Example 4.1

A linear water displacement is to be calculated. The following reservoir parameters are available:

Length	m[ft]	L	500 [1640]
Width	m[ft]	b	200 [656.2]
Thickness	m[ft]	h	10 [32.8]
Inclination	[$Grad$]	a	60
Porosity	[-]	f	0.20
Initial water saturation	[-]	S_{wi}	0.27
Permeability	m^2[md]	k	5.0×10^{-13} [506.6]
Oil:			
Formation volume factor B_{oi}	[-]	B_{oi}	1.22
Viscosity	Pas [cP]	μ_o	2×10^{-3} [2]
Density	kgm^{-3}[$lbm/cuft$]	ρ_o	700 [43.69]
Water:			
Formation volume factor B_{wi}	[-]	B_{wi}	1.01
Viscosity	Pas [cP]	μ_w	0.7×10^{-3} [0.7]

Density	$kgm^{-3}[lbm/cuft]$	ρ_w	980 [61.17]
Filtration velocity	$ms^{-1}[ft/s]$	u	$1.16\text{x}10^{-6}$ [$3.805\text{x}10^{-6}$]
Relative permeability	[-]	k_r	(see Tab.3.3.1)

Solution

The reservoir contains

$$\frac{L \cdot b \cdot h \cdot \phi(1 - S_{wi})}{B_{oi}} = 119670\ m^3 OOIP$$

In field units:

$$\frac{7758 \times 1640 \times 656.2 \times 32.8 \times (1/43560) \times 0.2 \times (1 - 0.27)}{1.22} =$$

$$= 7.5233 \times 10^5 bbl\ \ OOIP$$

The *fractional flow curve* is calculated with Eq. 4.24 in columns (4) and (5) in Table 4.1.

Table 4.1: Calculation of the Fractional Flow Curve

S_w (1)	k_{rw} (2)	k_{ro} (3)	(4)	f_w (5)
0.27	0.0000	1.000	0.0000	0.0000
0.35	0.0013	0.560	0.0066	0.0047
0.40	0.0050	0.440	0.0314	0.0244
0.45	0.0130	0.330	0.1012	0.0841
0.50	0.0250	0.235	0.2331	0.2050
0.55	0.0500	0.165	0.4640	0.4248
0.60	0.0800	0.115	0.6653	0.6261
0.65	0.1200	0.070	0.8304	0.8006
0.70	0.1650	0.045	0.9129	0.8918
0.75	0.2200	0.023	0.9647	0.9533
0.82	0.3100	0.000	1.0000	1.0000

Fig. 4.18 shows the f_w-curve. The tangent drawn from S_{wi} to the f_w-curve enables the determination of the front saturation: $S_{wF} = 0.65$, $\bar{S}_{wF} = 0.74$.

At breakthrough, the oil recovery (now identical with the displacement efficiency) is calculated using Eq. 4.27:

$$Column(4) = \frac{1}{1 + \frac{\mu_w}{k_{rw}}\frac{k_{ro}}{\mu_o}}$$

$$Column(5) = \left[1 - \frac{kk_{ro}(\rho_w - \rho_o)g\sin\alpha}{\mu_o u}\right] \times (4)$$

The displacement efficiency is

$$E_D = \frac{\bar{S}_{wF} - S_{wi}}{1 - S_{wi}} = \frac{0.74 - 0.27}{1 - 0.27} = 0.644 \tag{4.40}$$

I is defined as the produced (or injected) pore volume. It is obvious that

$$dE_D = \frac{1 - f_w}{S_{wi}} dI\,. \tag{4.41}$$

Until breakthrough, $f_w \equiv 0$ and therefore

$$E_{Dd} = \frac{I_d}{1 - S_{wi}}\,. \tag{4.42}$$

The function $E_D(I)$ is linear. After breakthrough, one must proceed as follows:

1. Values for $S_{wf} < \bar{S}_{w1} < \bar{S}_{w2} < ...$ are assumed at regular distances.
2. At every specific $\bar{S}_{wj}$ the corresponding E_{Dj} is determined from Eq. 4.40.
3. A tangent is drawn from the middle of the considered interval ($\bar{S}_{wj}$, $\bar{S}_{wj+1}$) to the f_w-curve. The tangent points are the f_{wj+1} values.
4. From the finite form of Eq. 4.41 ΔI is obtained:

$$\Delta_{j+1}E_D = E_{Dj+1} - E_{Dj} = \frac{1 - f_{wj+1}}{1 - S_{wi}}\Delta_{j+1}I \tag{4.43}$$

and

$$I = I_d + \sum_{j=0}^{m} \Delta_{j+1}I \tag{4.44}$$

Calculations (1) - (4) are demonstrated in Table 4.2. Results are displayed in Fig. 4.19.

Table 4.2: Calculation of the Recovery Curve

S_w	F_w	E_D	ΔE_D	ΔI	I
0.74	0.810	0.6438	0.0000	0.0000	0.4700
0.75	0.815	0.6575	0.0137	0.0541	0.5241
0.76	0.860	0.6712	0.0137	0.0714	0.5955
0.77	0.890	0.6849	0.0137	0.0909	0.6864
0.78	0.910	0.6986	0.0137	0.1111	0.7975
0.79	0.932	0.7123	0.0137	0.1471	0.9446
0.80	0.952	0.7260	0.0137	0.2084	1.1530
0.81	0.970	0.7397	0.0137	0.3334	1.4863
0.82	0.980	0.7534	0.0137	0.5000	1.9864

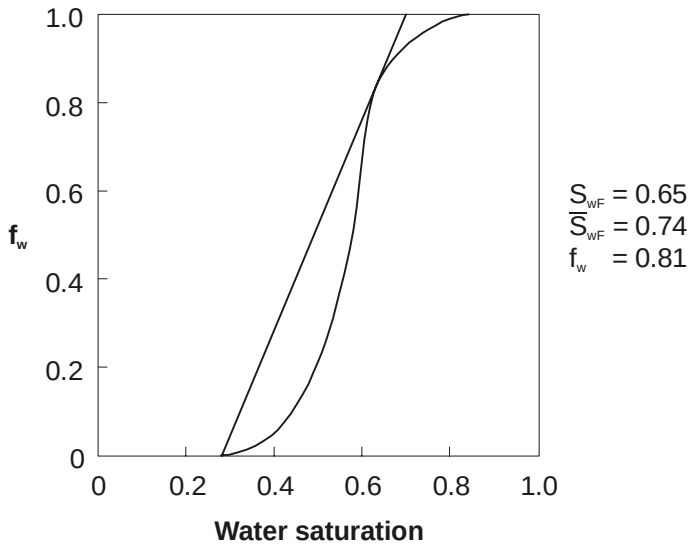

Figure 4.18: Fractional flow curve to Example 4.1

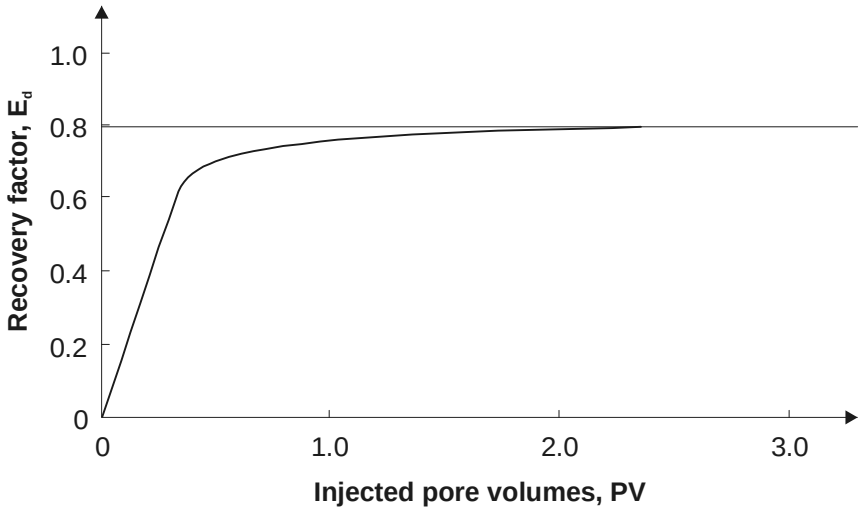

Figure 4.19: Oil recovery curve according to Example 4.1

Chapter 5

Sweep Efficiency

5.1 Mobility Ratio

In the theory of piston like displacement, it is assumed that ahead of the front only the displaced fluid - for example the oil - is flowing and the oil saturation is presumed as $S_{oi} = 1 - S_{wi}$, where S_{wi} is the initial immobile water saturation.

Behind the front, the displacing fluid is flowing - for example water - and the water saturation is $S_w = 1 - S_{or}$, where S_{or} is the immobile residual oil saturation. Further, the mobility ratio is defined as

$$M_{ow} = \frac{\lambda_w}{\lambda_o} = \frac{k_{rwM}}{\mu_w} \Big/ \frac{k_{roM}}{\mu_o} \tag{5.1}$$

where

λ_w, λ_o	-	are the water and oil mobilities
k_{rwM}	-	is the relative permeability of the water behind the front
k_{roM}	-	is the relative permeability of the oil before the front

The mobility ratio is essential for determining the characteristics of the displacement.

- If $M_{ow} \leq 1$ then the displaced fluid - the oil - is more mobile than the displacing fluid. This is beneficial for the displacement.
- If $M_{ow} > 1$ then the reverse situation is given.

The above definition is valid in a waterflooding in which there is no saturation gradient behind the waterflood front and consequently there is no ambiguity about the value of

displacing phase relative permeability. In case of a saturation gradient, the displacing phase mobility is defined at the average displacing fluid saturation - e.g. water saturation $\bar{S}_w$ - in the displaced pore volume of the reservoir. This definition has been proved by CRAIG *et al.*[7.](1955).

5.2 Stability of Displacement

The theory of BUCKLEY-LEVERETT[4.](1942) presumes that the displacing front proceeds in an uniform way. ENGELBERTS and KLINKENBERG[15.](1951) observed that in most cases so-called viscous fingers proceed ahead of the front. If the front catches up with the fingers then the displacing front can be regarded as stable, in the reverse case as unstable. In Fig. 5.1 illustrated cases the capillary force is zero and the fluid densities are equal. In case a) the Mobility Ratio M = 1. As it can be seen, the front is stable and the majority of the oil is displaced before breakthrough. In case b) M = 80. Early breakthrough and low displacement efficiency is manifested due to the viscous fingering.

Another aspect is that the capillary force and gravity can have a favorable effect on the stability of the front. Fig. 5.2 shows a displacement of oil from bottom to top by the heavier water which is the wetting fluid. Capillary forces tend to widen the finger and gravity tends to segregate the phases vertically. Both effects can be considered to be independent of the displacement velocity.

The tendency to instability increases with rising displacement velocity. If displacement proceeds slowly enough, time remains for the stabilization of the front through capillary forces and gravity. Reasons for the development of such a finger can be caused by local irregularities of the porous medium. The width of the finger depends directly on the extension of this inhomogeneity. If a porous medium is macroscopically considered homogeneous, this appearance will result in a flattening of the saturation profile.

If the development of the finger is due to a macroscopically detectable change of properties (in most cases the permeability) then the whole problem can be regarded as the movement of a front progressing in a stratified medium. Reservoirs are more or less stratified, which infers that viscous fingering is due to heterogeneity.

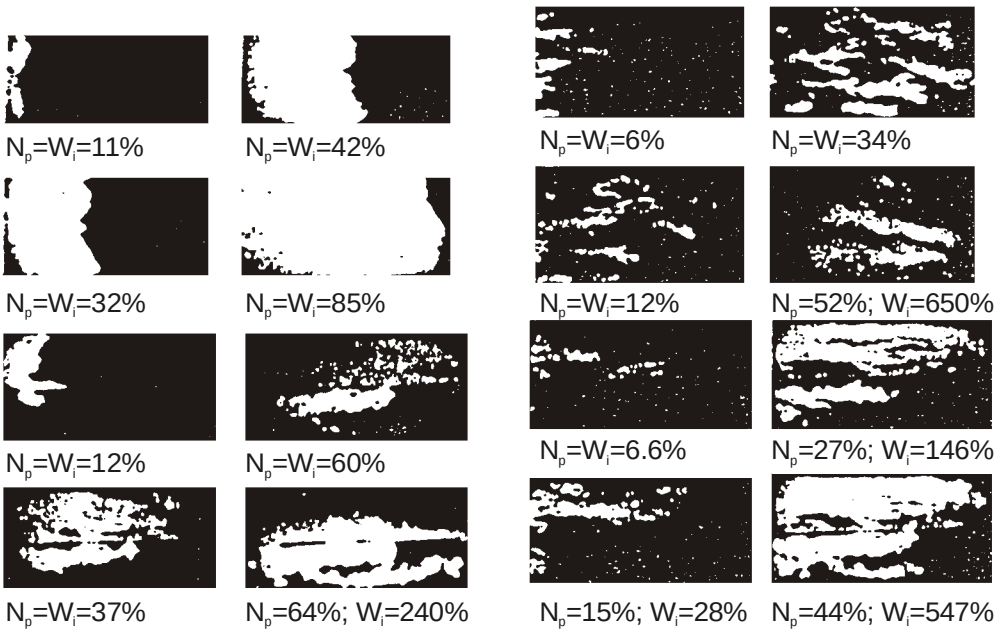

Figure 5.1: Linear water displacement demonstrated by a transparent three dimensional model (VAN MEURS 1957)

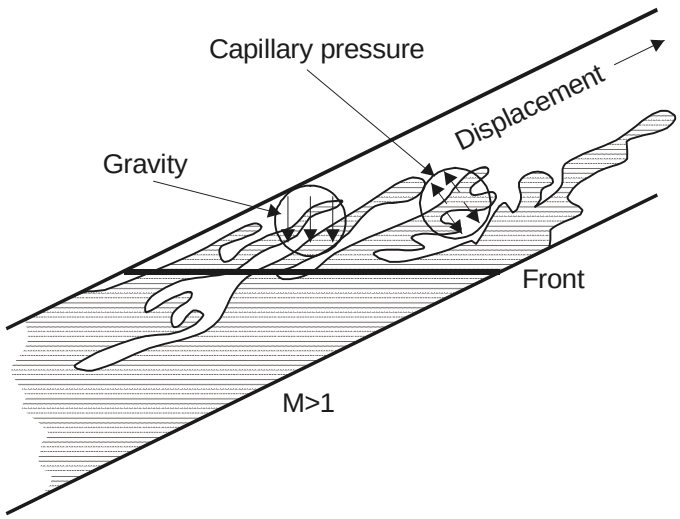

Figure 5.2: Capillary forces and gravity influence the development of a viscous fingering

5.3 Displacement in Dipping Layers

5.3.1 Position of the Displacing Front

Fig. 5.3 shows a non-horizontal layer in which the displaced and displacing fluid are in static equilibrium. In case $\rho_w > \rho_o$, the heavier displacing fluid is below and the interface will be horizontal, that means vertical to the vector of gravity $(\rho_w - \rho_o)g\vec{i}_3$. It is assumed that displacement is piston-like. Before the front only the displaced fluid with a mobility of k_{ro}/μ_o is flowing and behind the front only the displacing fluid with a mobility of k_{ro}/μ_w.

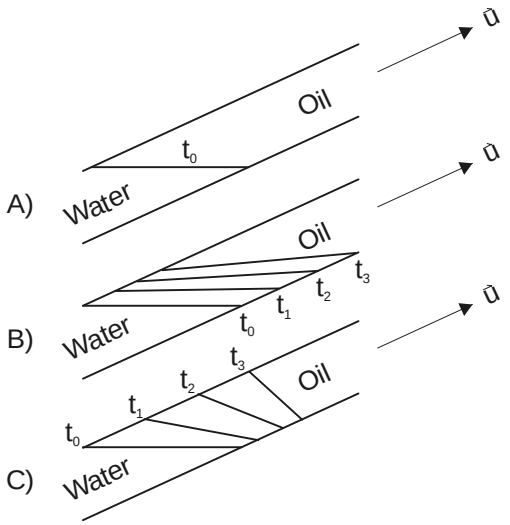

Figure 5.3: Initial position of the water-oil contact (a) and possible changes during displacement (b)(c)

In volume "*Fluid Flow in Porous Media"*, based on the results of DIETZ[12.](1953), it was proven that in this case the front is perpendiculare (orthogonal) to the vector $\vec{w}$:

$$\vec{w} = (\rho_w - \rho_o)g\vec{i}_3 + \frac{\vec{u}\mu_w}{kk_{rw}}(1 - M_{ow}) . \tag{5.2}$$

This position is pseudo-steady-state and stable, if

$$\rho_w > \rho_o \quad \text{and} \quad M_{ow} \le 1 . \tag{5.3}$$

If the displacement velocity increases, the front will become steeper (see Fig. 5.4).

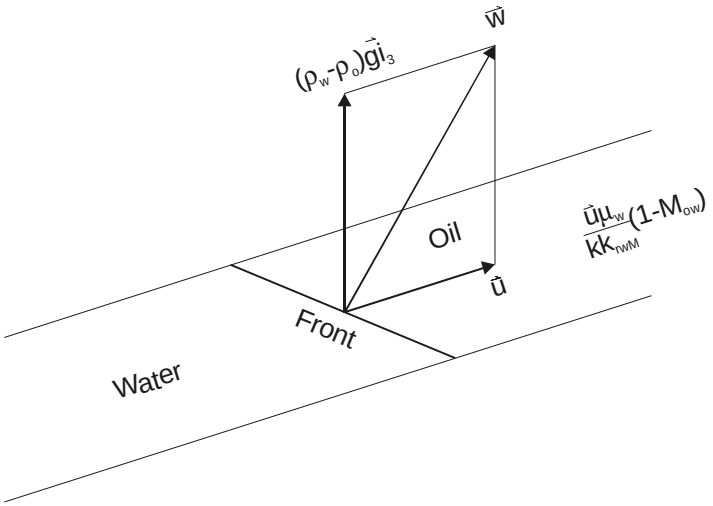

Figure 5.4: Position of the interface at opportune relation of mobilities ($M_{ow} \leq 1$)

In case

$$\rho_w > \rho_o \quad \text{but} \quad M_{ow} > 1\,, \tag{5.4}$$

the front will flatten with the increase of front velocity. If the velocity surpasses a certain critical value, then no more frontal displacement is possible. The displacing fluid underruns the displaced one.

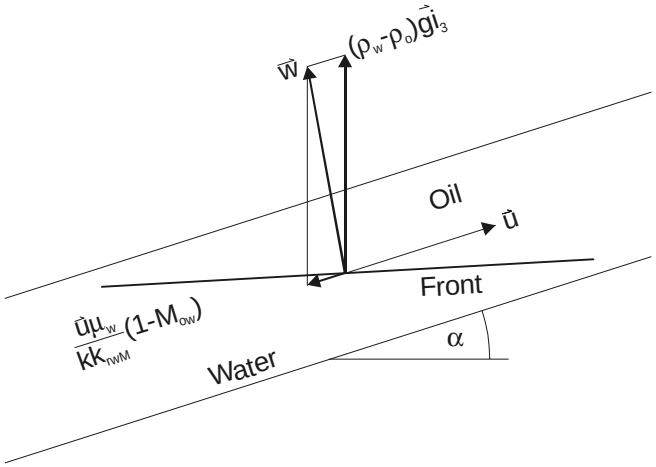

Figure 5.5: Position of the interface at an unfavorable mobility ratio ($M_{ow} > 1$)

This critical velocity can be calculated easily since the $\vec{w}$ is perpendicular to the axis of symmetry of the layer and the scalar product with $\vec{u}$ becomes zero (see Fig. 5.5).

$$u_c = -\frac{k(\rho_w - \rho_o)g\sin\alpha}{\frac{\mu_w}{k_{rwM}} - \frac{\mu_o}{k_{roM}}} = -\frac{kk_{rwM}(\rho_w - \rho_o)g\sin\alpha}{\mu_w(1 - M_{ow})}, \tag{5.5}$$

where u_c is the critical velocity.

If the displacement velocity exceeds the critical value, then the displacement is called *supercritical displacement.*

The critical velocity is a theoretical issue and has no practical importance. If $M > 1$ then in real field cases $u_c < 1$ m/year. No field can be operated with under this condition. In case of $M > 1$ the displacement process will be always supercritical.

5.3.2 Vertical Saturation Distribution

In case of an one-dimensional linear displacement by a wetting fluid, the capillary force effects an extension of the saturation profile. Nevertheless, this profile can be approximated by a discontinuity, because the extension is not significant. The real shape of the saturation profile can be calculated by numerical methods only which can take capillary forces into consideration too. Capillary forces play an important role in dipping layers. Fig. 5.6 shows a supercritical displacement of oil by water in a water-wet reservoir. Then considering a particle at the fluid-fluid interface, capillary forces are effective in the direction perpendicular to the interface and gravity in direction of $\vec{i}_3$.

Analysis of the components of these forces in the direction of displacement and perpendicular to this direction shows the importance of considering these forces. If the front velocity ranges between 0.1 - 0.3 m/d [0.3 - 1 ft/d] there will be enough time to achive the equilibrium between the capillary and gravity forces (at least a nearby equilibrium). On the left hand side of Fig. 5.7 the capillary pressure curve of the reservoir and the relative permeability curves are displayed.

The reading from the permeability curves is made nomogram-like following the doted line. The layer thickness *h* is messured vertical (apparent thickness) and not perpendicular to the layer (which is the true thickness).

The hydrostatic pressure difference between the top and the bottom of the layer is determined by the density of the wetting fluid (water). This pressure difference is considered in balance with the difference of the capillary pressures.

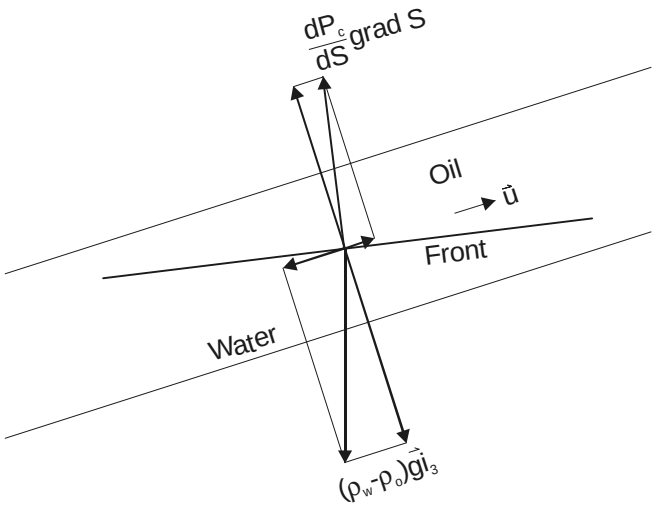

Figure 5.6: Influence of capillary forces and gravity on a supercritical displacement

At a thickness *h*, the difference in capillary pressure is

$$\Delta P_c = h\Delta\rho g\cos\alpha\,. \tag{5.6}$$

When regarding a specific section of the left hand diagram, the vertical distribution of saturation and the relative permeabilities can be determined. It is then simple to calculate the average saturation and relative permeabilities:

$$\bar{S}_w = \frac{1}{h}\int_o^h S_w(h)dh\,, \tag{5.7}$$

$$\bar{k}_{rw} = \frac{1}{h}\int_o^h k_{rw}(h)dh\,, \tag{5.8}$$

$$\bar{k}_{ro} = \frac{1}{h}\int_o^h k_{ro}(h)dh\,. \tag{5.9}$$

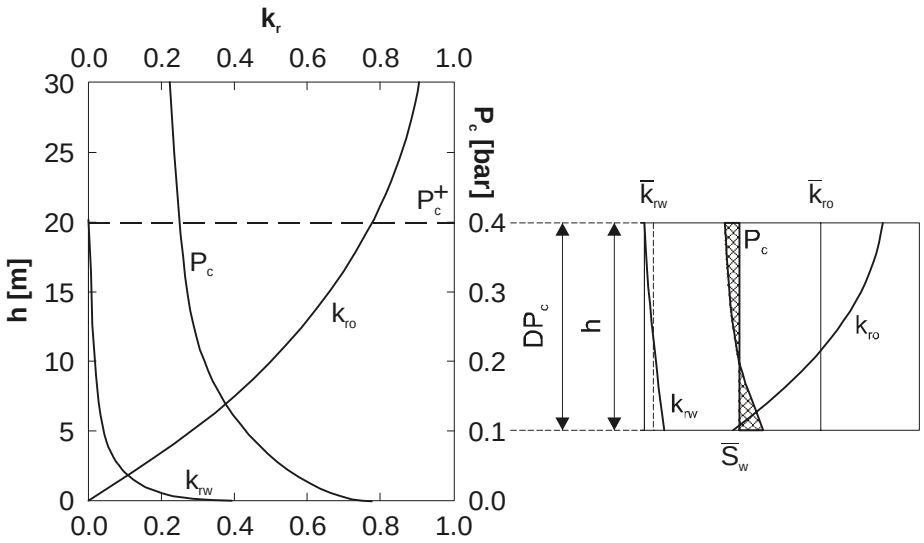

Figure 5.7: Calculation scheme of relative permeabilities for vertical equilibrium

By moving the distance h along the vertical axis, more corresponding values are obtained. Calculation of an average capillary pressure would be of no use. Thus, the capillary pressure at the top is referred to the saturation $\bar{S}_w$. The resulting notions are:

$$\bar{k}_{rw} = \bar{k}_{rw}(\bar{S}_w) \tag{5.10}$$

$$\bar{k}_{ro} = \bar{k}_{ro}(\bar{S}_w)$$

$$P_c^+ = P_c^+(\bar{S}_w)$$

$\bar{k}_{ro} = \bar{k}_{ro}(\bar{S}_w)$ The notions in Eq. are all functions of *h*.

Fig. 5.8 and Fig. 5.9 show the P_c^+ and $\bar{k}_r$-functions determined by Fig. 5.7 for $\Delta g \cos\alpha = 200\ kg/m^3 [12.5\ lbm/cuft]$ and h = 1, 5, 10, 15, 20 and 25 m [3.28, 16.4, 32.8, 49.2, 65.6 and 82.0 *ft*]. The integrals Eq. 5.7 - Eq. 5.9 transform the two dimensional displacement into a one dimensional linear problem, which allows the application of the BUCKLEY-LEVERETT[4.](1942) theory. The fractional flow curve is now calculated by the pseudo-relative permeability functions.

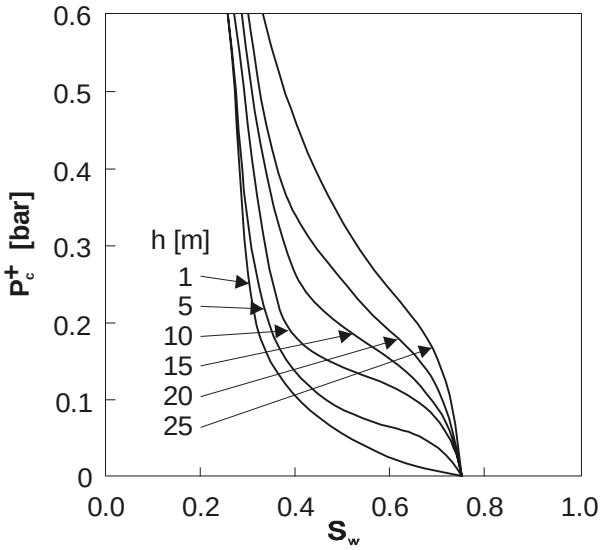

Figure 5.8: Pseudo-capillary pressure curves

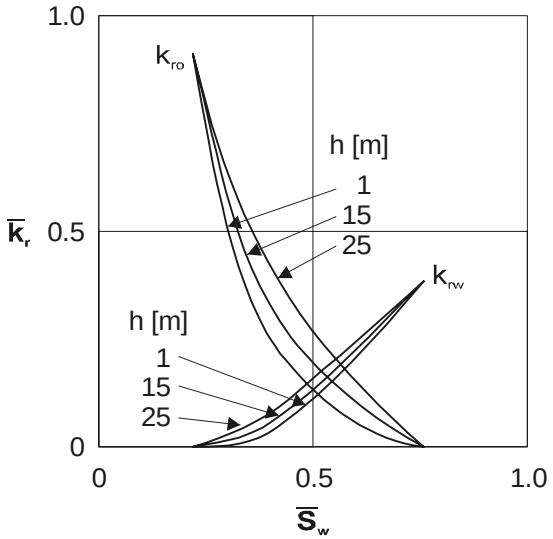

Figure 5.9: Pseudo-relative permeability curves

5.4 Displacement in Stratified Reservoirs

The following sections refer to water flooding, but are valid for all other kinds of displacement (water-gas, gas-oil) too.

5.4.1 Vertical Permeability Distribution

A hydrocarbon formation is rarely homogeneous in a vertical direction. Layers composed of various minerals and different petrophysical properties are positioned above and another. Often impermeable interbedding with thicknesses ranging from several mm to several meters exist and thus prevent *vertical cross* flow between the layers.

The influence of stratification on displacing processes not only depends on the parameters of the various layers, but also on the mobility ratio (M) and the difference in density of the fluids ($\Delta\rho$).

Experience has proven that the vertical distribution of permeability is often *log-normal* (see LAW[27.](1944)). This means that the number of sample representing equally large intervals will be regarded as a function of log *k*. When drawing this function, a GAUSS distribution is obtained and the curve of distribution results in a straight line on *probability diagram sheet* (see Fig. 5.10). The spread of the permeability is characterized by the *variation coefficient*

$$V = \frac{\sigma}{\bar{x}}.$$

σ is the standard deviation and $\bar{x}$ the expected value. In case of a normal distribution, the x-values are at a percentage of 15.9% smaller than $\bar{x} - \sigma$ and at a percentage of 84.1% larger than $\bar{x} + \sigma$.

The last mentioned value is usually defined as x_σ and therefore

$$V = \frac{\bar{x} - x_\sigma}{\bar{x}}.$$

Since $x = \log k$,

$$V = \frac{\log\bar{k} - (\log k)_\sigma}{\log k}. \qquad (5.11)$$

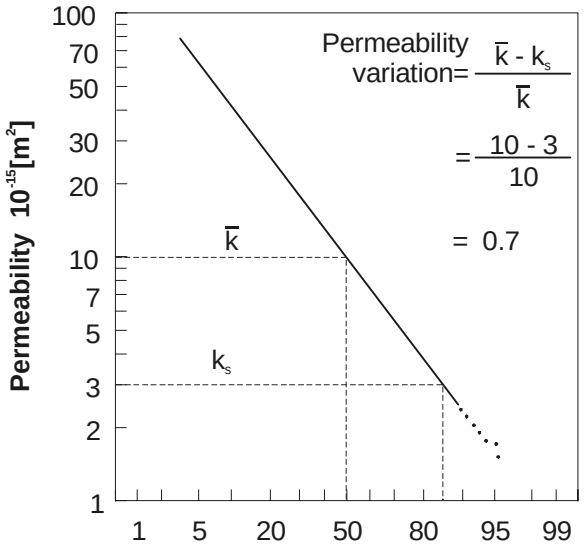

Figure 5.10: Log-normal distribution of permeability

Though it is not correct, the logarithm is often neglected in practice:

$$V \approx \frac{\bar{k} - k_\sigma}{\bar{k}}. \tag{5.12}$$

MILLER and LENTZ[30.](1947) divided the reservoir into *n* non-equally thick layers, ordered them by decreasing permeability and plotted the cumulative *permeability capacity* as a function of the cumulative *storage capacity*:

$$\frac{\sum_{i=1}^{j} h_i k_i}{\sum_{i=1}^{n} h_i k_i} = f\left[\frac{\sum_{i=1}^{j} h_i \phi_i}{\sum_{i=1}^{n} h_i \phi_i}\right]. \tag{5.13}$$

Fig. 5.11 shows such a function. The step function may be approximated by a continuous curve.

SCHMALZ and RAHME (1950) proposed the introduction of the so called LORENZ coefficient in order to characterize the heterogeneity:

$$LorenzCoefficient = \frac{surface\ \overline{ABCA}}{surface\ \overline{ADCA}} \tag{5.14}$$

The LORENZ coefficient ranges from 0 to 1. If it is zero, the layer is considered homogeneous. In case of a log-normal distribution the correlation between the *variation coefficient* and the LORENZ coefficient is shown in Fig. 5.12 In addition, the expected

values is identical with the geometrical average of the permeabilities when distributed log-normal.

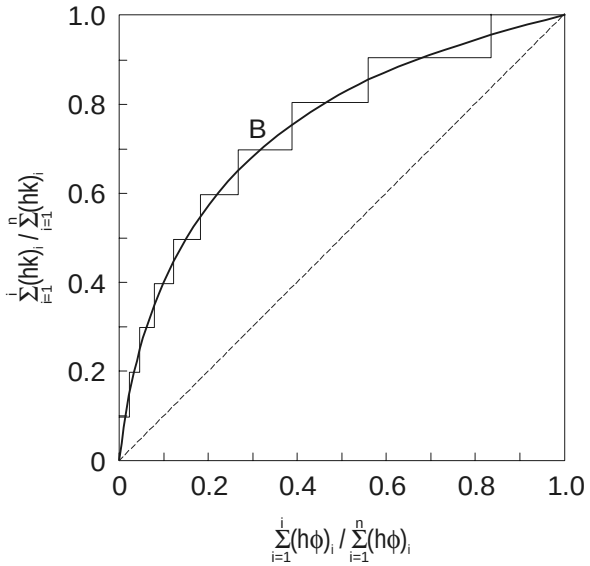

Figure 5.11: Distribution of the conductivity as a function of storage capacity

$$k = (k_1, k_2, ...k_n)^{1/n}. \tag{5.15}$$

WARREN and PRICE[40.](1961) proved the validity of this equation experimentally.

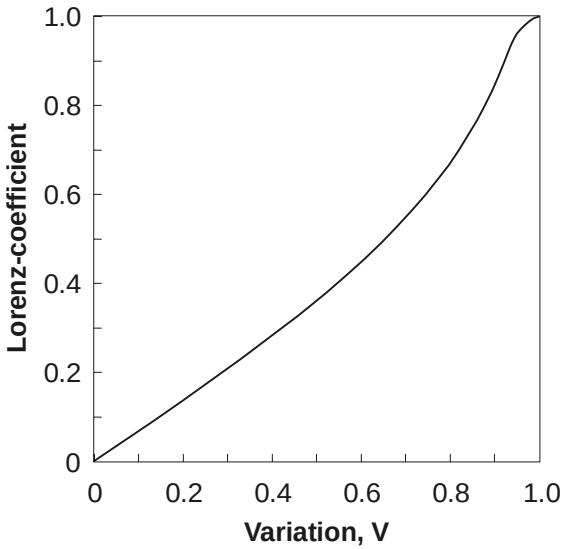

Figure 5.12: Correlation between the variation coefficient and LORENZ-coefficient

5.4.2 DYKSTRA-PARSONS Method

DYKSTRA (1949) and PARSONS (1951) assumed that a reservoir with the thickness H consist of n layers:

$$H = \sum_{j=1}^{n} h_j \tag{5.16}$$

Further, they assumed that

- the individual layers are homogeneous,
- all properties of the layers except permeability are the same,
- no cross flow between layers exists,
- displacement is piston like.

The individual layers are separated so no crossflow can occur. Therefore the sequence of the layers has no influence on the displacement and can be numbered according to decreasing permeability (Fig. 5.13).

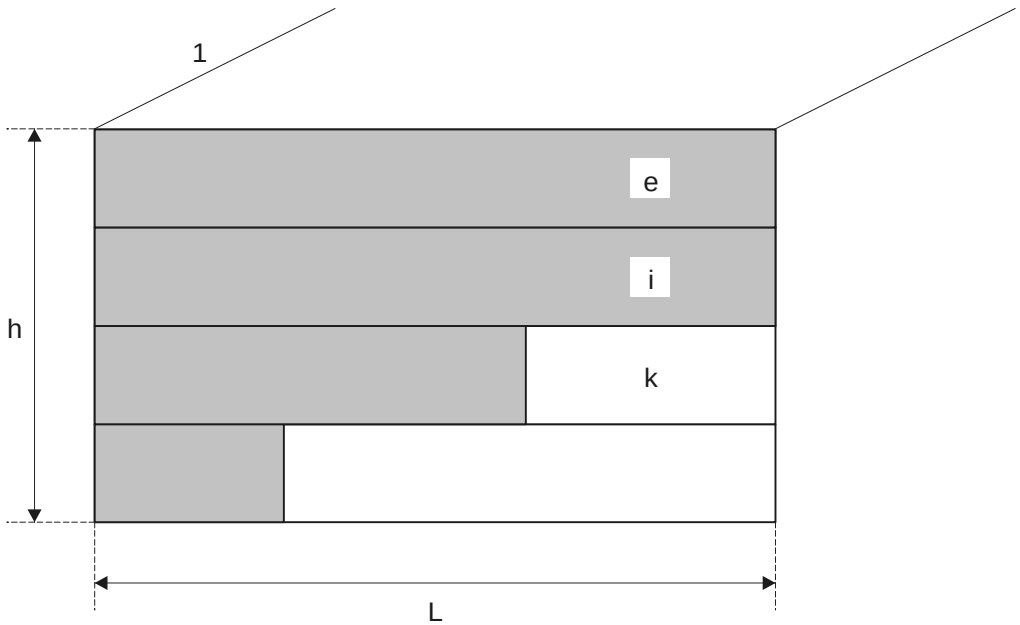

Figure 5.13: Stratified reservoir model

The displaceable amount of oil in layer j with a thickness of h_j is

$$L\phi h_j(1 - S_w - S_{or})\,. \tag{5.17}$$

The front velocity in a homogeneous layer is, at a mobility ratio $M \neq 1$ even at unchanged pressure drop Δp, not constant. If $M > 1$, the front velocity increases continuously, if $M < 1$ it will decrease. This was already derivated in *"Fluid Flow in Porous Media"*.

Based on these results, the position of the front in case of a linear displacement can be calculated as follows:

$$x = \frac{-ML + \sqrt{(ML)^2 - 2k\lambda_w \Delta p t(1-M)/\phi_D}}{1-M}, \tag{5.18}$$

and the flow velocity is

$$u = \frac{k\lambda_w \Delta p}{x_f + M(L - x_f)}, \tag{5.19}$$

where

$$\phi_D = \phi(1 - S_{wi} - S_{or}),$$

$$\lambda_w = k_{rw}/\mu_w.$$

In a stratified reservoir, water breaks through in layer j at time t_j. Then $x = L$ and $k = k_j$. Eq. 5.18 thus leads to

$$L(1-M) = -ML + \sqrt{(ML)^2 - 2k_j\lambda_w \Delta p t_j(1-M)/\phi_D}, \tag{5.20}$$

$$L^2(1-M^2) = -2k_j\lambda_w \Delta p t_j(1-M)/\phi_D$$

and finally to

$$-\frac{2\lambda_w \Delta p t_j}{\phi_D} = \frac{L^2}{k_j}(1+M). \tag{5.21}$$

Inserting Eq. 5.23 into Eq. 5.20 for all layers $i > j$ ($> k_{j+1} >$...) the position of the front is

$$\left(\frac{x}{L}\right)_i = \frac{-M + \sqrt{M^2 + (1-M^2)k_i/k_j}}{1-M}. \tag{5.22}$$

This term can also be considered as sweep efficiency of layer i at time t_j. Layers $i \leq j$ are completely swept out. The total sweep efficiency of the n layers is

$$E_I = \frac{1}{H}\left[\sum_{i=1}^{j} h_i + \frac{M}{1-M}\sum_{j=j+1}^{n} h_i - \frac{1}{M-1}\sum_{i=j+1}^{n} h_i\sqrt{M^2+(1-M^2)k_i/k_j}\right]. \tag{5.23}$$

The water production at the time t_j will be calculated as the fractional value:

$$f_w = \frac{\sum_{i=1}^{j} h_i u_i}{\sum_{i=1}^{n} h_i u_i}. \tag{5.24}$$

Because $x_f = L$ for all $i \le j$ so from Eq. 5.21

$$\sum_{i=1}^{j} h_i u_i = \frac{\lambda_w \Delta p}{L}\sum_{i=1}^{j} h_i k_i \tag{5.25}$$

and after inserting Eq. 5.24 in Eq. 5.21

$$\sum_{i=j+1}^{n} h_i u_i = \frac{\lambda_w \Delta p}{L}\sum_{i=j+1}^{n} \frac{h_i k_i}{\sqrt{M^2 + (1-M^2)k_i/k_j}} \tag{5.26}$$

Inserting Eq. 5.26 and Eq. 5.27 into Eq. 5.25 we get:

$$f_w = \frac{\sum_{i=1}^{j} k_i}{\sum_{i=1}^{j} k_i + \sum_{j+1}^{n} \frac{k_1}{\sqrt{M^2 + (1-M^2)k_i/k_j}}}. \tag{5.27}$$

During displacement, constant Δp was assumed. According to the different mobility of the phases, the water injection rate changes. Injectivity just as productivity is defined by the injectivity index:

$$J = \left(\frac{q}{\Delta p}\right)_{\Delta p \to 0}. \tag{5.28}$$

The relation

$$\gamma = \frac{J}{J_o} \tag{5.29}$$

is defined as the conductivity. J_o is the injectivity at time $t = 0$ when $x_f = 0$ for all layers.

Taken into consideration that the injection rate for a unit width of the layer i is

$$q_i = u_i h_i \tag{5.30}$$

and inserting Eq. 5.21and Eq. 5.24 in Eq. 5.27 we get the following expression:

$$\gamma = \frac{\sum_{i=1}^{j} \frac{h_i k_i \lambda_w}{L} + \sum_{j+1}^{n} \frac{h_i k_i \lambda_w}{ML + x_i(1-M)}}{\sum_{i=1}^{n} \frac{h_i k_i \lambda_w}{ML}} \tag{5.31}$$

$$= \frac{\sum_{i=1}^{j} h_i k_i + \sum_{j+1}^{n} \frac{h_i k_i}{\sqrt{M^2 + (1-M^2) k_i / k_j}}}{\frac{1}{M} \sum \int_{i=1}^{n} h_i k_i}$$

The change of conductivity with time is illustrated in Fig. 5.14.

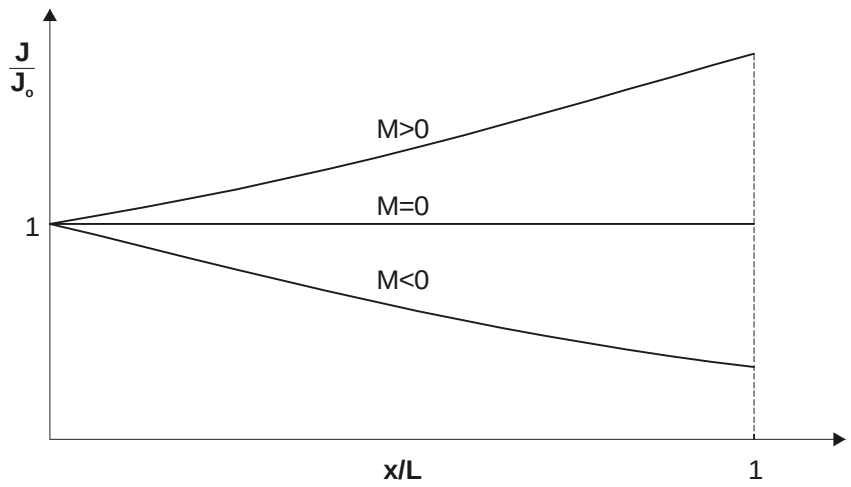

Figure 5.14: Injectivity vs. injected volume

5.4.3 JOHNSON Correlation

With help of a series of diagrams for a normal distribution of permeability, JOHNSON simplified the DYKSTRA-PARSONS calculation. In diagrams Fig. 5.15 - Fig. 5.19, the recovery factor E_R as a function of the Mobility Ratio and the Variation coefficient is plotted (Eq. 5.12). Usual values of the residual oil saturation, according to given mobility ratios were already taken into account.

These curves enable the determination of the values $E_R(1 - aS_{wi})$. The factor *a* is given. Example 5.1 shows the application of JOHNSON's method.

Example 5.1

The following data are given:

Variation coefficient	V	=	0.3
Mobility Ratio	M	=	2.6
S_{wi}		=	0.3

Determine the water displacement efficiency as a function of water-oil ratio.

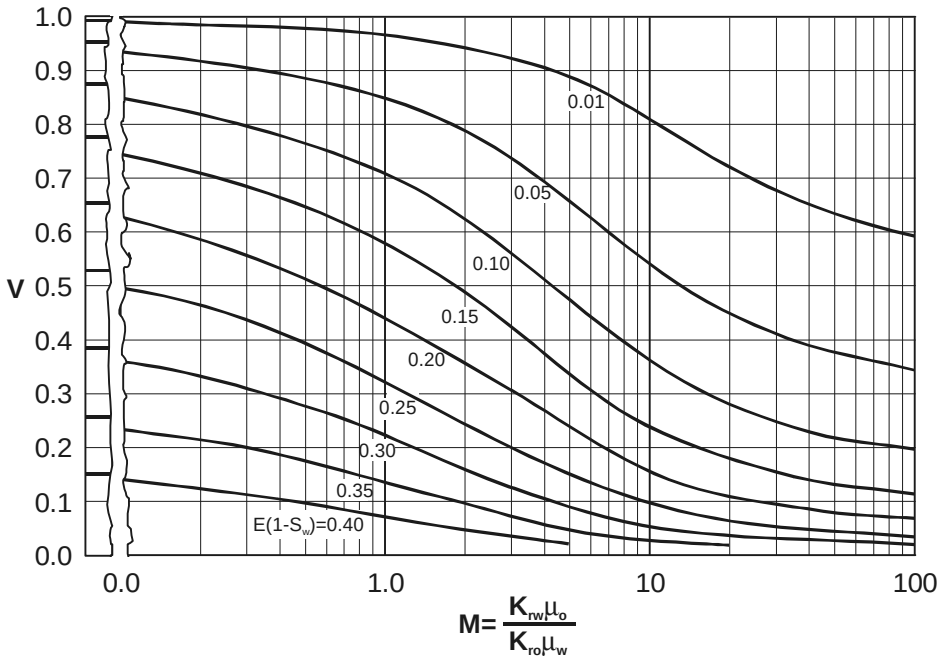

Figure 5.15: JOHNSON's (1956) correlation, WOR = 1

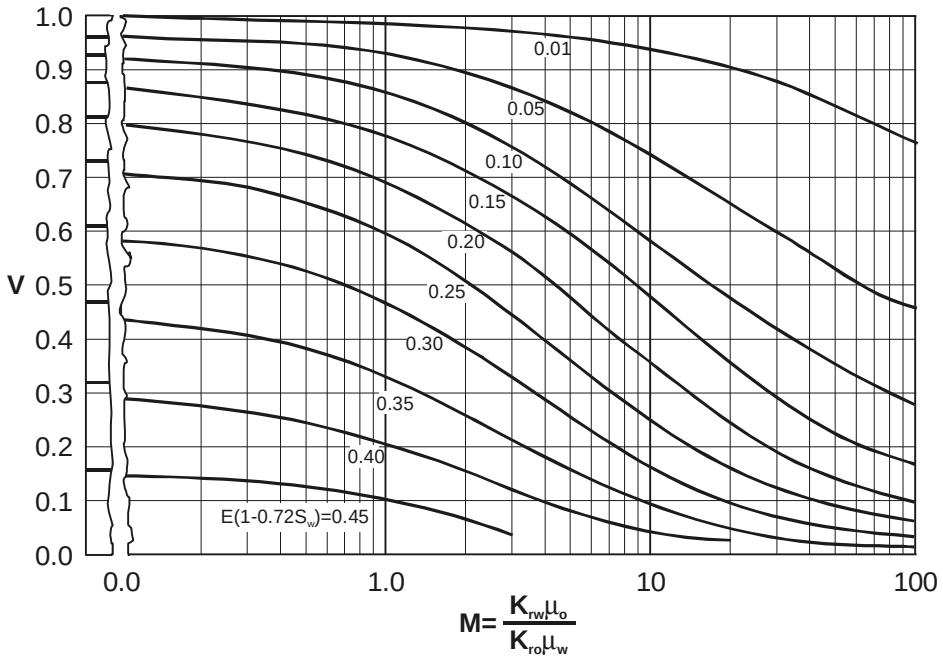

Figure 5.16: JOHNSON's (1956) correlation, WOR = 5

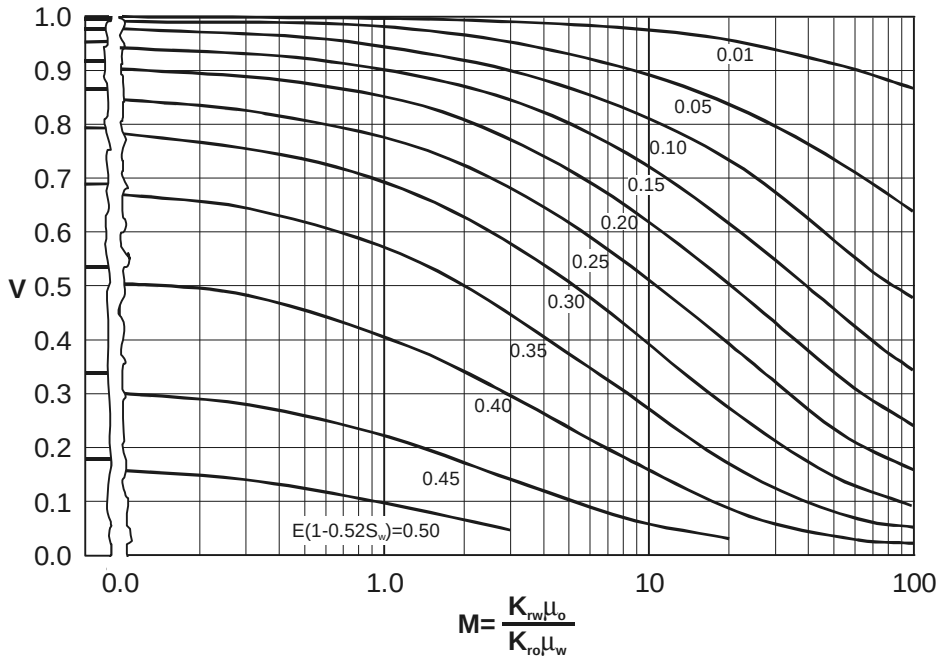

Figure 5.17: JOHNSON's (1956) correlation, WOR = 25

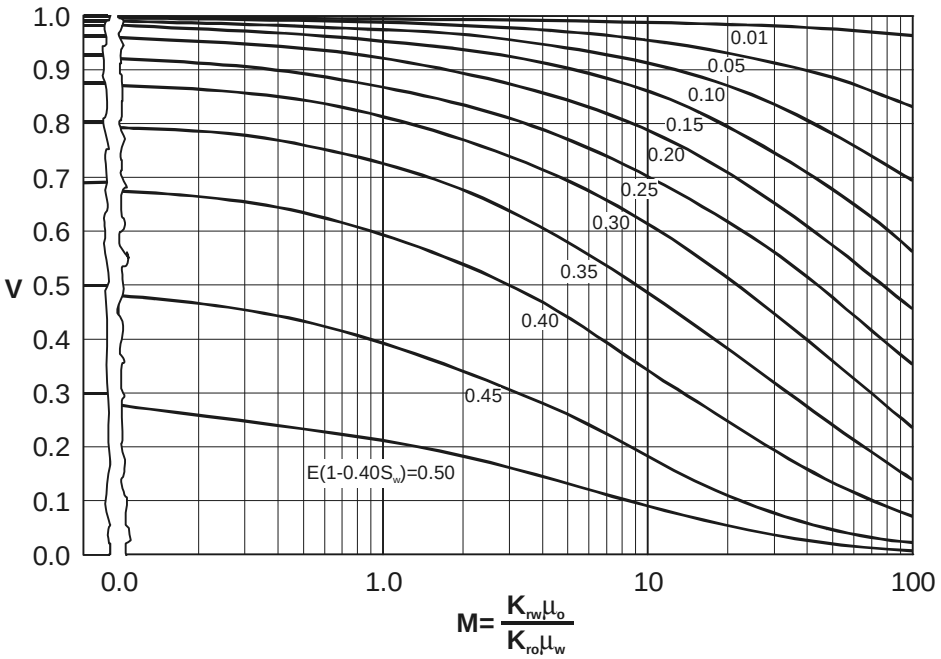

Figure 5.18: JOHNSON's (1956) correlation, WOR = 100

Solution

The values $E_R(1-aS_{wi})$ will be read from Fig. 5.15 to Fig. 5.18.

Table 5.1: Calculation of Recovery Factor by Johnson's Method

WOR	a	$E_R(1-aS_{wi})$	E_R
1	1.00	0.23	0.33
5	0.72	0.33	0.42
25	0.52	0.41	0.49
100	0.40	0.46	0.52

The calculation is summarized in Table 5.1 and the results are illustrated in Fig. 5.19.

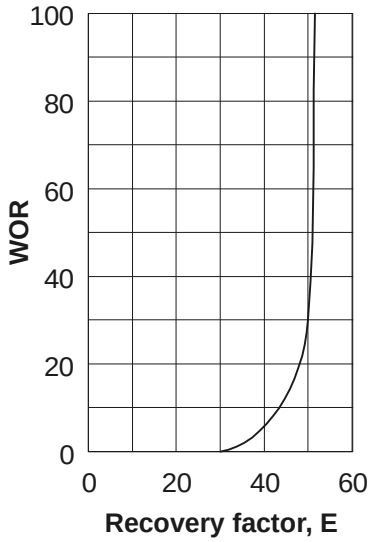

Figure 5.19: Solution after application of the JOHNSON's (1956) correlation.

5.4.4 Communicating Layers

In the absence of impermeable interbedding, a cross flow will exist between the layers of different permeabilities.

Let us imagine that a displacement proceeds isolated in a two layer formation up to a certain time and can therefore be calculated with the DYKSTRA-PARSONS[13.](1951) method. The positions of the front and distributions of pressure are shown in Fig. 5.20. Then the isolation is removed and fluid can flow between the layers due to differences in pressure. The direction of flow is given by the sign of the pressure difference.

Fig. 5.20 A) shows the case where $M < 1$, which means the mobility of the water is lower than that of oil. In the first part of the layer, the displacing fluid will proceed from the more permeable layer to the less permeable layer. In the second part, however, the displaced fluid (oil) will flow in reverse direction. The reverse situation is the case if $M > 1$. The idealized example illustrates the influence of the viscouos forces on the displacement efficiency.

- If the Mobility Ratio $M > 1$ than one part of the displacement fluid, injected in the higher permeable layer, invides the lower one and displace a part of the oil from the lower permeable layer into the higher one. This phenomenon accelerate the displacement front in the lower permeable layer and show down in the highr one. Therefore, the transition zone between the displacing and displaced fluid becomes smaller (the distance between the fronts) as in the isolated case.

- If $M > 1$ than the injected water tends to flow from the lower permeable layer into the higher one. The difference between the front velocities is larger in comparison to the

isolated case.

The cross flow depends on the permeability in a vertical direction (in most cases smaller than in an horizontal direction due to sedimentation and compaction), on the capillary force and on gravity.

If the layer thickness is rather small and vertical permeability large enough, then vertical equilibrium - caused by capillary forces and gravity - may be assumed. Therefore, methods used in Chapter 5.3.2 may also be applied here. The average saturation and the relative permeabilities are

$$\bar{S}_w = \frac{\int_0^H \phi(z) S_w(z)\,dz}{\int_0^H \phi(z)\,dz} = \frac{\sum_{j=1}^{n} \phi_j h_j \bar{S}_{wj}}{\sum_{j=1}^{n} \phi_j h_j}, \tag{5.32}$$

$$\bar{k}_{rw}(\bar{S}_w) = \frac{\int_0^H k(z) k_{rw}(z)\,dz}{\int_0^H k(z)\,dz} = \frac{\sum_{j=1}^{n} h_j k_j \bar{k}_{rwj}(S_w)}{\sum_{j=1}^{n} h_j k_j}, \tag{5.33}$$

$$\bar{k}_{ro}(\bar{S}_w) = \frac{\int_0^H k(z) k_{ro}(z)\,dz}{\int_0^H k(z)\,dz} = \frac{\sum_{j=1}^{n} h_j k_j \bar{k}_{roj}(S_w)}{\sum_{j=1}^{n} h_j k_j}. \tag{5.34}$$

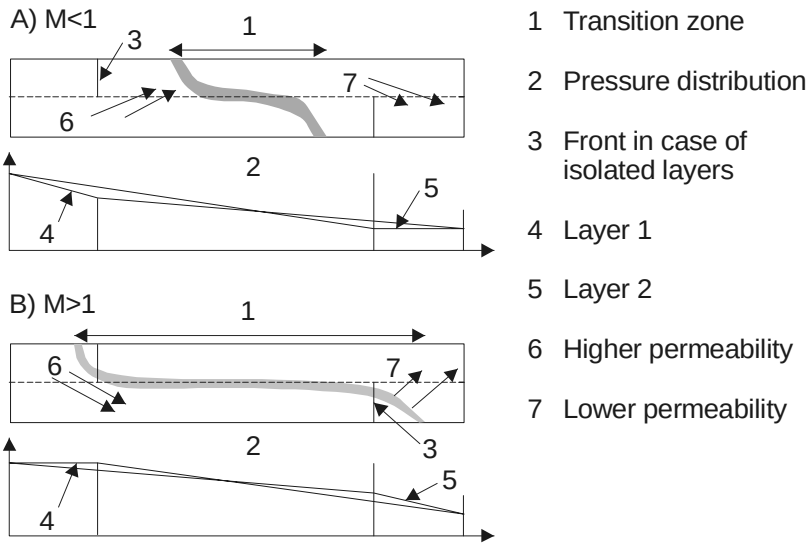

Figure 5.20: Water displacement in communicating layers

Calculations are again made according to the BUCKLEY-LEVERETT[4.](1942) theory, whereby the capillary force is neglected.

Example 5.2

The reservoir consists of three layers. The capillary pressure functions given in Fig. 5.1 are different in the particular layers but the relative permeability curves are the same for every layer. These curves are plotted with a staggered line in Fig. 5.23a. The layers have the following properties:

$$h_1 = 4m, \qquad \phi_1 = 0.25, \qquad k_1 = 10^{-12} m^2.$$

$$h_2 = 4m, \qquad \phi_2 = 0.20, \qquad k_2 = 0.5 \times 10^{-12} m^2.$$

$$h_3 = 4m, \qquad \phi_3 = 0.15, \qquad k_3 = 0.1 \times 10^{-12} m^2.$$

Reservoir fluids characteristics:

$$\rho_w - \rho_o = 200\ kg/m^3\ [12.48\ lbm/cuft]$$

$$\mu_w = 0.4 \times 10^{-3}\ Pas\ [0.4\ cP]$$

$$\mu_o = 2.0 \times 10^{-3}\ Pas\ [2.0\ cP]$$

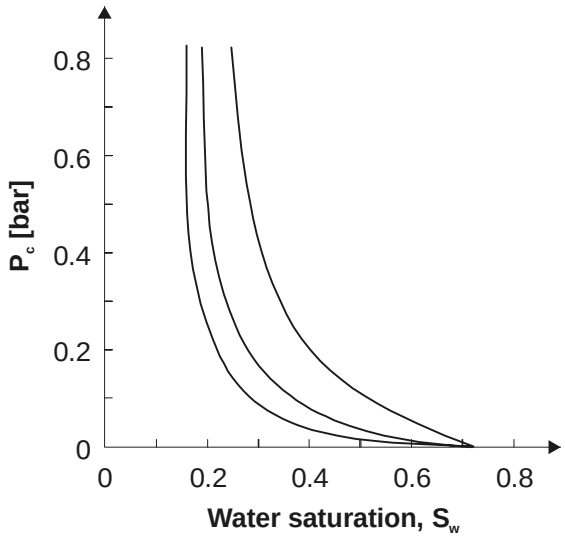

Figure 5.21: Stratified reservoir with vertical communication

The water displacement will be calculated for two cases:

1. Permeability decreases with the depth from layer to layer (sequence 1-2-3)
2. Permeability increases (sequence 3-2-1).

The vertical distributions of water saturation are for the two cases different (see Fig. 5.22). Such distributions can be constructed from the capillary pressure curves. At first arbitrary value of capillary pressure P_c^+ is chosen for the top of the layer. In Fig. 5.21, this corresponds to the height of h^+. From this point, the individual layer thickness is measured upwards in the right sequences. The sections with the P_c curves give the saturation distribution and the average saturations $\bar{S}_{w1}$, $\bar{S}_{w2}$, $\bar{S}_{w3}$ for the individual layers and the whole thickness $(\bar{S}_w)$ as well. The pseudo-relative permeability curves can be calculated on the basis of the saturation distributions using Eq. 5.33 and Eq. 5.34. The fractional flow curves can be calculated in the usual way. Table 5.2 gives the results of these calculation. Fig. 5.23 shows the *fractional flow curves*, and the displacement curves. In case of sequences 1-2-3, $S_{wf} = 0.654$. In case of 3-2-1, $S_{wf} = 0.36$.

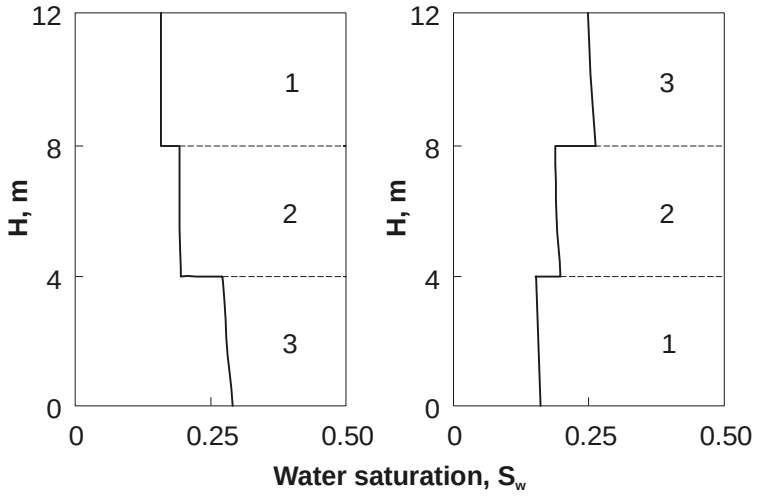

Figure 5.22: Vertical saturation distribution depending on the sequence of layers

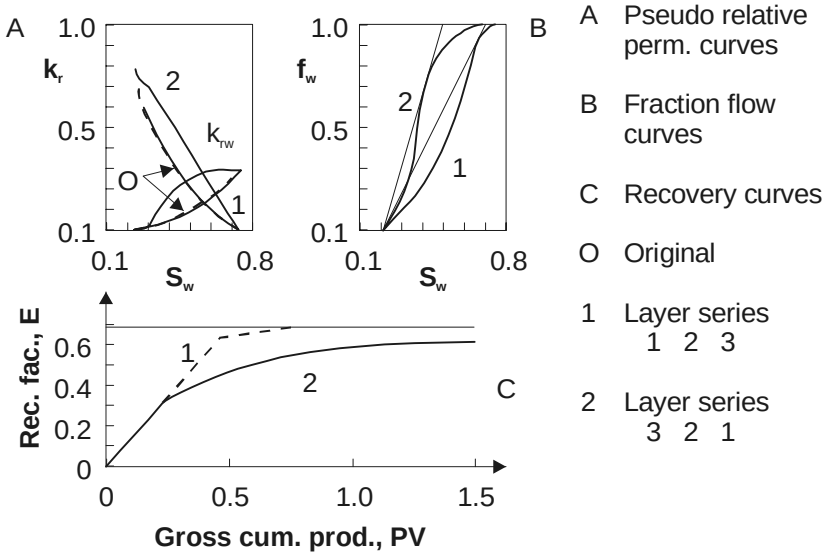

Figure 5.23: Displacement in heterogeneous reservoirs at increasing and decreasing permeability

5.4.5 Numerical Calculation of Water Flooding in Linear Stratified Layers

Numerical methods enable the solution of the multiphase flow equations for heterogeneous systems withoud simplifications.

In Volume 5 "*Numerical Reservoir Simulation*", these methods are described in detail. BERRUIN and MORSE[3.](1978) calculated at 328 m [1000 *ft*] long linear displacement with the help of a two dimensional, two phase (oil-water) fully implicit model. It consisted of 5 layers, each 3 *m* [10 *ft*] thick and with equal porosity. Vertical and horizontal permeabilities were the same. The variation coefficient is $V = 0.85$.

The reservoir data are the following:

Porosity	=	0.20	
Length	=	305 [1000]	*m* [*ft*]
Height	=	15.24 [50]	*m* [*ft*]
Bright	=	0.3048 [1]	*m* [*ft*]
B_o	=	1.0	
B_w	=	1.0	
ρ_o	=	710 [44.32]	kg/m^3 [*lbm/ft*]
ρ_w	=	1000 [62.42]	kg/m^3 [lbm/ft^3]
μ_o	=	0.005 [5]	*Pas* [*cP*]
μ_w	=	0.001 [1]	*Pas* [*cP*]
M	=	0.5	
k_v/k_h	=	1.0	

The permeability distributions are given in Table 5.3. In case 1, permeability decreases downwards. Without crossflow, oil recovery results in 0.56 at a WOR = 100.

All calculations considering crossflow gave better results. A decrease in displacing velocity effects an increase of oil recovery. At speeds of 1.2 *m/d* [4 *ft/d*] oil recovery comes to a value of 0.65. In case 2, permeability increases downwards. The most favorable oil recovery is obtained with isolated layers. Decreasing displacement velocity has an unfavorable effect on oil recovery. At a displacement velocity of 0.025 *m*/*d* [0.08 *ft/d*] oil recovery is only 0.2.

Table 5.2: Pseudo Permeability - and Fractional Flow Curve for Example 5.3

Sequence of Layers 1-2-3

P_c^+	$\bar{S}_w$	$\bar{k}_{rw}(S_w)$	$\bar{k}_{ro}(S_w)$	$f_w(S_w)$
0.00	0.750	0.340	0.000	1.000
0.05	0.704	0.276	0.049	0.965
0.10	0.588	0.152	0.232	0.766
0.15	0.486	0.081	0.420	0.491
0.20	0.355	0.032	0.591	0.211
0.25	0.369	0.013	0.692	0.086
0.30	0.253	0.008	0.756	0.052

Sequence of Layers 3-2-1

P_c^+	$\bar{S}_w$	$\bar{k}_{rw}(S_w)$	$\bar{k}_{ro}(S_w)$	$f_w(S_w)$
0.00	0.750	0.340	0.000	1.000
0.05	0.704	0.330	0.013	0.992
0.10	0.604	0.295	0.081	0.947
0.15	0.512	0.242	0.205	0.855
0.20	0.372	0.117	0.457	0.562
0.25	0.269	0.013	0.692	0.086
0.30	0.253	0.008	0.752	0.052

Table 5.3: Permeability Variation for Berruin and Morse Example

Sequence of Layer	Case 1	Case 1
1	1500.0	20.3
2	480.0	61.0
3	160.0	160.0
4	61.0	480.0
5	20.3	1500.0

Table 5.4: Displacement Velocities and Pressure Gradients for Berruin and Morse Example (metric units)

Displacement Velocity *m/d*	Horizontal Average Pressure Gradient *MPa/m*	Force of Gravity *M/Pa*
0.025	0.00009	0.003
0.120	0.00043	0.003
1.200	0.00500	0.003
2.400	0.01000	0.003
9.700	0.04300	0.003
38.700	0.15720	0.003

Table 5.5: Displacement Velocities and Pressure Gradients for Berruin and Morse Example (field units)

Displacement Velocity *ft/d*	Horizontal Average Pressure Gradient *psi/ft*	Force of Gravity *psi/ft*
0.082	0.004	0.13
0.394	0.019	0.13
3.937	0.221	0.13
7.874	0.470	0.13
31.820	1.910	0.13
126.970	6.950	0.13

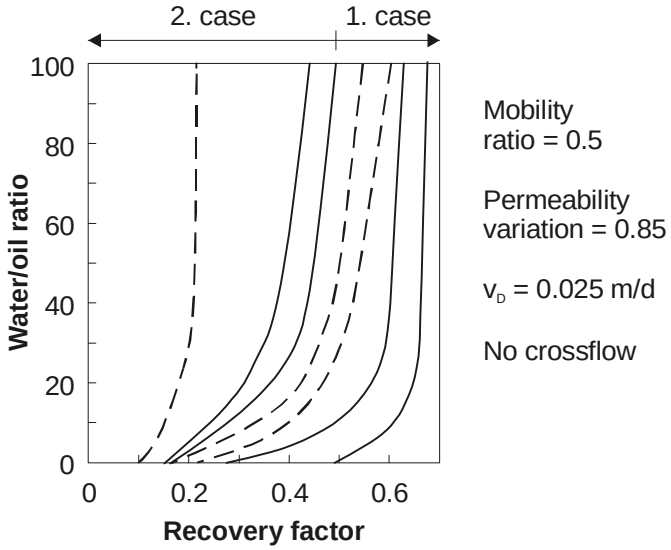

Figure 5.24: Water flooding in a stratified reservoir after BERRUIN and MORSE, 1978

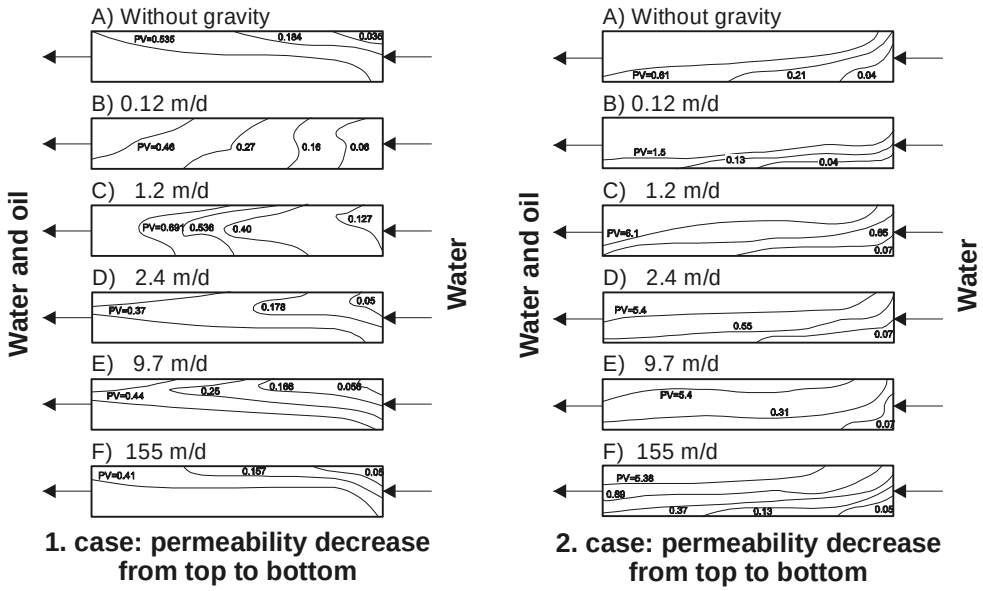

Figure 5.25: The position of the saturation profil S_w = 55 at various amounts of injected pore volume and displacement velocities after BERRUIN and MORSE, 1978

5.4.6 Areal Sweep Efficiency

Displacing mechanisms are not uniform in all sections of the reservoir due to

- the irregular distribution of displacing media and energy,
- anisotropy and heterogeneity in horizontal direction,
- punctiform production and injection (well pattern).

The areal sweep efficiency shows which part of the total reservoir area was flooded due to a certain displacing mechanism. Fig. 5.26 illustrates a regular well system with both production and injection wells. Due to symmetry, the determination of the sweep efficiency of the whole flooded area is possible based on a single pattern. The areal sweep efficiency is defined as

$$E_a = \frac{A^*}{A} = \frac{swept\ out\ area}{total\ area}. \tag{5.35}$$

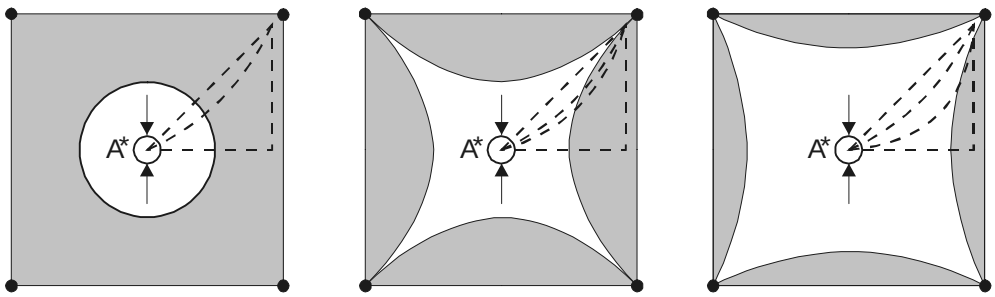

Figure 5.26: Definition of the areal sweep efficiency

A displacement is split by the breakthrough into two periods. The areal sweep efficiency increases further after breakthrough, but the extension of the flooded area proceeds more slowly since a certain amount of displacing medium is directly produced.

The term areal sweep efficiency is not only used for injection, but also for natural water influx and frontal gas displacement. In the following discussion only secondary recoveries (water flooding) are examined since the geometry of well pattern makes this easier. Fig. 5.27 shows several different well systems, whereby the relation of production and injections wells varies.

Two cases are to be distinguished: normal and inverted well pattern. In a normal well pattern, the production well is regarded as the center of the flooded area. In an inverted well pattern, the injection well is considered the center. In case of a five spot system both arrangements are the same. Fig. 5.28 shows the areal sweep efficiency at breakthrough as a function of the well distance. Unit mobilities ratio is assumed.

Fig. 5.29 shows the influence of the mobility ratio at $d/a = 1$. Correlations of the areal sweep efficiency with geometry, mobility ratio and injected quantity can be analysed with the help of mathematical, physical and analogous models. Due to the fact that all methods show errors, the results spread, but within acceptable limits.

Fig. 5.30 illustrates the areal sweep efficiency as a function of the *fractional flow value* f_1. (f_1 though has no relation to the BUCKLEY-LEVERETT theory since piston like displacement was assumed).

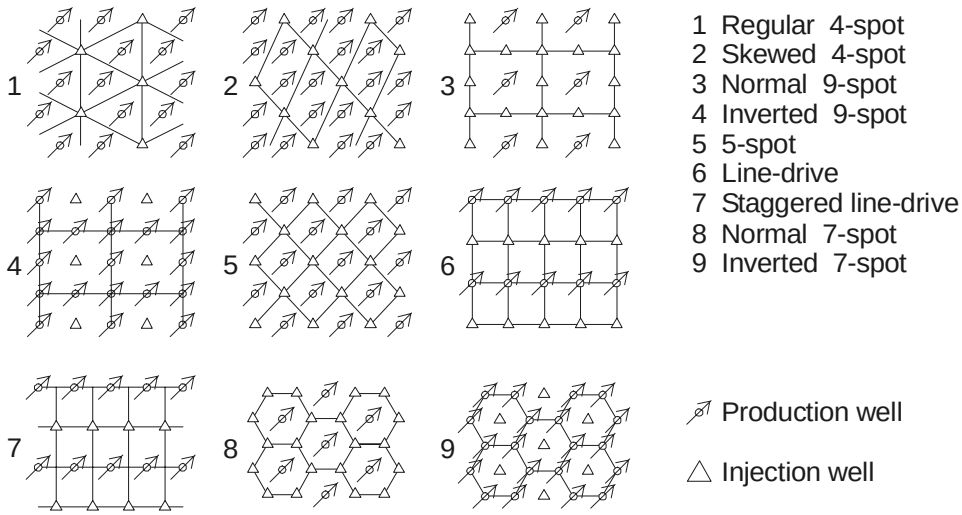

Figure 5.27: Well pattern for areal flooding (after CRAIG, 1971)

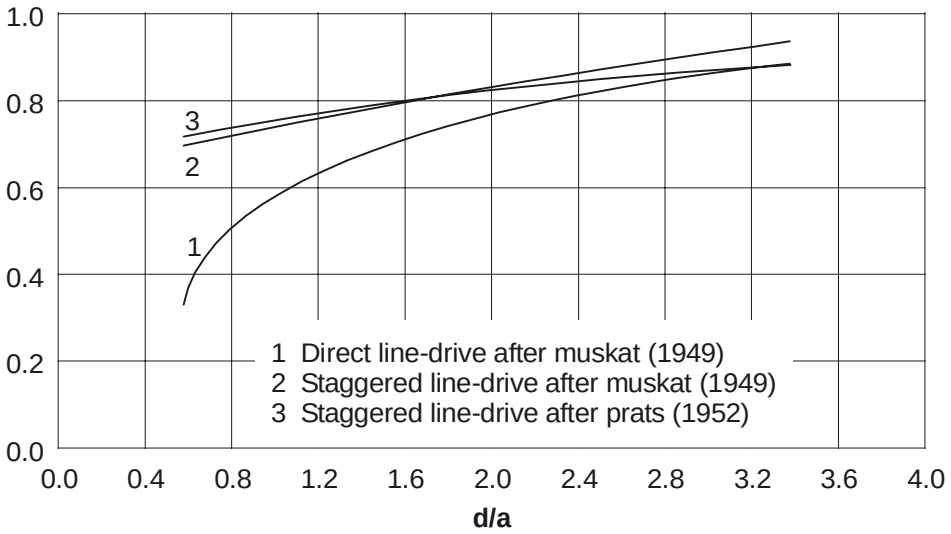

Figure 5.28: Areal sweep efficiency at a linear pattern and uniform mobility ratios at breakthrough (after CRAIG, 1971).

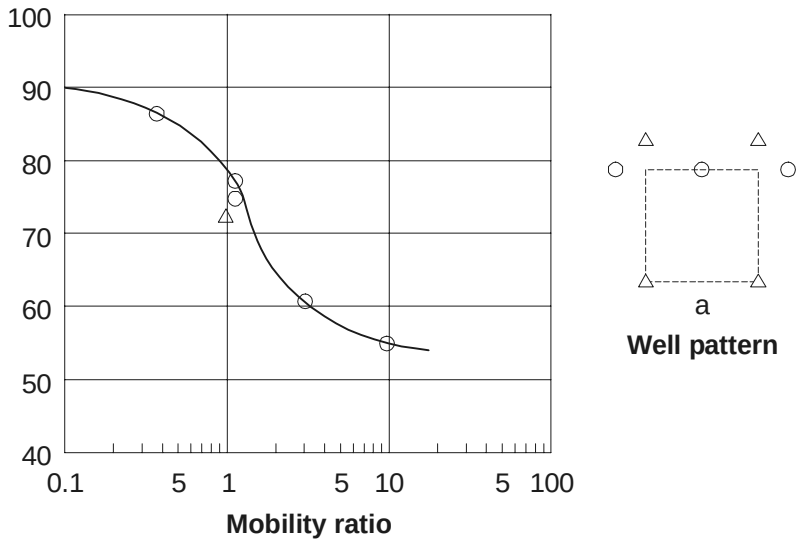

Figure 5.29: Areal sweep efficiency with a shifted linear pattern at breakthrough, d/a = 1 (after CRAIG, 1971).

Experiments by CAUDLE and WITTE[6.](1959) were conducted with miscible fluids for a five point, porous and permeable model. The swept out area was determined with the help of X-rays. f_1 indicates how much displacing fluid was produced.

Fig. 5.31 shows the areal sweep efficiency as a function of the relations between injected (V_I) and displaceable volume (V_D). The displaceable volume is defined as

$$V_D = A\phi h(S_{oi} - S_{or}) \tag{5.36}$$

The conductivity defined by Eq. 5.29 as a function of V_I/V_D is displayed in Fig. 5.31.

Example 5.3

Following data are given for a five-spot system:

A	=	2.5×10^5	m^2 [61.77 *ac*]	μ_o	=	5×10^{-3}	*Pas* [5 *cP*]
h	=	10	*m* [32.8 *ft*]	μ_w	=	0.8×10^{-3}	
ϕ	=	0.2		$k_{ro}(S_{oi})$	=	0.63	
S_{oi}	=	0.7		$k_{rw}(S_{oi})$	=	0.21	
S_{of}	=	0.4		B_o	=	1.25	
S_{or}	=	0.3		B_w	=	1	

Injection rate q_w = 500 m^3/d [3145 *bbl/d*].

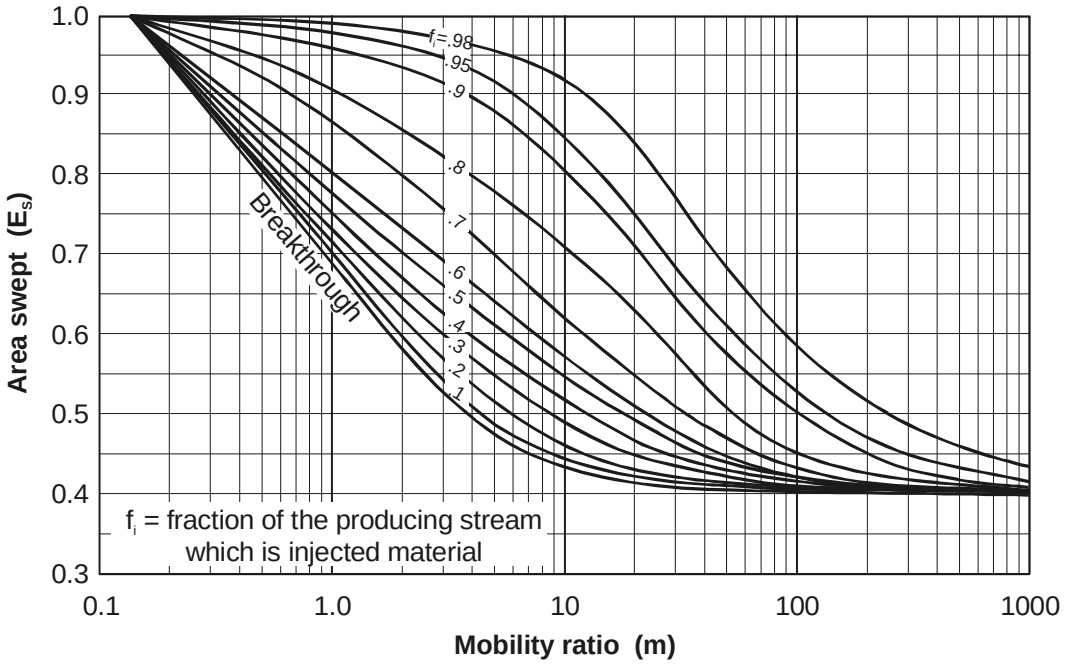

Figure 5.30: Areal sweep efficiency of a five point system and the mobility ratio as a function of the *fractional value* (after CAUDLE and WITTE, 1959).

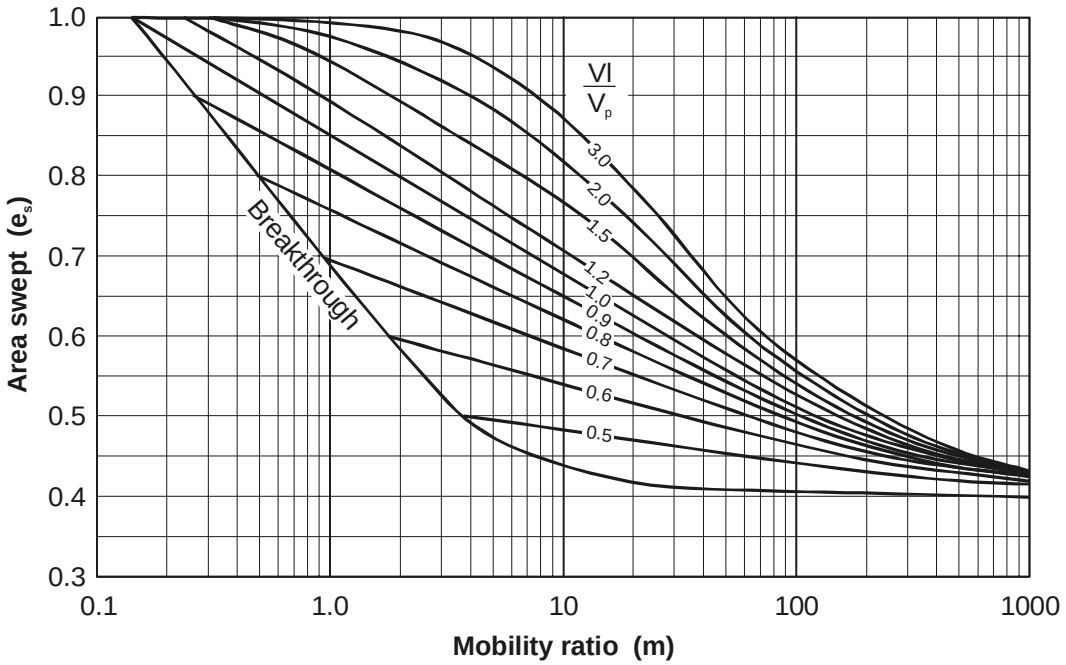

Figure 5.31: Areal sweep efficiency of a five-spot system as a function of the injected pore volume (after CAUDLE and WITTE, 1959)

The task is to calculate the time of breakthrough and the oil recovery after injection of 1 pore volume water.

Solution

The mobility ratio:

$$M = \frac{k_{rw}\mu_o}{k_{ro}\mu_w} = \frac{0.21 \times 5 \times 10^{-3}}{0.63 \times 0.8 \times 10^{-3}} = 2.08$$

At breakthrough the areal sweep efficiency results in $E_a = 0.6$ (see Fig. 5.30).

Produced oil:

$$N_p = \frac{Ah\phi(S_{oi} - S_{or})}{B_o} = \frac{2.5 \times 10^5 \times 10 \times 0.2(0.7 - 0.3) \times 0.6}{1.25} = 96000\ m^3$$

In field units:

$$N_p = \frac{7758 \times 61.77 \times 32.85 \times 0.2(0.7 - 0.3) \times 0.6}{1.25} = 603576\ bbl$$

Injected water until breakthrough:

$$W_i = \frac{N_p B_o}{B_w} = \frac{96000 \times 1.25}{1} = 120000\ m^3$$

In field units:

$$W_i = \frac{603576 \times 1.25}{1} = 754470\ bbl$$

Time of breakthrough:

$$t_d = \frac{W_i}{Q_w} = \frac{120000}{500} = 240\ d$$

In field units:

$$t_d = \frac{754470}{3145} = 240\ d$$

Porevolume:

$$V_p = Ah\phi = 2.5 \times 10^5 \times 10 \times 0.2 = 0.5 \times 10^6 \; m^3$$

In field units:

$$V_p = 61.77 \times 32.8 \times 0.2 = 405.21 \; ac\; ft$$

Displaceable volume:

$$V_D = V_p(S_{oi} - S_{or}) = 0.5 \times 10^6 \times 0.4 = 0.2 \times 10^6 \; m^3$$

$$V_p / V_D = \frac{0.5 \times 10^6}{0.2 \times 10^6} = 2.5$$

In field units:

$$V_D = 405.21 \times (0.7 - 0.3) \times 7758 = 1.257 \times 10^6 \; bbl$$

$$V_p / V_D = \frac{405.21}{1.257 \times 10^6 \times 1/7725} = 2.5$$

From Fig. 5.31, $E_A = 0.96$.

Then oil recovery results in

$$E = E_D E_A = \frac{S_{oi} - S_{or}}{S_{oi}} E_A = \frac{0.7 - 0.3}{0.7} \times 0.96 = 0.55 .$$

Remark: At breakthrough, it would be more appropriate to use the average oil saturation behind the front instead of the residual oil saturation. At a proceeding *water cut*, oil saturation in the flooded area converges to the residual oil saturation.

Example 5.4

The depression at breakthrough and after injection of 1 PV water is to be calculated with the values of Example 4.4.

At the initial time $t = 0$ (begin of injection) $\Delta p_o = 6$ *MPa* [870 *psi*].

Solution

From Fig. 5.31:

$$E_A = 0.60 \qquad \gamma = 1.45 \qquad \Delta p = \Delta p_o / \gamma = 4.1\ MPa\ [594.5\ psi]$$

$$E_A = 0.96 \qquad \gamma = 1.96 \qquad \Delta p = \Delta p_o / \gamma = 3.1\ MPa\ [449.5\ psi]$$

Similar diagrams as in Fig. 5.28 - Fig. 5.31 were set up for various other well systems and can be used as a first approximation.

For more precise calculations, numerical methods as in Chapter 5 are to be applied.

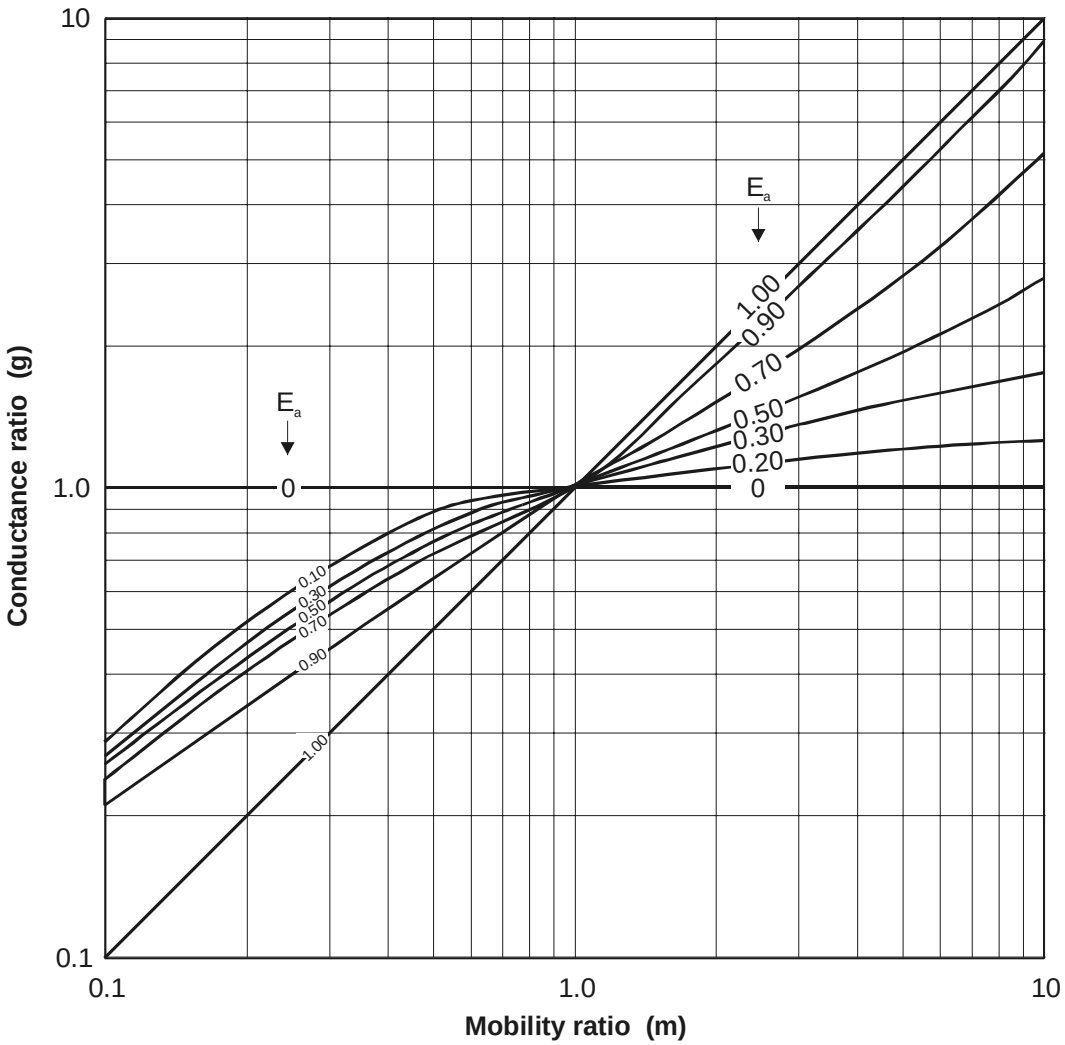

Figure 5.32: Conductance ratio γ as a function of mobility ratio and pattern area sweep efficiency for five-spot pattern (after CAUDLE and WITTE, 1959)

Chapter 6

Decline Curve Analysis

Decline curve analysis is an empirical method which applies oil production versus time plots to extrapolate an estimation of the future rates of production for a well. This method is not based on physical principles and so it can only be used as long as the mechanical conditions of the well (completion, production method etc.) and the drive forces in the reservoir are unchanged. Ignoring this limitation very often leads to failure.

The nominal decline rate D is defined as

$$D = -\frac{\frac{dq}{dt}}{q} = -\frac{d\ln q}{dt} \tag{6.1}$$

Three types of declines are commonly applied:

- Exponential (or constant percentage) decline,
- Hyperbolic decline
- Harmonic decline.

6.1 Exponential Decline

This method is based on the assumption that the decline rate D is constant throughout time. Integration of Eq. 6.1 leads to the rate time relationship:

$$-\int_{t_i}^{t} D dt = \int_{q_{oi}}^{q_o} d\ln q \tag{6.2}$$

$$-D(t - t_i) = \ln q_o - \ln q_{oi} \tag{6.3}$$

thus

$$q_o = q_{oi} e^{-D(t-t_i)} \tag{6.4}$$

By using a decimal logarithm instead of *ln*, Eq. 6.3 can be written as

$$\log q_o = 0,434 D(t-t_i) + \log q_{oi} \tag{6.5}$$

The cumulative production can be calculated easily:

$$Q_o(\Delta t) = \int_{t_i}^{t} q_o(t)dt = \int_{t_i}^{t} q_{oi} e^{-D(t-t_i)} dt = \frac{q_{oi} - q_o}{D} \tag{6.6}$$

and so

$$q_o = q_{oi} - DQ_o(\Delta t) \tag{6.7}$$

The time interval is

$$\Delta t = t - t_i \tag{6.8}$$

Now log q_o *vs.t* and/or q_o vs. Q_o can be plotted.

Despite the Eq. 6.5 and Eq. 6.7, both are straight lines with a slope of 0.434 *D* and *D* respectively. The remaining time to abondonment or until an economic limit of production rate (q_{oa}) is reached, is calculated from Eq. 6.5:

$$t_a = t_i + \frac{2.303}{D} \log \frac{q_{oi}}{q_{oa}} \tag{6.9}$$

The reserve at the time t_i is

$$Q_{oa} = \frac{q_{oi} - q_{oa}}{D} \tag{6.10}$$

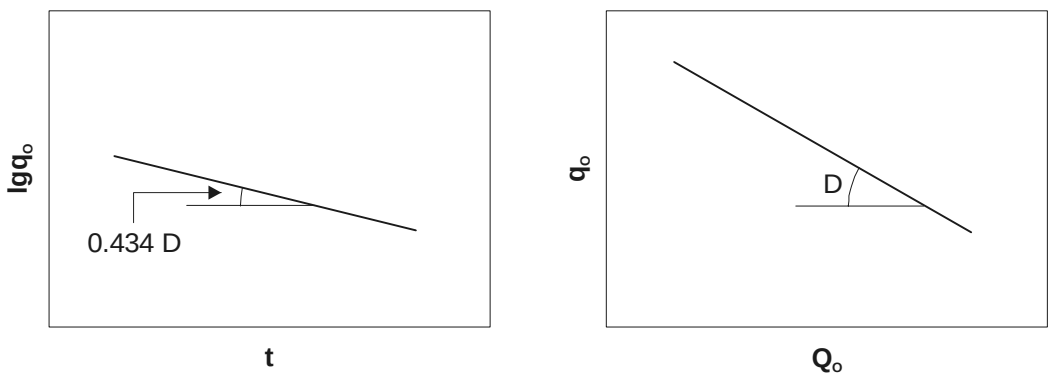

Figure 6.1: Exponential decline plot

6.2 Hyperbolic Decline

This method is based on the assumption that the decline rate D is proportional to the nth power of the rate q_o:

$$D = -\frac{\frac{dq_o}{dt}}{q_o} = bq_o^n \tag{6.11}$$

where b and n are constant. The initial value of the decline rate is

$$D_i = bq_{oi}^n \tag{6.12}$$

and so Eq. 6.11 can be written in the following form:

$$-\frac{dq_o}{dt} = \frac{D_i}{q_{oi}^n} q_o^{n+1} \tag{6.13}$$

After integration of Eq. 6.13,

$$-\int_{q_{oi}}^{q_o} \frac{dq_o}{q_o^{n+1}} = \int_{t_i}^{t} \frac{D_i}{q_{oi}^n} dt \tag{6.14}$$

$$\frac{1}{n}\left(\frac{1}{q_o^n} - \frac{1}{q_{oi}^n}\right) = \frac{D_i}{q_{oi}^n}(t - t_i) \tag{6.15}$$

or

$$q_o = q_{oi}[1 + nD_i(t - t_i)]^{-\frac{1}{n}} \tag{6.16}$$

The cumulative production can be calculated in the following way:

$$Q_o(\Delta t) = \int_{t_i}^{t} q_o(t)dt = \int_{t_i}^{t} q_{oi}[1 + nD_i(t - t_i)]^{-\frac{1}{n}} dt \tag{6.17}$$

$$= \frac{q_{oi}}{D_i(n-1)}[1 + nD_i(t - t_i)]^{\frac{n-1}{n}}$$

The hyperbolic decline curve is not as simply plotted as the exponential or the harmonic one. The best way is to use a computer for curve fitting.

6.3 Harmonic Decline

The harmonic decline is a special case of the hyperbolic one. Eq. 6.16 for $n = 1$ is

$$q_o = q_{oi}[1 + D_i(t - t_i)]^{-1} = q_{oi}[1 + D_i \Delta t]^{-1} \tag{6.18}$$

The cumulative production can be calculated as

$$Q_o(\Delta t) = \int_{t_i}^{t} q_o dt = \int_{t_i}^{t} \frac{q_{oi}}{1 + D_i(t - t_i)} dt = \frac{q_{oi}}{D_i} \ln[1 + D(t - t_i)] \tag{6.19}$$

After substitution of Eq. 6.18 into Eq. 6.19,

$$Q_o(\Delta t) = 2.3027 \frac{q_{oi}}{D_i} \log \frac{q_{oi}}{q_o} \tag{6.20}$$

or

$$\log q_o = -0.434 \frac{D_i}{q_{oi}} Q_o(\Delta t) + \log q_{oi} \tag{6.21}$$

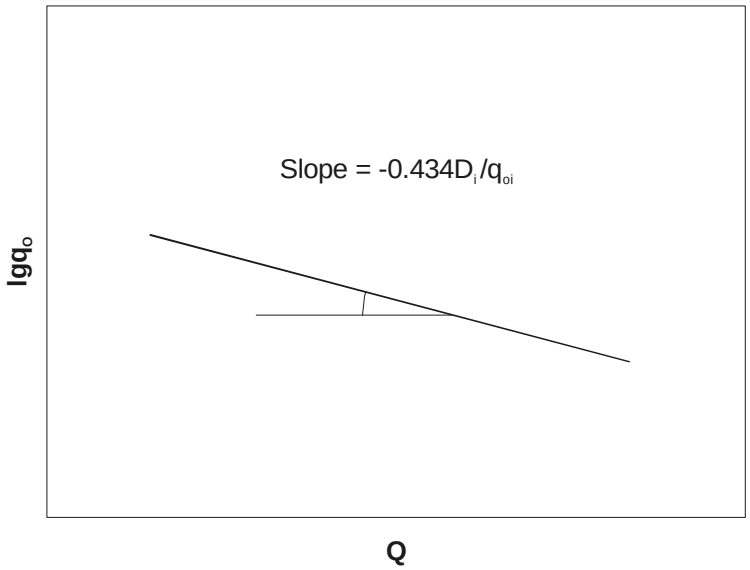

Figure 6.2: Harmonic decline plot

Now $\log q_o$ *vs.* Q_o is plotted. In spite of Eq. 6.21, the harmonic decline curve is a straight line in the considered coordinates with a slope of

$$0.434 D_i / q_{oi} = 0.434 b\,. \tag{6.22}$$

b is the constant in Eq. 6.11.

Chapter 7

References

1. Archi, G.E.: "The Electrical Resistivity Logs as an Aid in Determining Some Reservoir Characteristics", Trans.,AIME (1942), 146, 54-61.
2. Arps, J.J., Brons, F., van Everdingen, A.F., Buchwald, R.W. and Schmidt, A.E.: "A Statistical Study of Recovery Efficiency", Bull., 14D API (1967).
3. Berruin, N.A. and Morse, R.A.: "Effect of Flooding Rate and Permeability ordering on Waterflooding Stratified Reservoir", SPE paper 7158 (1978).
4. Buckley, S.E and Leverett, M.C: "Mechanism of Fluid Displacement in Sands", Am. Inst. Min. Metall. Eng., Trans.,AIME, V. 146, (1942), 107-111.
5. Carter, R.D. and Tracey, G.W.: "An Improved Method for Calculating Water Influx", Trans., AIME, 219, (1960), 415-417.
6. Caudle, B.H. and Witte, M.D.: "Production Potential Changes During Sweep-Out in a Five-Spot System", J. Pet. Eng., (Dec.1959), 446-8, Trans., AIME, 216, (1959).
7. Craig, F.F., Jr., Geffen, T.M. and Morse, R.A.: "Oil Recovery Performance of Pattern Gas of Water Injection Operations from Model Tests", Trans., AIME, 204, (1955), 7-15.
8. Craig, F.F., Jr.: "The Reservoir Engineering Aspects of Waterflooding", Monograph Voume 3 of the Henry L. Doherty Series, New York/Dallas (1971), 135 p.
9. Craft, B.C.: "Applied Petroleum Reservoir Engineering", Prentice-Hall, Inc., Englewood Cliffs, N.J. (1959), 126, 206, 224.
10. McCray, A.W.: "Petroleum Evaluations and Economic Decisions", Prentice-Hall, Inc., Englewood Cliffs, New Jersey (1975).
11. Darcy, H.: "Les Fontaines Publiques de la Ville de Dijon", Victor Dalmont, Paris.
12. Dietz, D.N.: "A Theoretical Approach to the Problem of Encroaching By-Passing Edge Water", Akad. van Wetenschappen, Amsterdam, Proc. B56 (1953), 83-92.
13. Dykstra, H. and Parsons, R.L.: "The Prediction of Waterflood Performance with Variation in Permeability Profile", Prod. Monthly (1950), 15, 9-12.
14. Earlougher, R.C., Jr.: "Advances in Well Test Analysis", Monographs Series, SPE,

(1977); Trans., AIME 5, Dallas.

15. Engelberts, W.F. and Klinkenberg, L.J.: "Laboratory Experiments on the Displacement of Oil by Water from Packs of Granular Material", Proc. Third World Pet. Cong., The Hague (1951), Sec. II, 544.

16. Van Everdingen, A.F. and Hurst, W.: "The Application of the Laplace Transformations to Flow Problems in Reservoirs", Trans., AIME, 186, (1949), 305-324.

17. Fetkovich, M.J.: "A Simplified Approach to Water Influx Calculations - Finite Aquifer Systems", J.Pet.Tech. (July 1971), 814-818.

18. Frick, T.C.: "Petroleum Production Handbook", McGraw-Hill Book Cx o. Inc., New York (1962), II.Chapt. 32, 5-22.

19. Havlena, D. and Odeh, A.S.: "The Material Balance as an Equation of a Straight Line", J.Pet.Tech., (Aug. 1963), 896-900; Trans., AIME, 228, (1963).

20. Heinemann, Z.E. and Weinhardt, B.: "Reservoir Fluids," Textbook, Leoben (2001).

21. Heinemann, Z.E.: "Flow in Porous Media", Textbook, Leoben (1988), 161 pp.

22. Heinemann, Z.E.: "Well Testing", Textbook, Leoben (1991).

23. Holmgren, C.R. and Morse, R.A.: "Effect of Free Gas Saturation on Oil Recovery by Waterflooding", Trans., AIME, 192, (1951), 135-140.

24. Hurst, W.: "Water Influx into a Reservoir and its Application to the Equation of Volumetric Balance", Trans., AIME, 151, (1943), 57-72.

25. Jonhnston, C.E. Jr.: "Prediction of Oil Recovery by Water Flood - A Simplified Graphical Treatment of the Dykstra-Parsons Method", Trans., AIME, 207, (1956), 345-346.

26. Kyte, J.R., Stanclift, R.J. Jr., Stephan, S.C., Jr. and Rappaport, L.A.: "Mechanism of Water Flooding in The Presence of Free Gas", Trans., AIME, 207, (1956), 215-221.

27. Law, J.: "Statistical Approach to the Intersitial Heterogeneity of Sand Reservoirs", Trans., AIME, 155, (1944), 202-222.

28. Martinez, A.R. *at al*.: "Classification and Nomenclature System for Petroleum and Petroleum Reserves", Proc. of the 11th World Petr. Congress, Vol. 2, (1983) John WILEY & Sons, Chichester, 325-39.

29. Matthews, C.S. and Russel, D.G.: "Pressure Buildup and Flow Tests in Wells", Monograph Series, SPE (1967) 1.

30. Miller, M.G. and Lentz, M.R.: "Performance of Bodcaw Reservoir Performance under Cycling Operation Compared to Field Data", Drilling Prod. Pract., API (1947), 128-49.

31. Van Meurs, F.: "The Use of Transparent Three-Dimensional Models for Studying the Mechanism of Flow Processes in Oil Reservoirs", Trans., AIME (1957), 210, 295-301.

32. Muskat, M. and Taylor, M.O.: "Effect of Reservoir Fluid and Rock Characteristics on Production Histories of Gas-drive Reservoirs", Trans., AIME (1946), 165, 78-93.

33. Pirson, S.J.: "Elements of Oil Reservoir Engineering", 2nd ed., McGraw-Hill Book Co., Inc. New York (1958), 608p.

34. Prats, M.: "The Breakthrough Sweep Efficiency of a Staggered Line Drive", Trans., AIME, 207, (1956), 361-362.

35. Schilthuis, R.J.: "Active Oil and Rerservoir Engergy", Trans., AIME, 118, (1936), 33-52.

36. Stiles, W.E.: "Use of Permeability Distribution in Water Flood Calculations", Trans., AIME, 186, (1949), 9-13.

37. Tarner, J.: "Oil Weekly", (June 12, 1944).

38. Tracy, G.W.: "Simplified Form of the Material Balance Equation", Trans., AIME, 204, (1955), 243-8.

39. Walstrom, J.E., Mueller, T.D. and McFarlane: "Evaluation Uncertainty in Engineering Calculations", J. Pet. Tech. (Dec. 1967), 1595.

40. Warren, J.E. and Price, H.S.: "Flow in Heterogeneous Porous Media", Proc. Pet. Eng. J. (1961), 153-169.

41. Vogt, J.P. and Wang, B.: "Accurate Formulas for Calculating the Water Influx Superposition Integral", paper SPE 17066 presented 1987 at the Eastern Regional Meeting, Pittsburgh, Pennsylvania, Oct. 21-23.